PRODUCTION OF API X60 AND X70 GRADE STEEL PLATES BY THERMOMECHANICAL CONTROLLED ROLLING

A MASTER'S THESIS

in

Metallurgical and Materials Engineering

Atılım University

by

SEREN GÜNEŞ

JUNE 2018

PRODUCTION OF API X60 AND X70 GRADE STEEL PLATES BY THERMOMECHANICAL CONTROLLED ROLLING

A THESIS SUBMITTED TO

THE GRADUATE SCHOOL OF NATURAL AND APPLIED SCIENCES

OF

ATILIM UNIVERSITY

BY

SEREN GÜNEŞ

IN PARTIAL FULFILLMENT OF THE REQUIREMENTS FOR THE DEGREE OF

MASTER OF SCIENCE

IN

THE DEPARTMENT OF

METALLURGICAL AND MATERIALS ENGINEERING

JUNE 2018

Approval of the Graduate School of Natural and Applied Sciences, Atılım University.

_____

Prof.Dr. Ali KARA

Director

I certify that this thesis satisfies all the requirements as a thesis for the degree of Master of Science.

_____

Prof.Dr. Naci SEVİNÇ

Head of Department

This is to certify that we have read the thesis "Production of API X60 and X70 Grade Steel Plates by Thermomechanical Controlled Rolling" submitted by Seren Güneş and that in our opinion it is fully adequate, in scope and quality, as a thesis for the degree of Master of Science.

_____

Asst.Prof.Dr. Erkan KONCA

Supervisor

Examining Committee Members

Prof.Dr. Bilgehan ÖGEL _____

Asst.Prof.Dr. Kâzım TUR _____

Asst.Prof.Dr. Erkan KONCA _____

Date: (June 29, 2018)

I declare and guarantee that all data, knowledge and information in this document has been obtained, processed and presented in accordance with academic rules and ethical conduct. Based on these rules and conduct, I have fully cited and referenced all material and results that are not original to this work.

Name, Last name: Seren GÜNEŞ

Signature:

ABSTRACT

PRODUCTION OF API X60 AND X70 GRADE STEEL PLATES BY THERMOMECHANICAL CONTROLLED ROLLING

Güneş, Seren

M.S., Metallurgical and Materials Engineering Department

Supervisor: Asst.Prof.Dr. Erkan Konca

June 2018, 125 pages

This study was undertaken as an initial work to determine the rolling and cooling conditions for the production of API PSL2 X60M and X70M grade steels plates. Two full size Nb-Ti-V microalloyed steel slabs of 200 mm thickness with compositions compliant to the API specification were sliced into 14 small size slabs and these small slabs were subjected to different thermomechanical controlled rolling and accelerated cooling operations to produce 20 mm thick plates. Specifically, the effects of i) finish rolling temperature, ii) partitioning of the total reduction between the rough and finish rolling phases, and iii) accelerated cooling using water shower were studied. Mechanical tests (tensile, impact and drop weight tear test-DWTT) and metallographic examinations of the samples taken from the trial production plates were done. The conditions that could produce fine grained ferritic microstructures with mechanical properties satisfying the API PSL 2 requirements for API X60 steel plates solely by controlled rolling were determined. On the other hand, the use of accelerated cooling in addition to controlled rolling was required for the production of API X70 grade steel plates.

Keywords: Thermomechanical controlled rolling, Thermomechanical controlled processing, Production of steel plates, API X60, API X70, Accelerated cooling

ÖZ

TERMOMEKANİK DENETİMLİ HADDELEME YÖNTEMİ İLE API X60 VE X70 SINIFI ÇELİK LEVHA ÜRETİMİ

Güneş, Seren

Yüksek Lisans, Metalurji ve Malzeme Mühendisliği Bölümü

Tez Yöneticisi: Dr. Öğr. Üyesi Erkan Konca

Haziran 2018, 125 sayfa

Bu çalışma, API PSL2 X60M ve X70M sınıflarında çelik levha üretimi için haddeleme ve soğutma koşullarını belirlemek üzere bir ön çalışma olarak gerçekleştirilmiştir. Kimyasal kompozisyonları ilgili API spesifikasyonuna uygun 200 mm kalınlığında iki adet tam boy Nb-Ti-V mikroalaşımlı çelik slab, 14 adet küçük slaba dilimlenmiş ve bu slab dilimlerine 20 mm kalınlığında levha üretmek üzere farklı koşullarda termomekanik haddeleme ve hızlandırılmış soğutma işlemleri uygulanmıştır. Özel olarak; i) bitirme haddelemesi sıcaklığı, ii) toplam ezmenin kaba ve bitime haddelemesi arasındaki dağılımı ve iii) duşlu masa kullanarak hızlandırılmış soğutma uygulamanın etkileri çalışılmıştır. Deneme üretimi levhalardan alınan numunelerin mekanik testleri (çekme, darbe ve düşürme ağırlıklı yırtma deneyi-DWTT) ve metalografik incelemeleri gerçekleştirilmiştir. API PSL 2 kapsamında X60 sınıfı çelik levhalar için istenen mekanik özellikleri karşılayan ince taneli ferritik içyapıların tek başına denetimli haddeleme ile üretilebildiği koşullar belirlenmiştir. Öte yandan, API X70 sınıfı çelik levha üretimi için denetimli haddelemeye ek olarak hızlandırılmış soğutmanın da uygulanması gerekmiştir.

Anahtar Kelimeler: Termomekanik denetimli haddeleme, Termomekanik denetimli işlem, Çelik levha üretimi, API X60, API X70, Hızlandırılmış soğutma

To My Parents

ACKNOWLEDGMENTS

I express sincere appreciation to my supervisor Asst.Prof.Dr. Erkan Konca for his guidance and insight throughout the research.

This study is carried out in plate rolling mill in an integrated iron and steel company. I express thanks to my managers Serkan Dikeç and Kamber Aygören who supported me and also my colleagues, Çağlar Duran, Tuncay İbiş, Asım Sırrı Özkan, Burak Dinar for the production of plates, Kaan Tanrıöver, Ibrahim Akdümbek, Çağıl Yılmaner for performing of mechanical tests and DWTT, Abdullah Sezer and Dilara Çimen for their assistance on the microstructural analysis and grain size calculations with Clemex Vision Program.

I also offer sincere thanks to my family for their patience and support during this period.

TABLE OF CONTENTS

LIST OF TABLES

LIST OF FIGURES

LIST OF ABBREVIATIONS

API : American Petroleum Institute

BOF : Basic Oxygen Furnace

HSLA : High Strength Low Alloyed Steel

A_{c1} : Austenite formation start temperature on heating

A_{c3} : Full austenitization temperature on heating

A_{r1} : Eutectoid transformation temperature on cooling

A_{r3} : Start temperature for ferrite formation from austenite on cooling

DWTT : Drop Weight Tear Test

SEM : Scanning Electron Microscope

TCR : Thermomechanical Controlled Rolling

TMCP : Thermomechanical Controlled Processing

CE : Carbon Equivalent

T_{nr} : Non-recrystallization temperature of austenite

TTT : Time - Temperature - Transformation

CCT : Continuous Cooling Transformation

CHAPTER 1

INTRODUCTION

1.1. Steels for Natural Gas and Petroleum Pipelines

More than 300,000 kilometers of liquid petroleum and natural gas pipelines are present traverse in the world that connects the producing areas to refineries. Pipelines are safe, efficient and unseen. They move crude oil from oil fields on land and offshore to refineries where it is turned into fuels and other products, Also the most significant advantage of pipelines is that they operate 24 hours a day, seven days a week [1].

Line-pipe steels, used for transporting crude oil or natural gas over a long distance, should be stronger, tougher, larger and thicker for cost reduction and high pressure transportation [1].

All over the world, American Petroleum Institute (API) standard pipes are used in petroleum and natural gas industry. For years, API X52 and X60 grades of steels were used for these pipes. Later high strength requirements caused to the development of X65, X70 and X80 grades steels. In addition to high strength, high impact strength and weldability have also become important for these steels [2].

It is known that approximately 20% of the petroleum and natural gas deposits in the world are located in the North Pole area. However, most of the refineries are in West Europe and North America since petroleum products are mainly used in there. The use of high strength steels is mandatory for fast and safe transportation. On the other hand, higher strength steels can reduce the thickness of the pipes and therefore reduce the weight and thereby provide economy [3].

The main characteristics of these steels are as follows:

- High strength,
- High impact toughness,
- High weldability,
- High ductility.

1.2. API Pipeline Steel Grades

API Specification 5L - Specification for Line Pipe is a kind of guidebook for API pipeline steels. This standard defines requirements for seamless and welded steel pipes for use in pipeline transportation systems in the petroleum and natural gas industries. Level PSL 1 provides a standard quality level for line pipe and Level PSL 2 has additional mandatory requirements for chemical composition, notch toughness and strength properties [4].

Although the chemical compositions of the steel pipes (Table 1) used in the petroleum and gas industry are defined by the specifications of American Petroleum Institute, production method is left to the producers [4].

Therefore, the production methods of API grades may differ according to the steel producer internal workings, the main expected purpose is to achieve the desired mechanical properties [4].

Table 1 API 5L Specification delivery condition

PSL	Delivery Condition	Steel Grade
PSL 1	As-rolled, normalizing rolled, thermomechanical rolled, thermomechanical formed, normalizing formed, normalized, normalized and tempered or quenched and tempered	X60, X70
PSL 2	Normalizing rolled, normalizing formed, normalized or normalized and tempered	X60N, X70N
PSL 2	Quenched and tempered	X60Q, X70Q
PSL 2	Thermomechanical rolled or thermomechanical formed	X60M, X70M

1.3. API Specifications for X60 and X70 Grades

The similar chemical compositions for the X60, X70 grades according to API Specification 5L are shown in Table 2 and Table 3 [4].

Table 2 Chemical composition (wt.%) of API X60 and X70 grades

Grade	C max	Si max	Mn max	P max	S max	V max	Nb max	Ti max	Cu max	Ni max	Cr max	Mo max
PSL1/ X60	0.26	-	1.40	0.030	0.030	Nb + V + Ti ≤ 0.15			-	-	-	-
PSL1/ X70	0.26	-	1.40	0.030	0.030	Nb + V + Ti ≤ 0.15			-	-	-	-
PSL2/ X60N	0.24	0.45	1.40	0.025	0.015	0.10	0.05	0.04	0.50	0.50	0.50	0.50
PSL2/ X60Q	0.18	0.45	1.70	0.025	0.015	0.10	0.05	0.04	0.50	0.50	0.50	0.50
PSL2/ X70Q	0.18	0.45	1.80	0.025	0.015	0.10	0.05	0.04	0.50	0.50	0.50	0.50
PSL2/ X60M	0.12	0.45	1.60	0.025	0.015	Nb + V + Ti ≤ 0.15			0.50	0.50	0.50	0.50
PSL2/ X70M	0.12	0.45	1.70	0.025	0.015	Nb + V + Ti ≤ 0.15			0.50	0.50	0.50	0.50

Table 3 Carbon Equivalent limit values of API X60 and X70 Grades.

Grade	$CE_{IIW(*)}$	$CE_{pcm(*)}$
PSL1/X60	0.43	0.25
PSL1/X70	0.43	0.25
PSL2/X60N	As agreed	
PSL2/X60Q	0.43	0.25
PSL2/X70Q	0.43	0.25
PSL2/X60M	0.43	0.25
PSL2/X70M	0.43	0.25

(*) The CE_{IIW} limits apply if C > 0.12 % and the CE_{pcm} limits apply if C ≤ 0.12 %.

Mechanical property requirements for X60 and X70 grades in API 5L specification are shown in Table 4 [4].

Table 4 Mechanical property requirements of API X60 and X70 grades

Grade	Yield Strength (MPa)	Tensile Strength (MPa)	YS / TS Ratio (max)	% EL (min)	Impact (°C - J)	DWTT(*)
PSL1/X60	415	520	-	24	-	
PSL1/X70	485	570	-	22	-	
PSL2/X60M PSL2/X60N PSL2/X60Q	415-565	520-760	0.93	24	0°C - 40J	≥ 85 %
PSL2/X70M PSL2/X70Q	485-635	570-760	0.93	22	0°C - 68J	≥ 85 %

(*) Drop Weight Tear Test (DWTT) is explained in Chapters 2 and 3.

1.4. Motivation and Objectives of the Current Work

Line pipes produced from steels plates are preferred over the pipes that are produced from coils since they can transport oil and natural gas at higher flow rates due to their higher thickness and larger diameters. API steels play an important role in the development of petroleum industry in all over the world [5].

Therefore, there is a strong international market for the API 5L PSL2 specification like X60 and higher grade steel plates.

The objective of this work is to find out the processing conditions that would enable the production of API 5L PSL2 X60M and X70M grade steel plates by thermomechanical controlled rolling at Plate Rolling Mill. For this objective, 200 mm thick slabs with compositions compliant to X60M and X70M grades were cut into small slabs and they were rolled into 20 mm thick plates under various rolling and cooling conditions. Mechanical tests and metallographic examinations of the samples taken from these plates were performed to determine the successful rolling conditions.

CHAPTER 2

BACKGROUND, THEORY & LITERATURE SURVEY

2.1. Plate Production

2.1.1. Steel Production Process

Steel production operations are carried out in the Basic Oxygen Furnace (BOF). The crude iron that is produced in the blast furnace is charged to the BOF. Combination of liquid crude iron, scrap and alloying elements are used to make the desired quality. The carbon amount in the liquid crude iron is reduced by means of pure oxygen blowing method. The oxygen initiates a series of exothermic reactions, including the oxidation of such impurities as carbon, silicon, phosphorus, sulphur and manganese. Deoxidation of steel is achieved by addition of aluminum and silicon. Finally, liquid crude iron is converted into liquid steel [6].

Secondary metallurgy process includes the remedial actions necessary to improve the properties of the alloyed liquid steel. Liquid steel, both chemically and thermally, is heterogeneous. For this reason, the steel is subjected to temperature and chemical homogenization by mixing with argon gas in a second ladle processing station. Al and Si are burned with oxygen [7].

After the temperature and chemical composition of steel in the secondary metallurgical process are adjusted, it is passed through a movable mold cavity and dynamically solidified and then converted into slabs called as continuous casting process [7].

2.1.2. Plate Rolling Process

Plate production starts with the preparation of slabs and cutting the slabs into the desired dimensions. The small slab dimensions must be determined depending on the thickness, width and length of the main slab. Small slab is used as a semi-finished product for plate production.

Small slabs are heated to a range of about 1200-1250°C for 2-3 hours in order to get austenite phase. They are sent to the plate production unit as shown in Figure 1 by the help of the transfer tables. The oxide layer formed on the small slab surfaces during the heating is cleaned by spraying pressurized water before the rolling operation. The rolling operation is carried out by rolling as forward and backward movement of the small slab [8, 9].

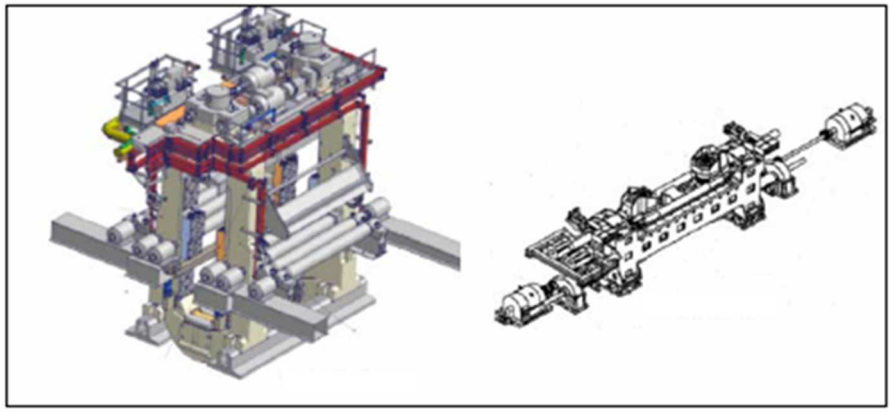

Figure 1 Plate rolling unit

Plate rolling methods include rotational rolling and direct rolling depending on the order width of the product [10].

Direct Rolling:

Slabs are directly rolled (Figure 2a) when the width of the ordered plates is not greater than the width of the slab.

Rotational Rolling:

When the width of the ordered plate is larger than the width of the slab, rotation operation is applied to the slab (Figure 2b) and the length of the slab is rolled as the width of the slab. According to this operation, before the first pass of rolling, the length of the slab is adjusted related to the product order width.

On the other hand, a second rotational rolling is applied for the higher order width. In this case, the product is rotated in the first pass and in the third pass (Figure 2c). The length and the width are adjusted related to the product order width and length.

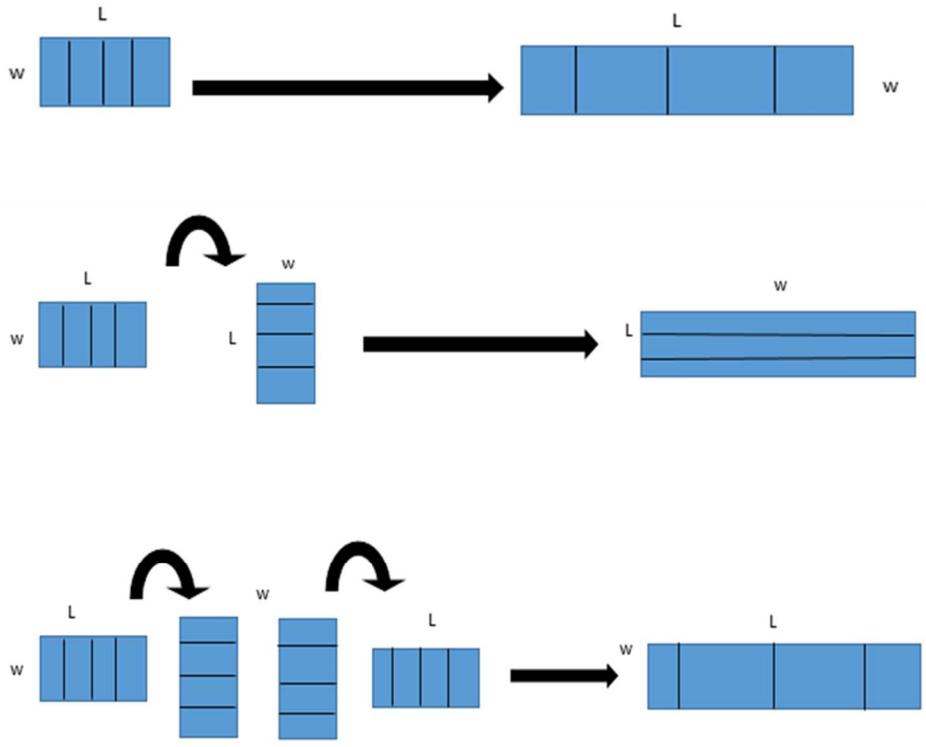

Figure 2 a) Direct, b) rotational, and c) double rotational rolling

Rolling Pass

The optimization strategy uses the basic models and takes into account a number of constraints and limits in order to determine the optimal rolling schedule. Dimensions of initial product, temperature of initial product, material laws and rolling mill parameters are the entry parameters. Exit thickness, width and temperature required are the target parameters. These parameters are needed for a rolling schedule calculation. A rolling schedule is a sequence of several rolling passes (Figure 3) to reduce the product from its initial state to its target dimensions. All these passes must respect the mill equipment and product constraints [9, 10].

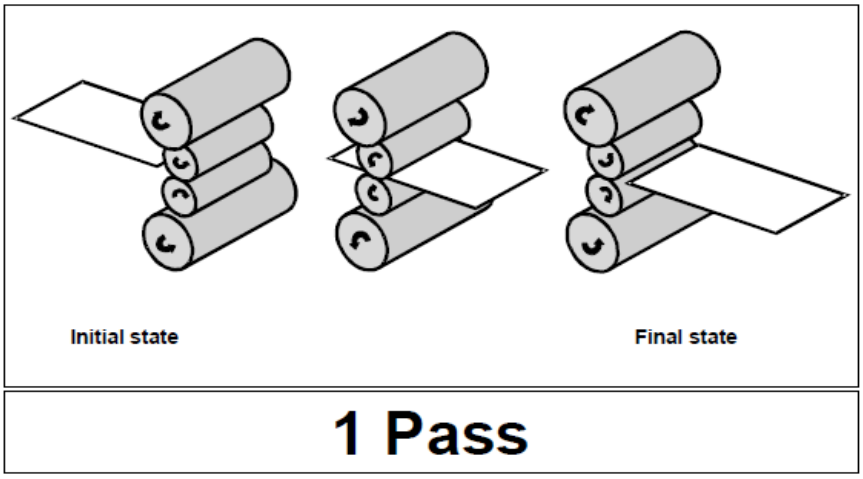

Figure 3 One pass rolling

A rolling phase (Figure 4) is characterized by an uninterrupted sequence of rolling passes which constitute a "finite" step of the rolling process with the objective of obtaining a particular state of the product. Each phase is defined by the "start-of-phase" product dimensions and by the "end-of phase" target product dimensions [10].

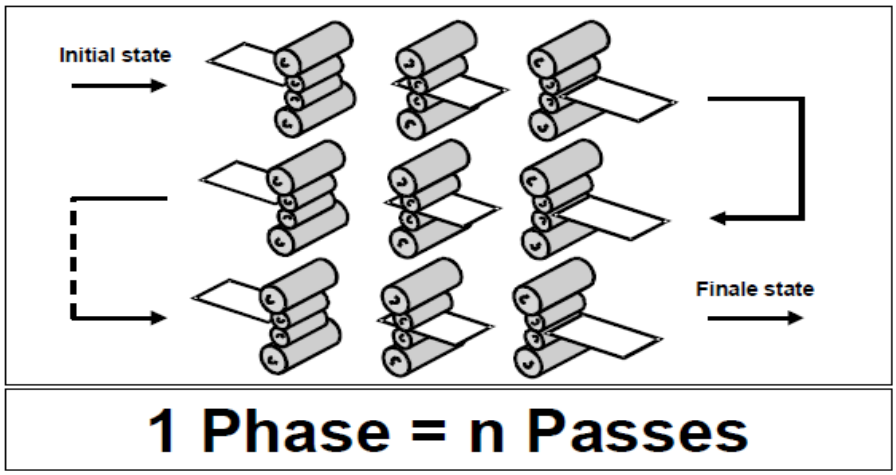

Figure 4 A rolling phase

Basically, the rolling schedule optimization consists in determining a pass sequence that is optimal in terms of productivity and product quality, from a given initial thickness to the target thickness [10].

Plate rolling process includes two groups as conventional hot rolling and controlled hot rolling. Hot rolling is the conventional method of steel processing. In order to gain some mechanical properties to steel, normalizing, quenching and tempering methods can be applied as conventional methods of heat treatment. These methods are performed in a furnace and are applied to steel products after rolling is completed [11].

2.1.2.1. Conventional Hot Rolling of Plates

In conventional hot rolling, final shape of the plate is given at high temperatures above A_{r3} critical temperature. Reduction from slab to plate starts and finishes in austenite phase. Due to high temperature, recrystallization and grain growth occur during rolling so regular grain structure cannot be obtained. This rolling method is usually used for non-alloyed steels where strength and hardness are not required [12].

2.1.2.2. Normalizing Rolling

Normalizing rolling is a kind of thermomechanical rolling method in which the rolling last pass is given in the normalizing temperature range about 920°C. This can involve hold-periods during the rolling process to allow plates to cool before rolling is resumed. During rolling austenite phase is completely recrystallized but at low temperatures there is no grain growth and as a result the material will have the same conditions as the air cooling conditions after normalizing heat treatment after the last pass. Normalized rolling is used in all plate rolling mills since the rolling output temperature is around or higher than 900°C, depending on the rolling mill and load rates. Controlled rolling can increase strength, refine grain size, improve fracture toughness and may eliminate the need for normalizing. On the other hand, if plate temperatures are not uniform, controlled rolling can lead to property variability between different regions of the plate so thickness is important factor and high roll pressures are required for thick plates at low rolling temperatures [11].

2.2. Plate Rolling for API Grades

2.2.1. Strengthening Mechanisms for Steel Plates

Since 1970, many demands have been come out to the pipe manufacturers for the development of higher strength steels for pipelines. Generally, welded large diameter pipeline is preferable for transportation oil and gas, since it provides the highest throughput. API X70 and upper grades are generally used for the construction of long distance pipelines. As the request for strength increases, the method of hot rolling changes from conventional hot rolling and normalizing process to thermomechanical control rolling and thermomechanical control process [13].

The development of high strength API grades are shown in Figure 5. API X60 grade can be reached with hot rolling and normalizing conditions, but for API X70 grade production thermomechanical controlled rolling method is needed. In addition to controlled rolling, accelerated cooling process is necessary in order to produce API X70 and upper grades [13].

The most important companies for the production of API Grades as a plate, are placed in United States such as ArcelorMittal Global R & D - East Chicago, SSAB Americas, Nucor Steel Hertford County. The other important ones are Nippon Steel & Sumitomo Metal Corporation and JFE Steel Corporation in Japan, Tata Steel Europe Ltd. in Netherlands, and NLMK Europe in Belgium.

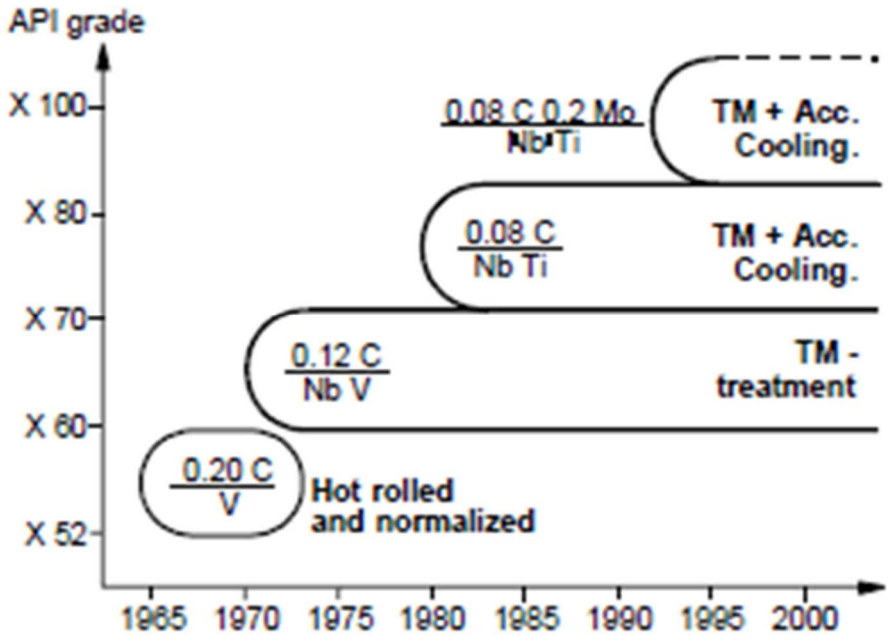

Figure 5 Development of high strength steels [13]

In general, the most effective way to increase the strength in steels is to increase the carbon content. However, as carbon is increased, the impact strength and weldability are negatively affected so in order to maintain high toughness and weldability, percent of C levels of steel should be kept low. For this reason, it is aimed to increase the strength of steel by using different mechanisms. One of them is to decrease the grain size so as to increase the strength of steel. Especially in steels with low carbon content, ferrite grain size should be reduced as much as possible to increase strength. The small ferrite grain size does not negatively affect the weldability and ductility of steel. On the contrary, smaller ferrite grain sizes result in higher mechanical properties and impact strength of steel (Figure 6) [2].

High strength low alloyed steels are hot rolled products meeting the yield strength requirements specified in related standards with low carbon and low alloy content, thus by applying controlled rolling mechanical properties should be further improved. Besides controlled rolling, it is needed to restrict grain growth so the presence of nitrides and carbonitrides prevent the growth of austenite grains at the beginning. The smaller austenite grains result in smaller final ferrite grains [2].

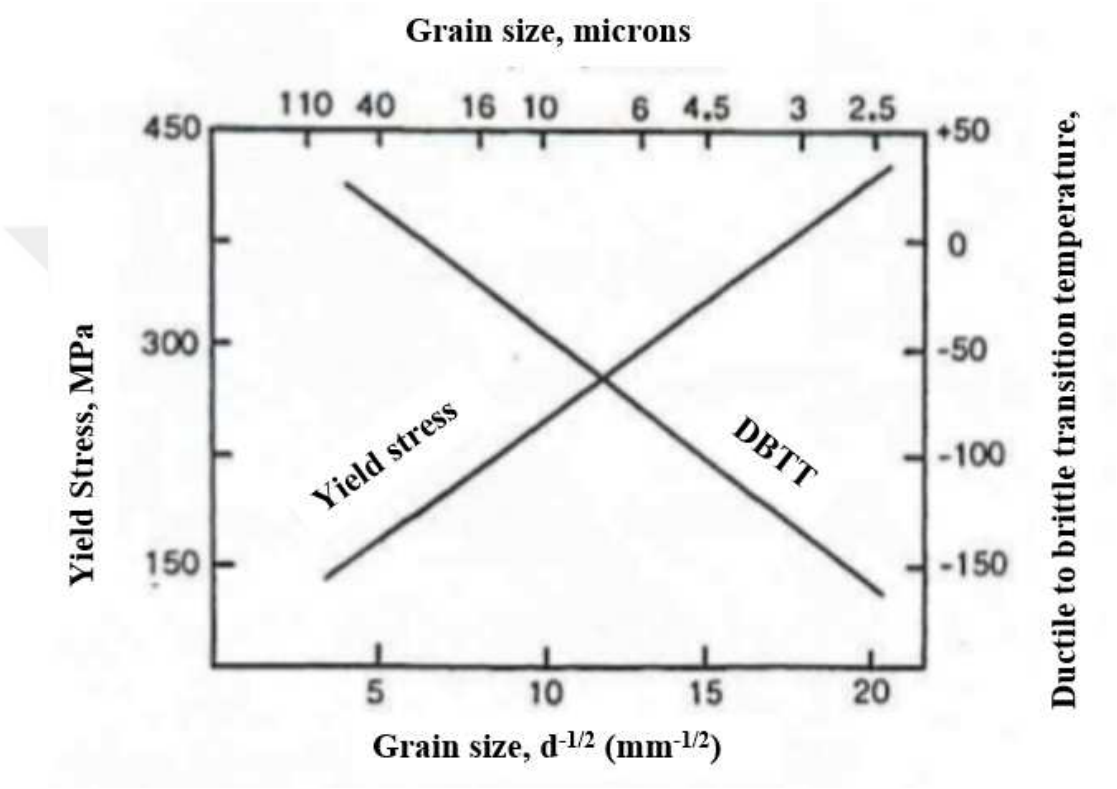

Figure 6 Effect of grain size on yield strength and ductile to brittle transition temperature [14].

The effect of alloying elements is most effective on steels compared to other metals.

Niobium, Vanadium and Titanium

Generally microalloying methods for increasing the strength of carbon-manganese steels is by the additions of small amount niobium (Nb), titanium (Ti), vanadium (V). They have the same purpose as to restrict recrystallization and grain growth of the austenite during hot rolling that results in grain refinement of ferrite and to provide extra strengthening to ferrite with the formation of alloy precipitates [15].

These elements increase the yield and tensile strength of the steel by reducing the grain size. They can be used single, double and triple compositions in steel. They increase the strength by precipitation hardening mechanism as well as grain size refinements. They also have an ability to form carbides. Formation of carbides, nitrides or carbon nitrides retard the recrystallization so increasing the non- recrystallization temperature (T_{nr}), increasing in strength and toughness [16, 17].

The variation of the non-recrystallization temperature of austenite with micro alloying element content can be seen in Figure 7.

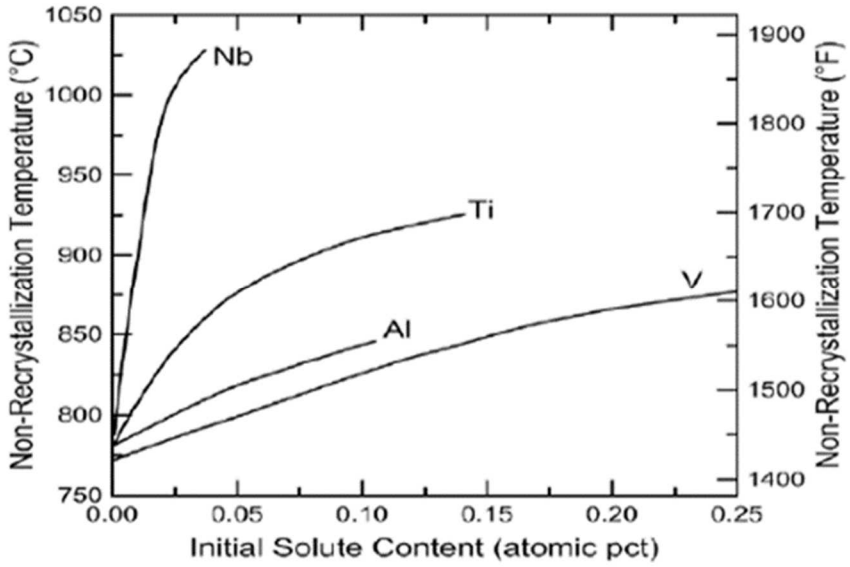

Figure 7 The effect of alloying elements on the non-recrystallization temperature

Niobium is needed for retarding austenite recrystallization, precipitation hardening, and also controlling transformation and improving weldability thus it is evolved to use in low carbon steels for improving strength [18].

Carbon

The basic alloying element in steel is carbon that gives hardening to steel. Carbon improves the yield and tensile strength of the steel but reduces percentage elongation, formability and weldability. Therefore, in API grades, carbon contents are kept as low as possible [16, 17, 19].

Manganese

Manganese improves the strength of steel due to hardenability and increase the welding ability of steels. Manganese has an ability to form carbides in steel. However, the effect of manganese on high-carbon steels is greater than on low-carbon steels [16, 17, 19].

Silicon

Silicon is used in steel because it is used as a deoxidizer. Elongation, yield-tensile strength and elasticity increases with the silicon but it decreases formability of steel. As the amount of silicon in steel decreases, the rate of descaling increases [16, 17, 19].

Phosphorus

Phosphorus is an undesired element in steel. Although it increases yield and tensile strength, it has a negative effect on the steels as decreasing elongation and bending ability [16, 17, 19].

Sulphur

Sulfur is a residue element from the steel production and is tried to be removed from the steel as much as possible due to the undesirable effects. It makes the steel brittle so rolling of steel becomes hard. Sulfur, significantly reduces the toughness and ductility of the steel, also affects weldability property negatively. In addition, its effect on yield and tensile strength is negligible [16, 17].

Copper (Cu)

Although copper element increases the yield and tensile strength of steel, it decreases the percentage elongation and formability property. Ductility seriously decreases but it is generally added because of increasing corrosion resistance and hardness of steel [16, 17, 19].

Nickel (Ni)

Nickel increases the impact toughness of steel. In addition, it improves weldability, plastic deformation and fatigue properties. Nickel has an effect to improve corrosion resistance [16, 17].

Chromium (Cr)

Chromium provides corrosion and oxidation resistance and increases hardenability of steel. It improves the heat resistance of the steel and prevents descaling [16, 17, 19].

Molybdenum (Mo)

Molybdenum increases the tensile strength of the steel and weldability due to its resistance to heat. In addition, it prevents grain growth and improves hardenability of ferrite phase in steel but formability decreases with molybdenum [16, 17, 19].

Carbon Equivalent (CE)

Carbon is an element to strengthen steel effectively, but increasing in carbon content result in deteriorating of toughness and weldability of steel. In welding, the carbon equivalent formulas $CE_{(IIW)}$ and $CE_{(Pcm)}$ as following should be calculated with carbon and related other alloying elements content [20]. $CE_{(IIW)}$ is the most common one from Intertional Institude of Welding and $CE_{(Pcm)}$ is an alternative formula which is developed for high strength low carbon steels.

$$CE_{(IIW)}=C+Mn/6+(Cr+Mo+V)/5+(Cu+Ni)/15 \quad \text{(eq. 1)}$$

$$CE_{(Pcm)}=C+Si/30+Mn/20+Cu/20+Ni/60+Cr/20+Mo/15+V/10+5B \quad \text{(eq. 2)}$$

Since weldability is crucial for line-pipe steels, reducing carbon content is needed to improve the weldability and toughness of steel remarkably [20].

2.2.2. Thermomechanical Control Rolling

Thermomechanical Controlled Rolling (TCR) is an advanced process of controlled rolling that involves control of temperature and reduction rates during the rolling operation. The facilities have the capability of accurately measuring plate temperature at multiple locations to control the uniformity of temperature during the rolling process. TCR processing can provide a very refined and uniform grain structure result in increasing in strength, toughness, and ductility [21, 22].

TCR is the process that takes place in the temperature range at which the austenite is not recrystallized thus rolling in low temperature causes the austenite grain structure to take the pancake form which later transforms to fine grained ferritic-pearlitic structure (Figure 8). The final three pass during rolling is given above a temperature at which the austenite begins to transform into ferrite in this case low rolling temperatures indicates that the grain structure of the steel is reduced. By the last three passes, deformation starts above the A_{r3} phase transformation temperature and is finished below A_{r3} temperature in dual phase region with ferrite and austenite [9, 11, 22].

2.2.3. Thermomechanical Controlled Processing (TMCP)

If improved properties are required, post-rolling heat treatments can be applied to modify the strength, ductility, and fracture toughness of the steel and control of temperature during the rolling process can lead to property enhancement without the need for additional heat treatment. Thermomechanical controlled processing (TMCP) is an effective post-rolling heat treatment to introduce more precise control of temperature during the rolling process. TMCP is achieved by controlled rolling followed by cooling with water at a high rate of cooling, called as accelerated cooling for transformation control. Heating and cooling are incorporated directly during the rolling process [23-25].

In plate production accelerated cooling is a type of cooling with water and it is applied after rolling is finished (Figure 8). This way the mechanical properties and toughness of product are improved by preventing the grain growth of the steel and thus properties can be achieved with lower alloy elements resulting cost reduction. Currently, there are only a limited number of mills that have this capability for plate production [19].

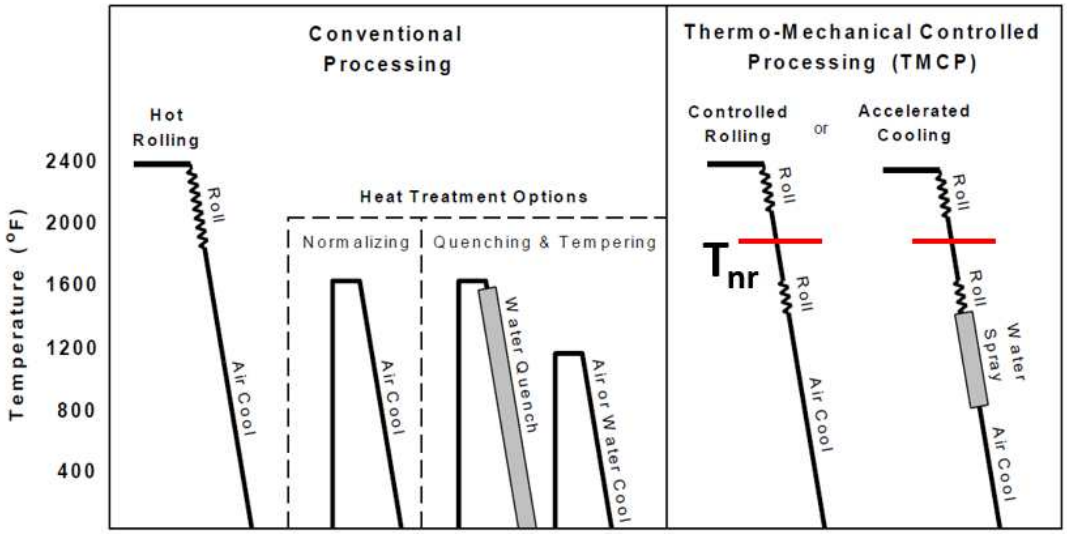

Figure 8 Temperature-Time histories for conventional, TCR and TCMP methods of plate production [22].

CHAPTER 3

EXPERIMENTAL

3.1. Trials to Produce API X60 and X70 Steel Plates

3.1.1. Selection of the Slabs

As stated in section 1.4, this study is undertaken to determine the rolling conditions for the production of API X60 and API X70 grade steels by thermomechanical controlled rolling. Slab is needed for rolling of plates which its shape is like rectangular prism. The dimensions of slabs are approximately 200mm*1000mm*12000mm and the target of the final dimensions of product are approximately 20mm*1000mm*6000mm as thickness, width and length, respectively. While manufacturing of plates, number of rolling passes are important. The target dimensions of plate are produced by reversing mill and the number of passes depend on the final dimensions of the plate.

The chemical compositions of the slabs used for the trials are given in Table 5 and their calculated carbon equivalent values of the slabs used for the trials are given in Table 6.

Table 5 The chemical compositions (max wt.%) of the slabs used

	C	Si	Mn	P	S	V	Nb	Ti	Cu	Ni	Cr	Mo
API X60 and X70 (max)	0.12	0.45	1.60	0.025	0.015	Nb + V + Ti ≤ 0.15			0.50	0.50	0.50	0.50
Slab (max)	0.010	0.25	1.60	0.025	0.010	0.01	0.06	0.03	0.10	0.10	0.20	0.15

Table 6 The carbon equivalent values (wt.%) of the slabs used

	C_{IIW}	C_{Pcm}
API X60 and X70 (max)	0.43	0.25
Slab-1	0.40	0.18
Slab-2	0.40	0.19

3.1.2. TTT and CCT Curves of the Slab Compositions

JMatPro-V10 software was used to construct TTT (Time- Temperature - Transformation) and CCT (Continuous Cooling Transformation) diagrams (Figure 9-12) for the slab compositions given in Table 5 [26].

For the construction of the diagrams austenitization temperature was taken as 1050°C which is the about the minimum recrystallization temperature (T_{nr}) of austenite for the given compositions. ASTM grain size number according to ASTM E112 is taken as "6" [27, 28].

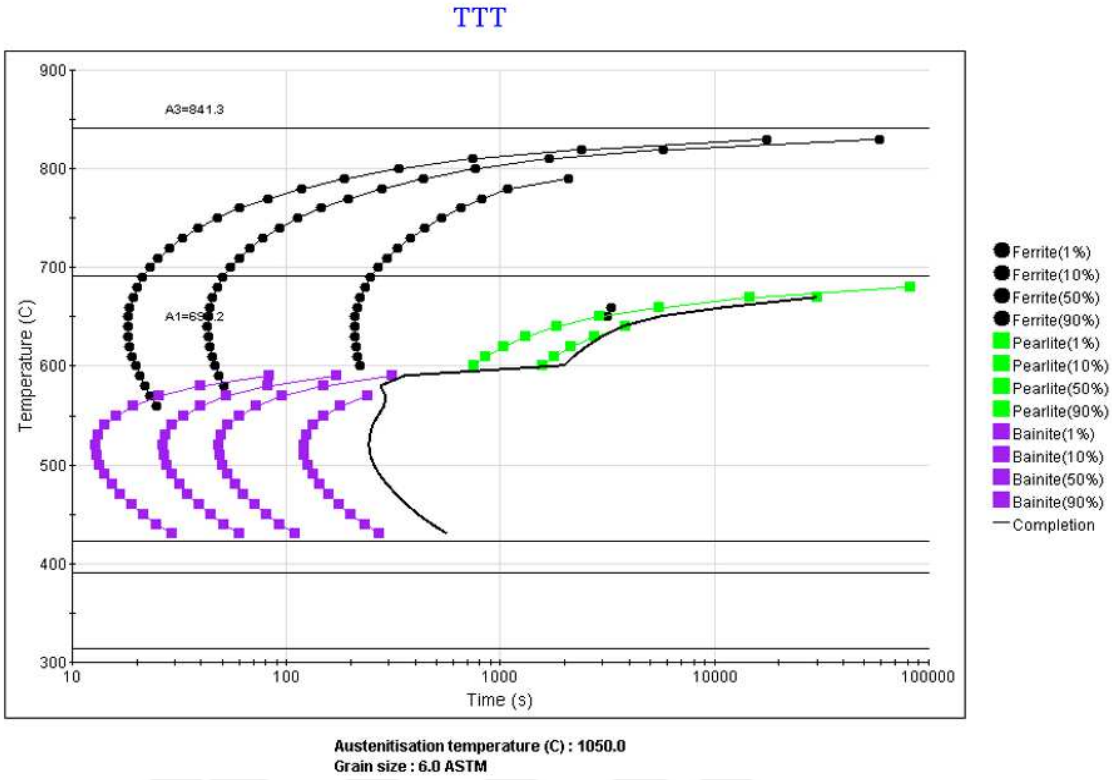

Figure 9 TTT diagram for Slab1

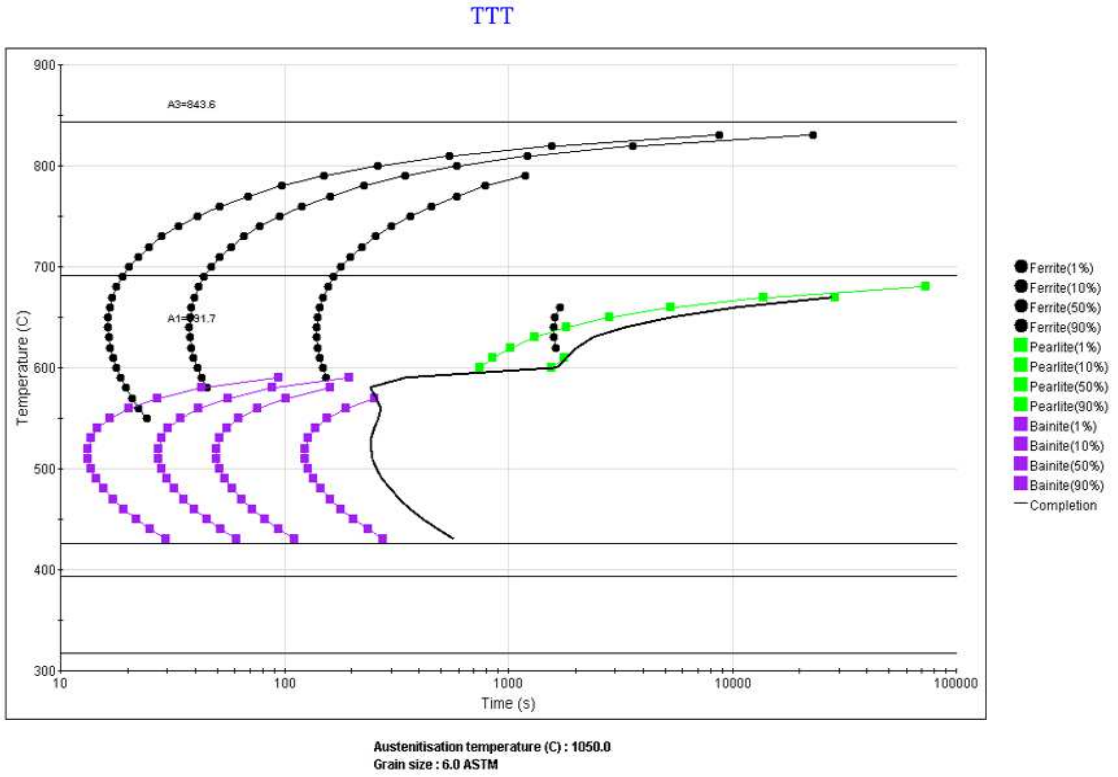

Figure 10 TTT diagram for Slab2

The critical temperatures were calculated as A_3 = 841°C and A_1 = 690°C for the slab-1 composition, and A_3 = 844°C and A_1 = 691°C for the slab-2 composition as shown on the TTT diagrams.

Steel of composition less than 0.76 wt. % carbon is designated as "hypoeutectoid" steel. For a hypoeutectoid steel that is very slowly cooled from austenite phase, ferrite starts to form below the critical temperature A_3. Remaining austenite goes into eutectoid reaction to form pearlite when the temperature is further lowered to A_1 temperature [29].

Ferritic-bainitic microstructure is expected at room temperature when the production conditions are determined on the diagram for both slabs at relatively high cooling rates. Controlled slower cooling conditions should produce ferritic-pearlitic structures according to the CCT diagrams (Figure 11 and Figure 12) [29].

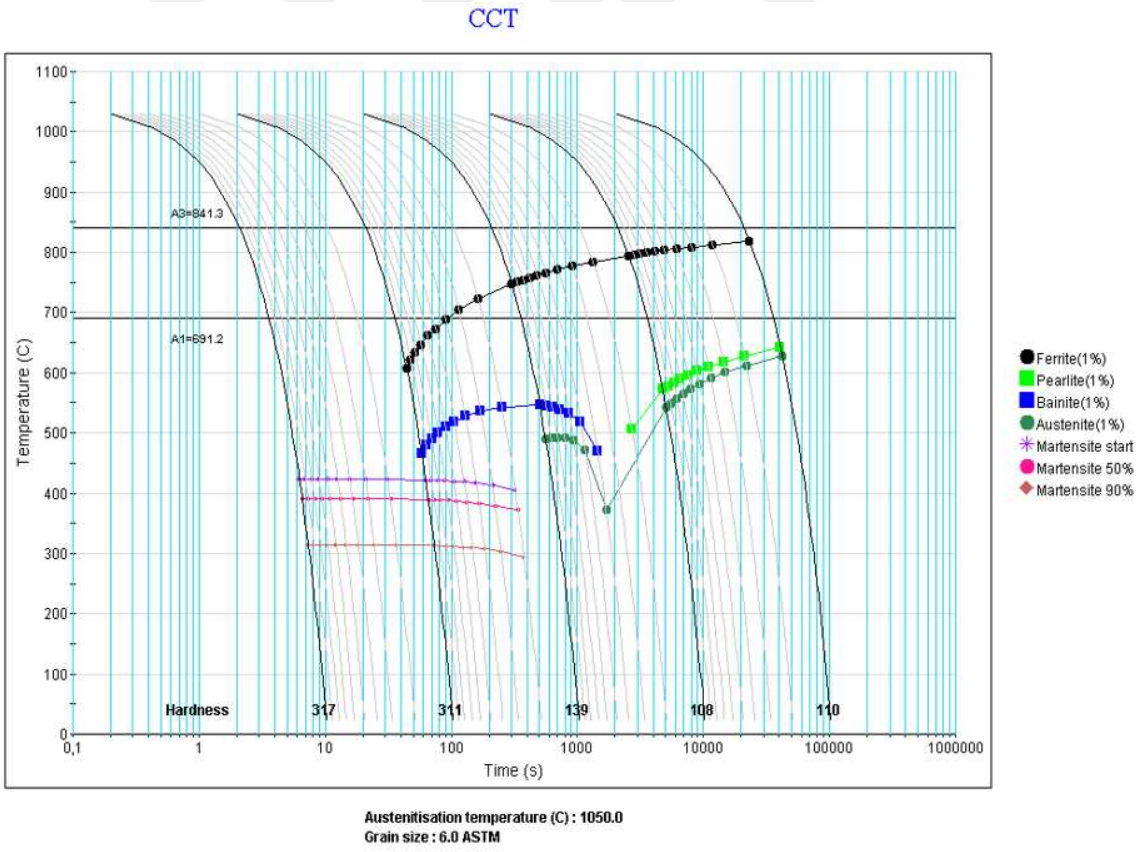

Figure 11 CTT diagram for Slab1

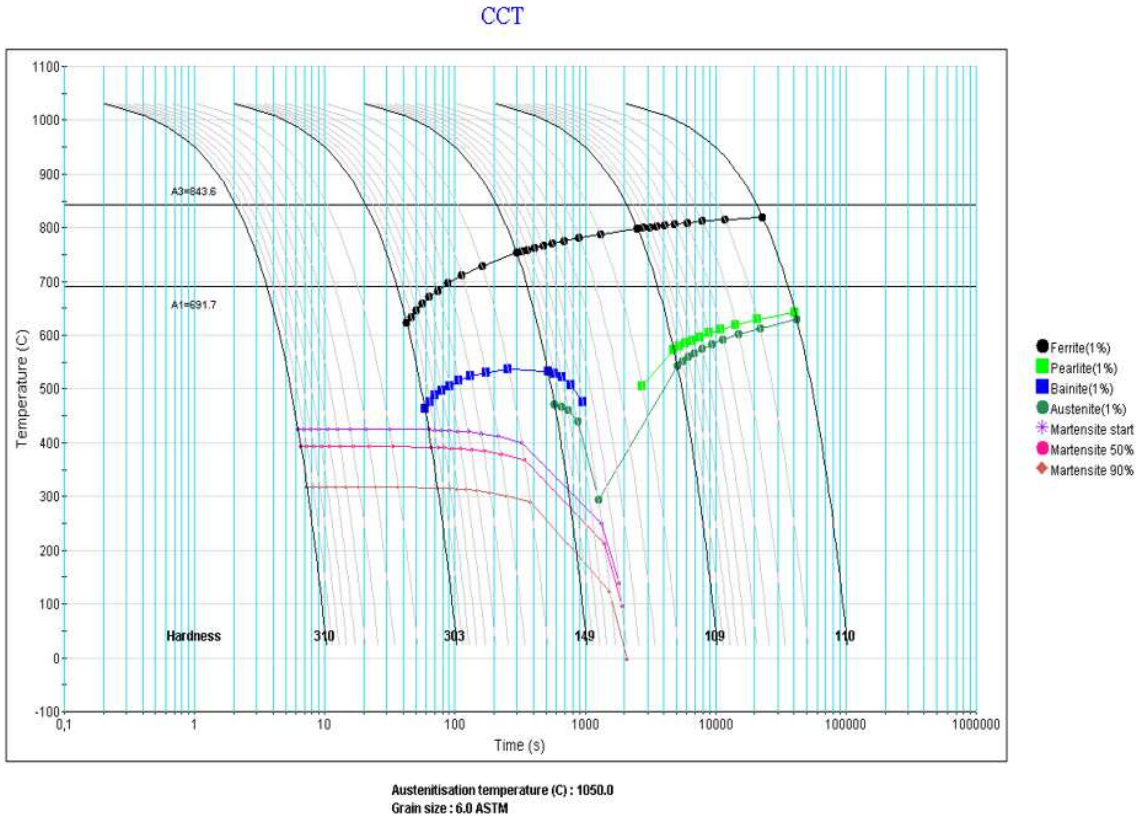

Figure 12 CTT diagram for Slab2

Ferritic nucleation starts at a temperature of around 840°C under equilibrium conditions. According to CCT diagram the formation of ferrite-bainite phases or ferrite-pearlite microstructures are observed depending on the rate of cooling. Ferritic transformation temperatures are also seen to decrease with increasing rate of cooling. In addition, martensite phase may also be seen at very high cooling rates.

3.1.3. Calculation of Critical Temperatures (T_{nr}, A_{r1}, A_{r3})

The transformation temperatures are critical temperatures in production of steel products. During heating process, A_{c1} is the temperature at which the transformation starts from ferrite-pearlite to austenite phase ($\alpha \rightarrow \alpha + \gamma$) and A_{c3} is the temperature at which the structure is completely converted to austenite phase (γ). During cooling process, A_{r3} is the beginning temperature of transformation from austenite to ferrite phase and A_{r1} is the eutectoid transformation temperature [30, 31].

The A_{r3} temperature is a critical value in the rolling process since austenite phase (γ) begins to transform to ferrite phase (α). The A_{r3} phase transformation temperature gives a temperature limit indicating whether the rolling is to be carried out in the austenite (γ) zone or in the transformation zone (γ + α) (Figure 13) [32].

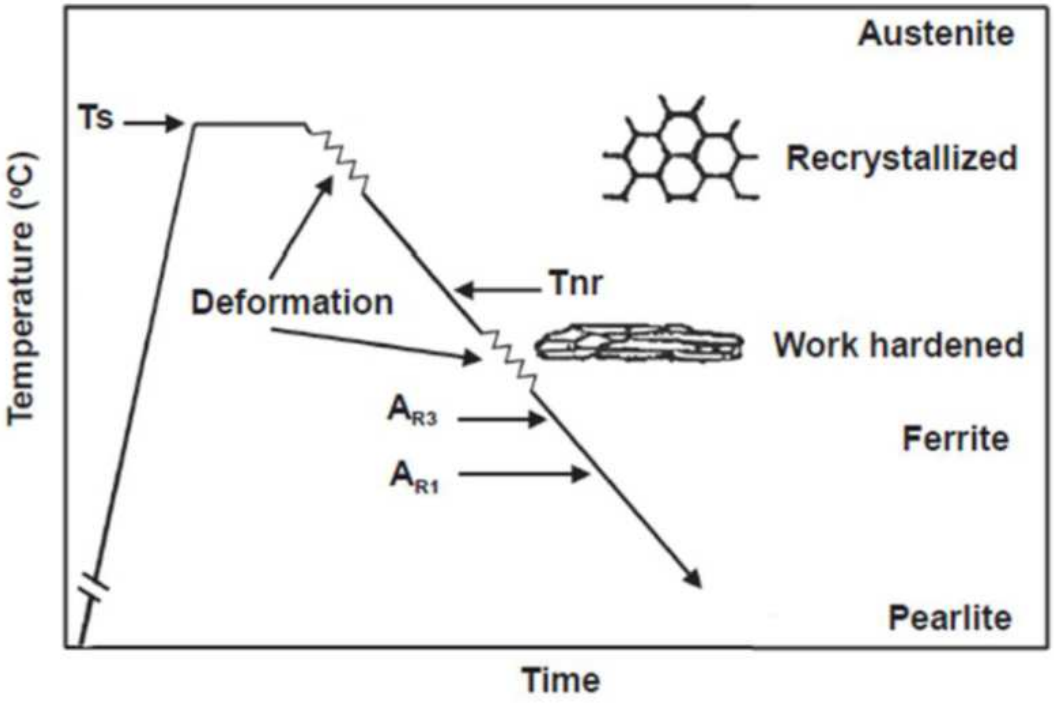

Figure 13 The critical temperatures in thermo-mechanical processing [33]

One of the important factors for grain size of ferrite is the prior austenite grain size and deformation temperature conditions. During the thermo-mechanical processing, the steel is first heated to the austenitization temperature and then soaked at these temperatures for certain interval of time [33].

Recrystallization mechanism in an austenite phase is critical in order to get the desired microstructure and mechanical properties. T_{nr} is the non-recrystallization temperature also called as the recrystallization stop temperature for austenite [34].

The role of T_{nr} is very important in increasing the strength of the material. When material is deformed above T_{nr}, equaxied recrystallization grains occurs then become large due to grain coarsening. On the other hand, when the deformation occurs below

T_{nr} it leads to work hardening like pancake structure and therefore increases the number of nucleation sites for the austenite-to-ferrite transformation [33].

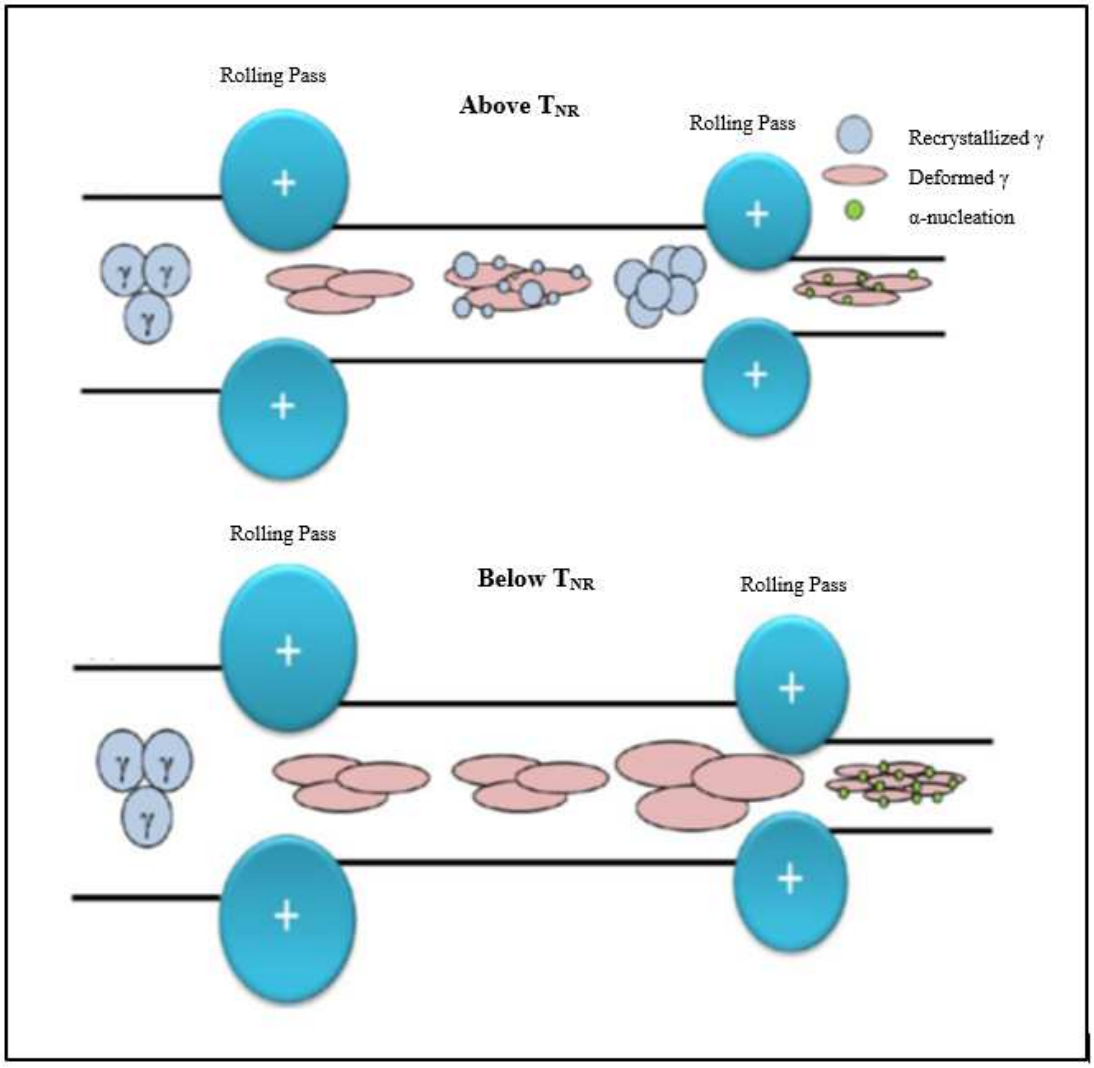

Figure 14 Relation between rolling and T_{nr} temperature [34].

T_{nr} can be calculated using empirical formula [33].

Boratto Equation: (eq. 3)

$$T_{nr} = 887 + 464\mathbf{C} + (6445\ \mathbf{Nb} - 644\sqrt{\mathbf{Nb}}) + (732\mathbf{V} - 230\sqrt{\mathbf{V}}) + 890\mathbf{Ti} + 363\mathbf{Al} - 357\mathbf{Si}$$

Bai Equation: (eq. 4)

$$T_{nr} = 174 \log [\mathbf{Nb}\ (\mathbf{C} + (12/14)\ \mathbf{N})] + 1444$$

According to the Boratto and Bai equations T_{nr} of slab-1 is 1069°C and 1040°C, and T_{nr} of slab-2 is about 1054°C and 1040°C, respectively.

Cooling process is started from the austenite single phase region above Ar_3 temperature after hot rolling operation is finished and different microstructures are obtained by air cooling or cooling with water [35].

A_{r3} (°C) = 910 -310**C** -80**Mn**- 20**Cu** -15**Cr** -55**Ni** -80**Mo** + 0.35(**t**-8) where, t: plate thickness in mm [36].

According to Quchi equation A_{r3} temperature is calculated as approximately 748°C for slab-1 and 753°C for slab-2.

3.1.4. Rolling Conditions (Rolling Schedules)

As mentioned before, the dimensions of original (full size) slabs were approximately 200mm*1000mm*12000mm. In order to get small slabs (i.e. baby slabs), the original slabs were cut in length so thickness and width of slabs did not change but the lengths were fell to 2000-3000 mm. The target of the final dimensions of product are approximately 20mm*1000mm*6000mm as thickness, width and length, respectively.

Baby slabs are heated approximately to 1200°C in order to reach the homogeneous austenite phase of steel in the slab furnace. Then, they were taken into the rolling process. According to the operational practice, 8-10 rolling passes are needed in order to reach the final dimensions.

The non-recrystallization temperature of the given slab is about 1060°C according to the Boratto equation so the rough rolling temperature should be at least about 1060°C before rolling starts. Controlled rolling thickness is considered as 3T (that is 3x20 = 60mm) because of reduction ratio of steel to get smaller grains in microstructure. In addition, in order to investigate the effect of thickness to start controlled rolling, 2T (40 mm) and 4T (80 mm) were also tried out as controlled rolling thickness values.

Controlled temperature while rolling should be taken in consideration in the last 3 passes because of the transformation of austenite to the expected structures like ferrite, pearlite or bainite. The thermomechanical rolling temperatures are the experimental variables and the temperatures are selected above the A_{r3} temperature according to Quchi equation which was calculated as approximately 750°C.

A total of 14 baby slabs were used for the trials in two series according to the industrial conditions. In the first series, six baby slabs were rolled and then after the evaluation of results, the other eight baby slabs were rolled. The number of baby slabs were different in the two parts due to the dimensions of slab furnace.

In the first series, the aim was to observe the effect of rolling temperatures on the internal structure and mechanical properties of steel plates. B-Slab1 was rolled with conventional plate rolling practice (Figure 15).

Figure 15 Conventional rolling of plates

B-Slab2, B-Slab3, B-Slab4, B-Slab5, B-Slab6 were rolled in rough mill from 200 mm to 60 mm and kept until the specified controlled temperature (Figure 16). From 60 mm to 20 mm they were rolled within the controlled rolling temperatures that were set as

950°C, 900°C, 850°C, 800°C for B-Slab2, B-Slab3, B-Slab4, and B-Slab5, respectively.

Figure 16 Waiting step before TCR

After the rolling process, the final products were taken to the cooling region and cooled slowly in air and to prevent distortion, batch cooling was applied as shown in Figure 17.

Figure 17 Air cooling zone after TCR

The last one, called B-Slab6, was rolled in 800°C controlled temperature then cooled quickly by applying a shower of water to shorten the cooling time.

In the second series of rolling experiments, the aim was to observe the effect of accelerated cooling on the microstructure and mechanical properties of steel plates.

B-Slab7 was conventionally rolled, air cooled until the temperature of plate was 800°C, and then cooled by supplying a shower of water. B-Slab8, B-Slab9, B-Slab10, B-Slab11, were rolled from 200 mm to 60 mm in rough mill and from 60 mm to 20 mm with controlled rolling temperatures as 950°C, 850°C, 800°C, 750°C, respectively. Then they were cooled by supplying a shower of water as shown in Figure 18.

Figure 18 Accelerated cooling of plates using water shower

In order to see the reduction ratio effect on plates with TCR, B-Slab12 was rolled from 40 mm to 20 mm with controlled rolling temperature of 800°C and cooled with water shower. The other two baby slabs (B-Slab13 and B-Slab14) were rolled from 80 mm to 20 mm with TCR. B-Slab13 was cooled in air and B-Slab14 was cooled with water shower.

The rolling and cooling conditions of baby slabs are given in figures as B-Slab1 in Figure 19, B-Slab7 in Figure 20, B-Slab2 in Figure 21, B-Slab8 in Figure 22, B-Slab3 in Figure 23, B-Slab4 in Figure24, B-Slab9 in Figure 25, B-Slab5 in Figure 26, B-Slab10 in Figure 27, B-Slab11 in Figure 28, B-Slab14 in Figure 29, B-Slab13 in Figure 30 and B-Slab12 in Figure 31.

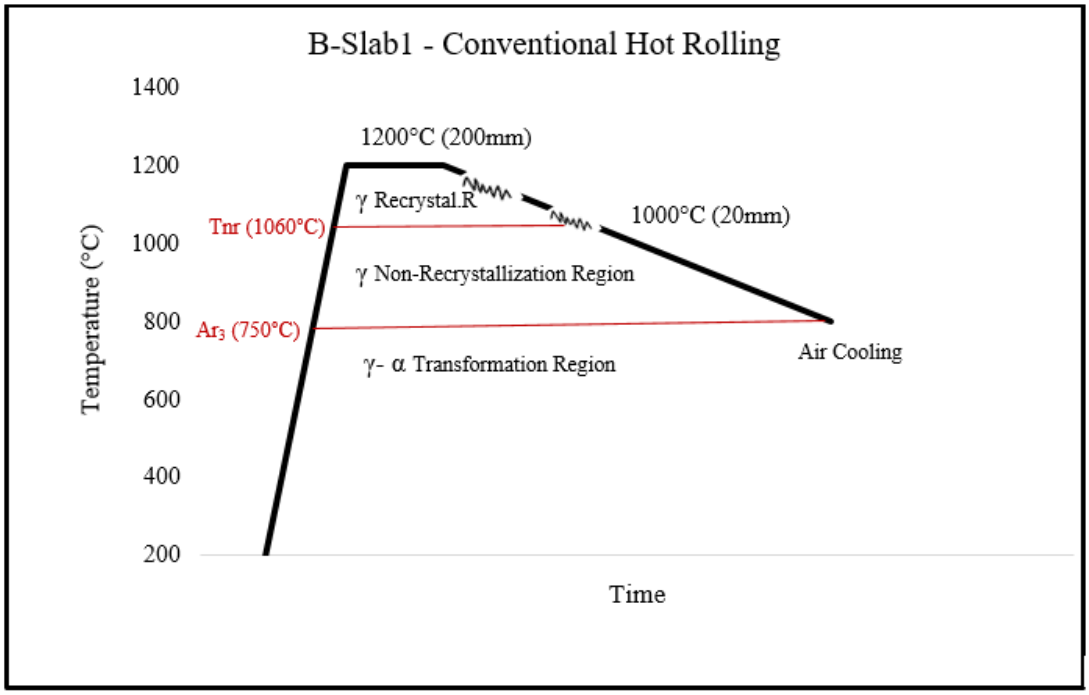

Figure 19 Rolling and cooling conditions of B-Slab1

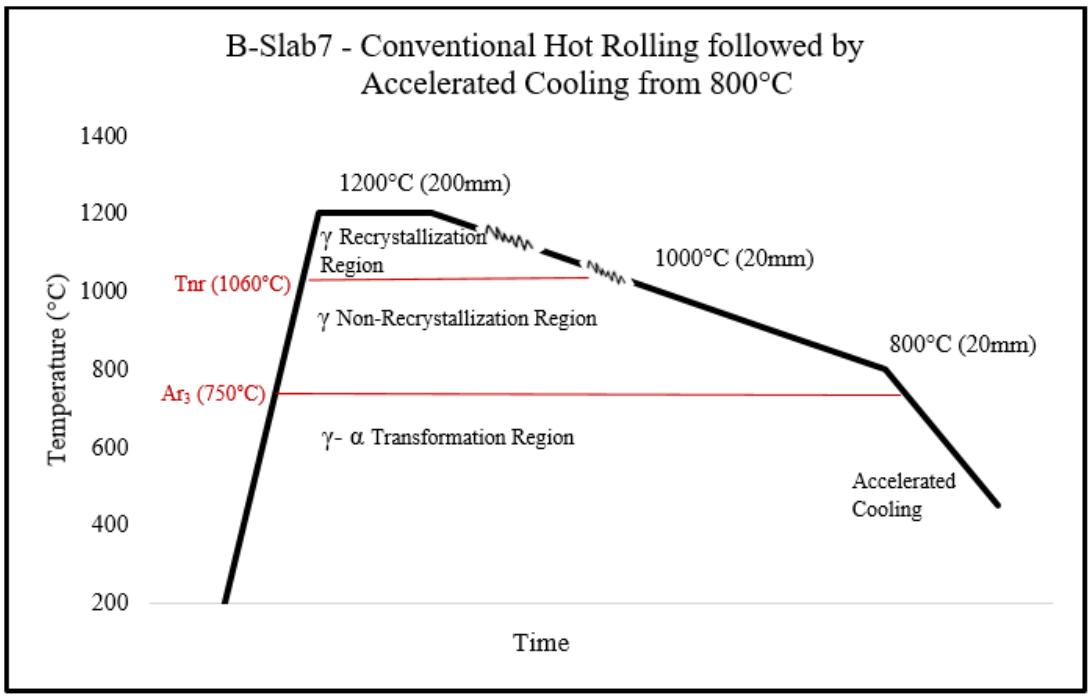

Figure 20 Rolling and cooling conditions of B-Slab7

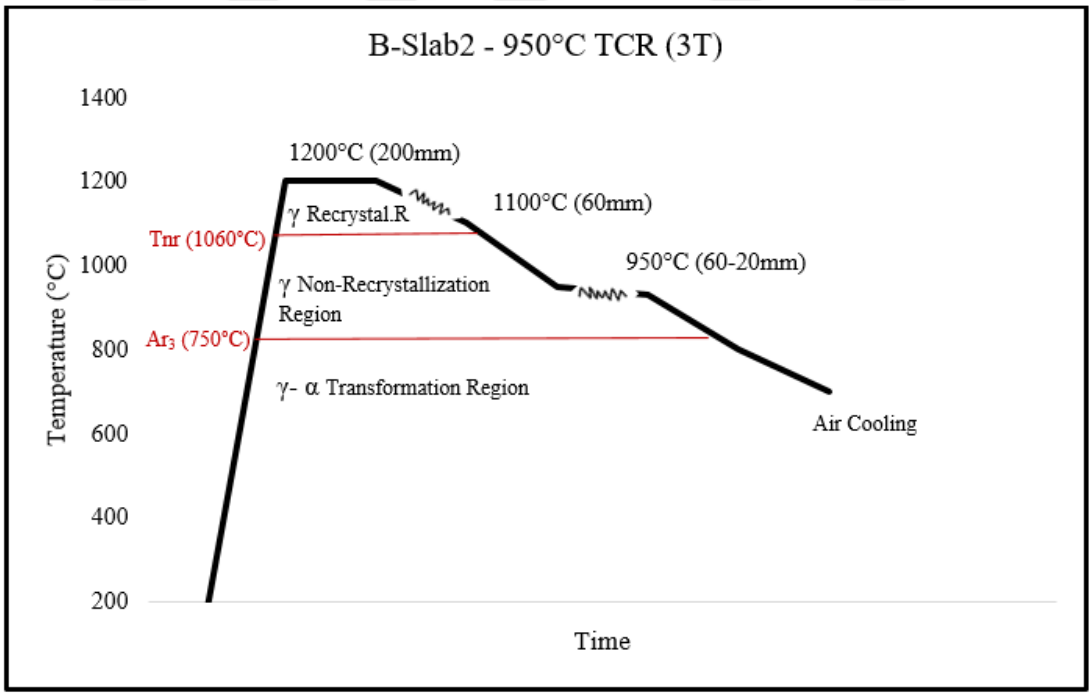

Figure 21 Rolling and cooling conditions of B-Slab2

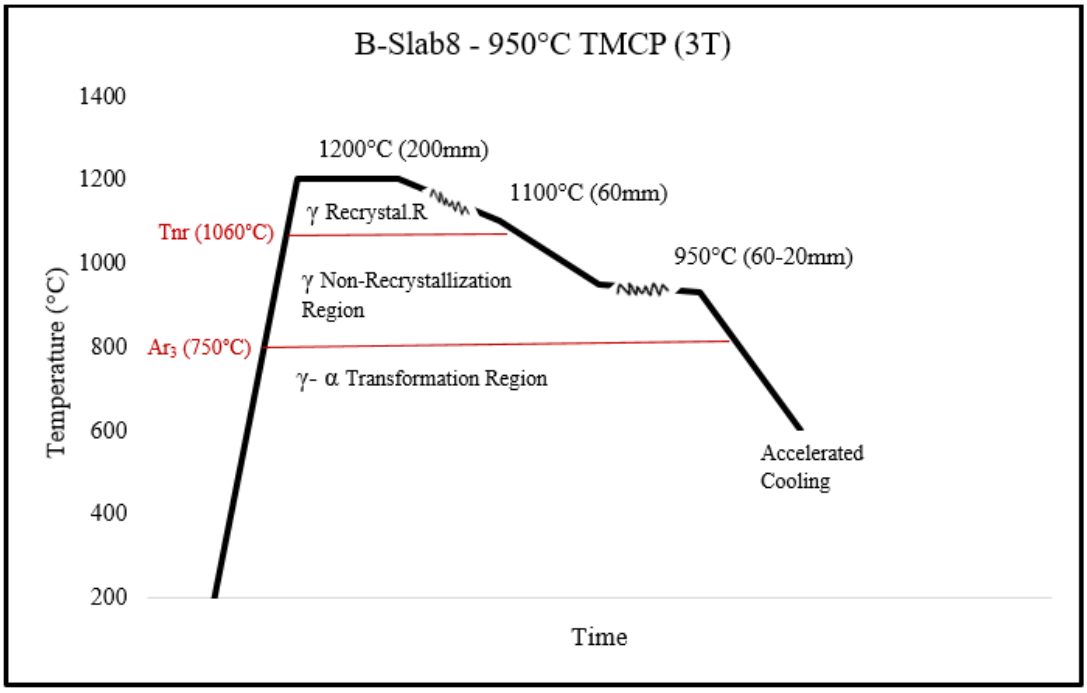

Figure 22 Rolling and cooling conditions of B-Slab8

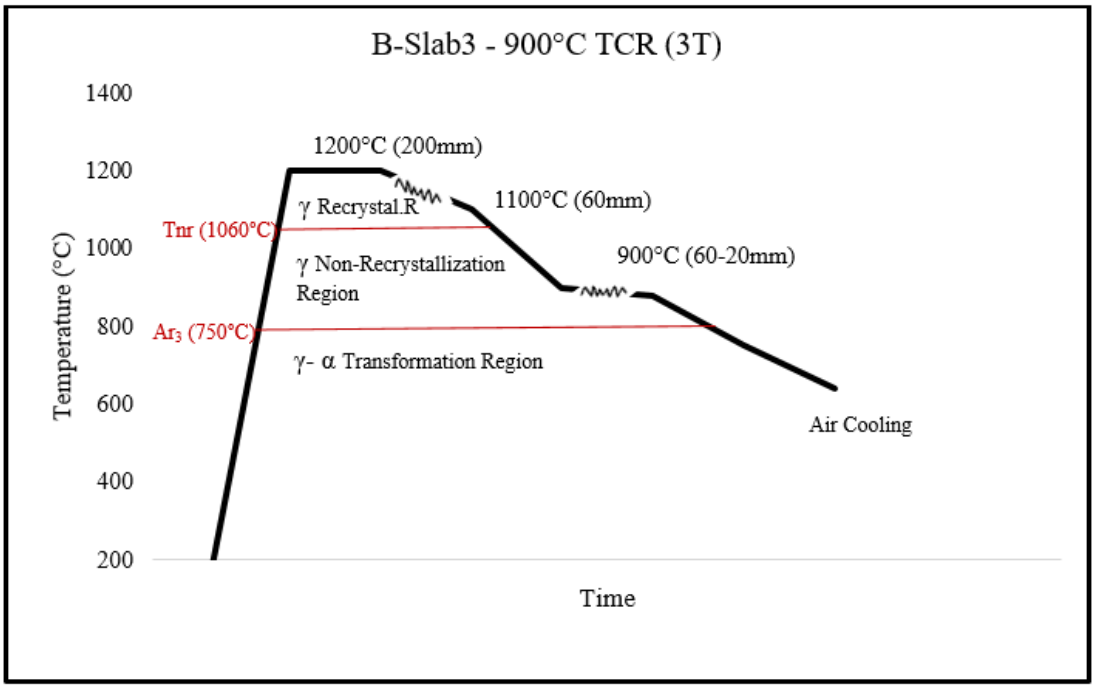

Figure 23 Rolling and cooling conditions of B-Slab3

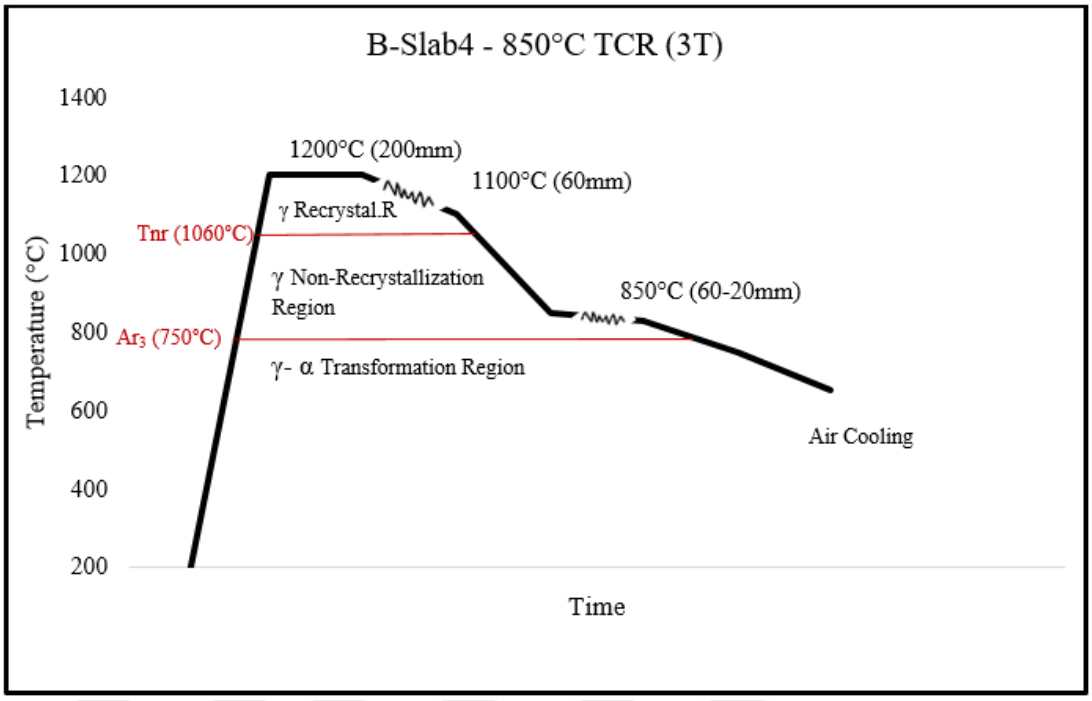

Figure 24 Rolling and cooling conditions of B-Slab4

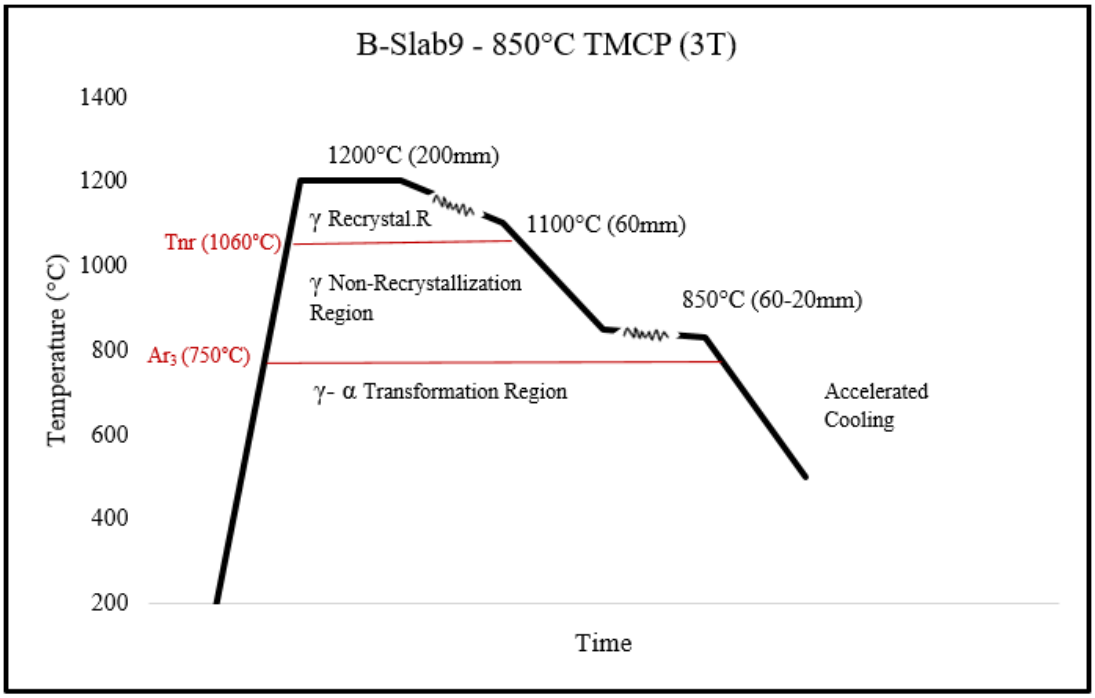

Figure 25 Rolling and cooling conditions of B-Slab9

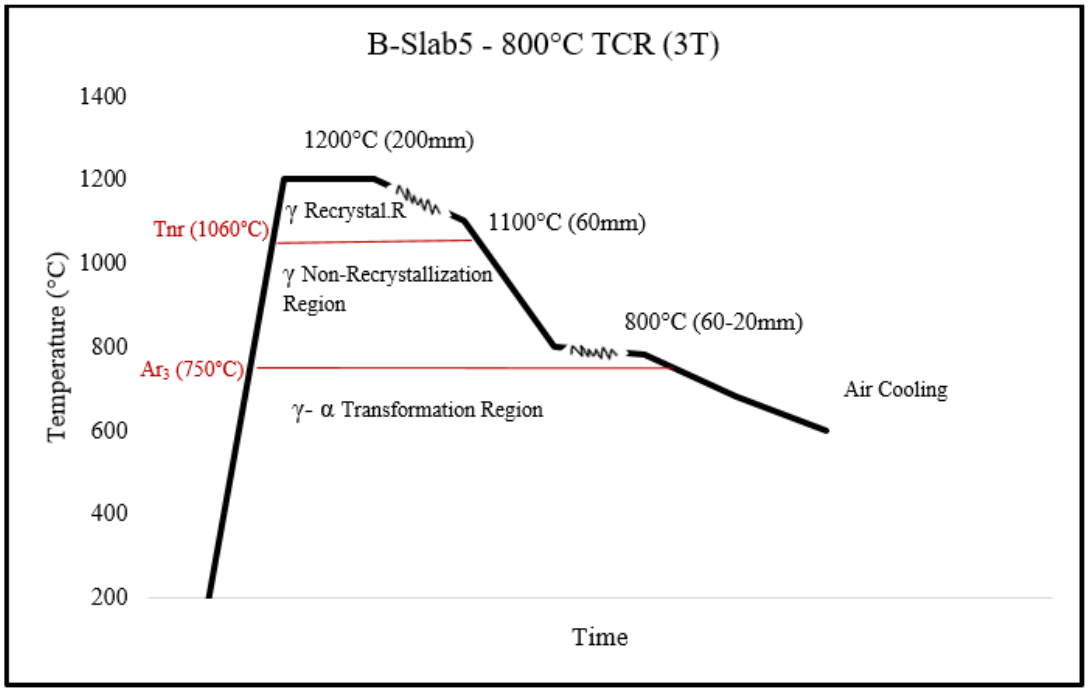

Figure 26 Rolling and cooling conditions of B-Slab5

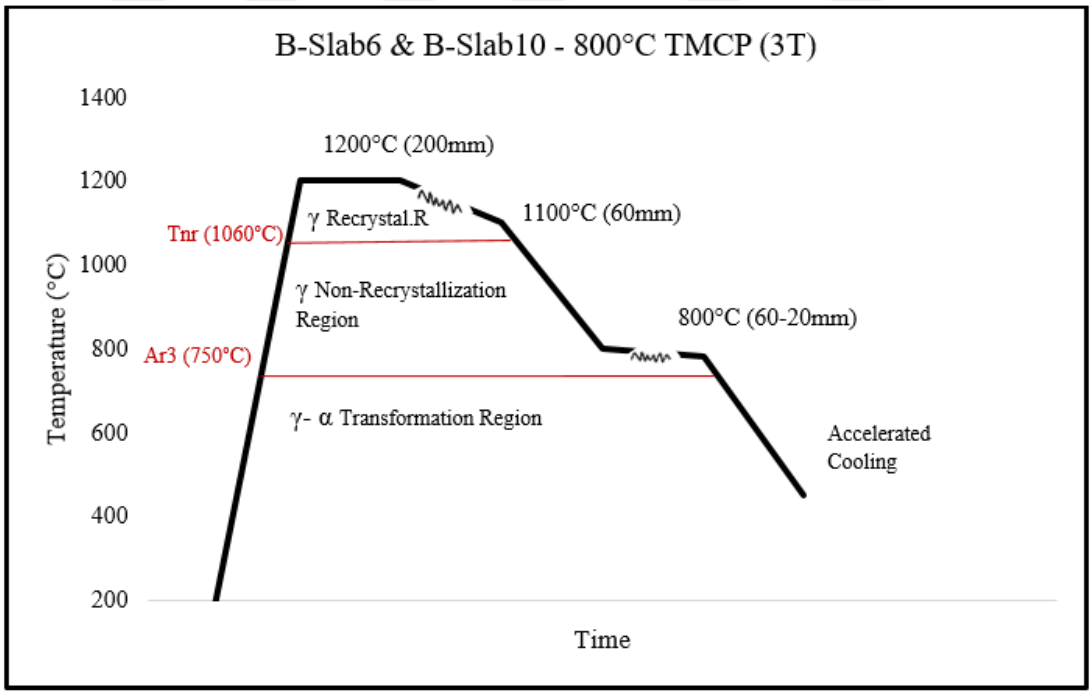

Figure 27 Rolling and cooling conditions of B-Slab6 & B-Slab10

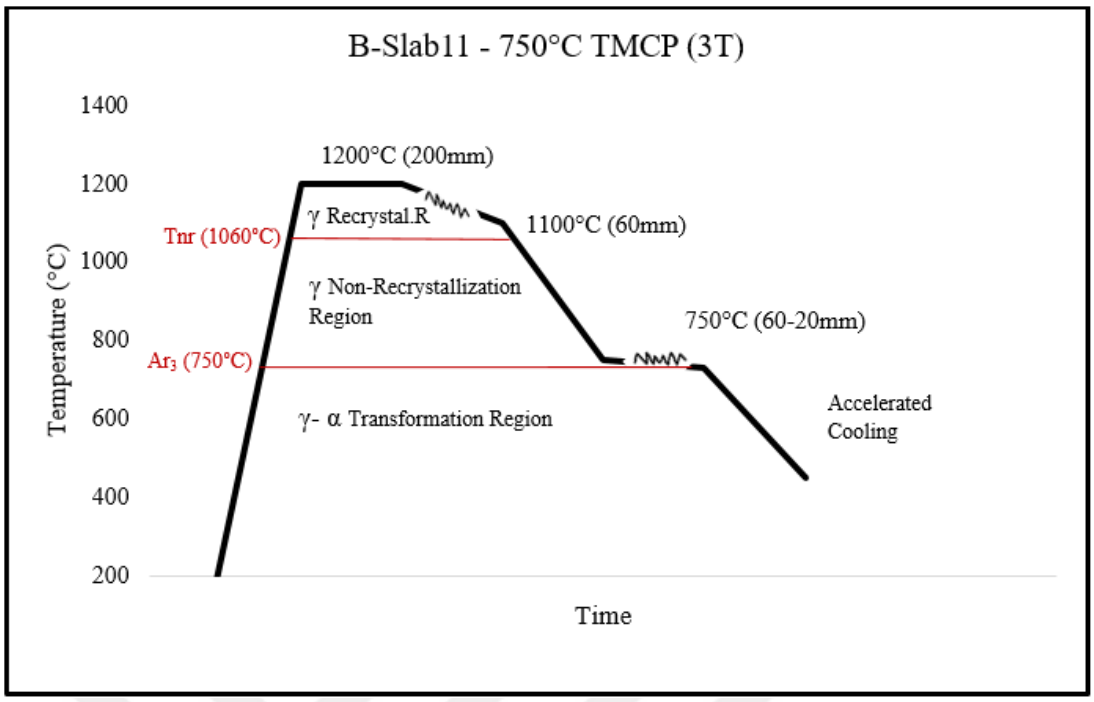

Figure 28 Rolling and cooling conditions of B-Slab11

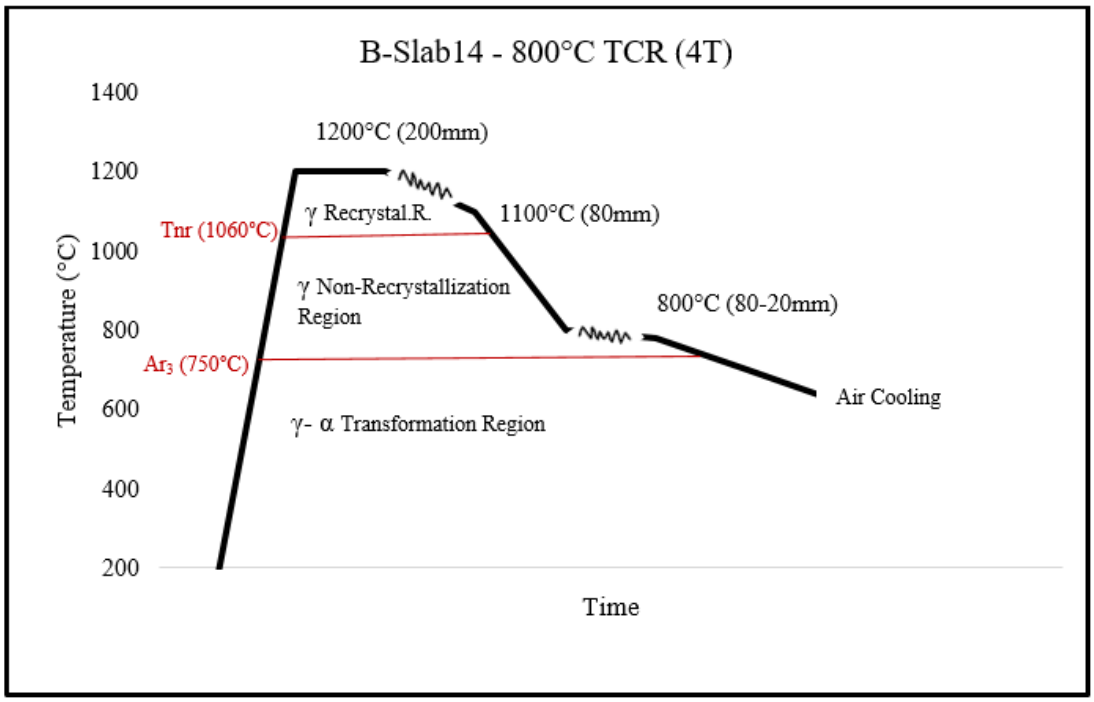

Figure 29 Rolling and cooling conditions of B-Slab14

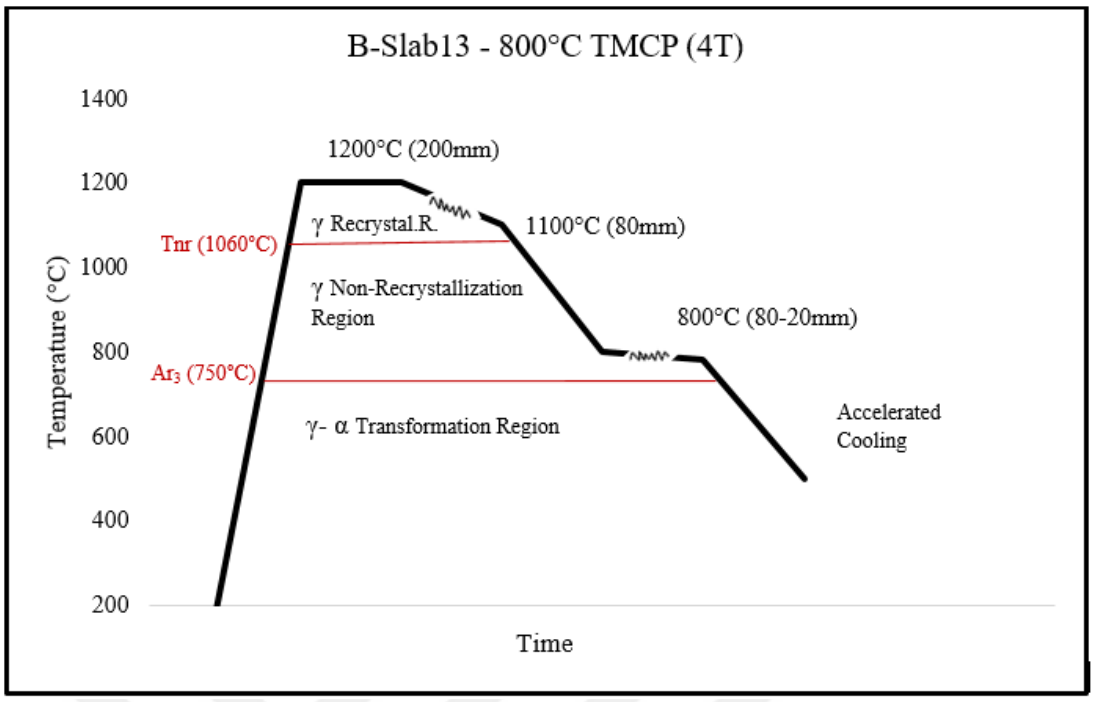

Figure 30 Rolling and cooling conditions of B-Slab13

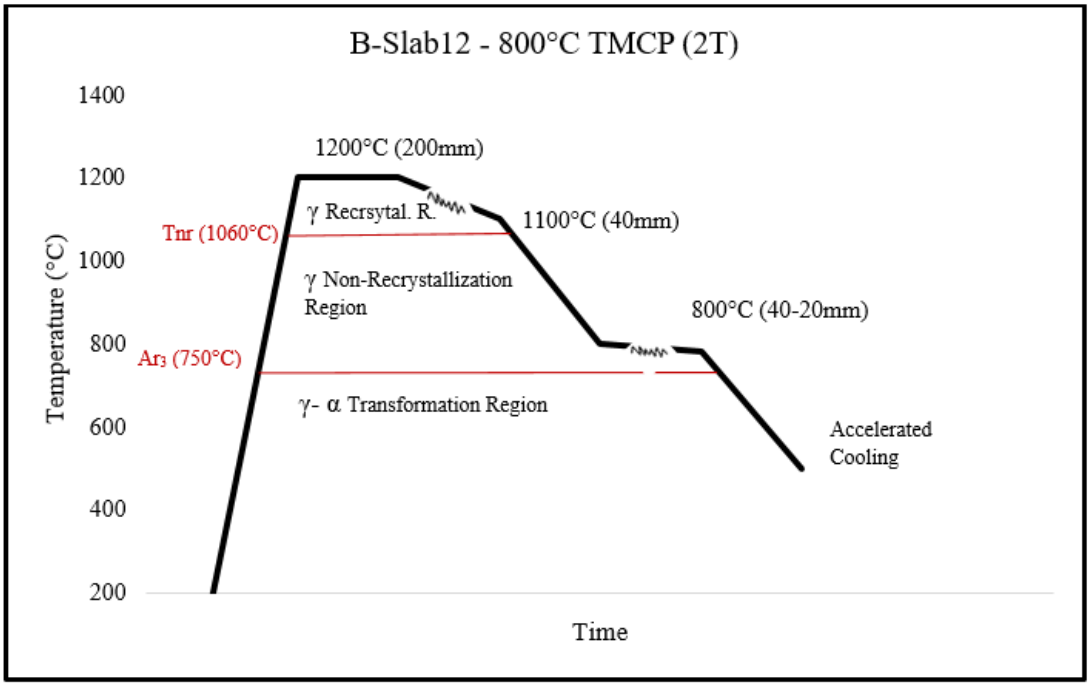

Figure 31 Rolling and cooling conditions of B-Slab12

Experimental rolling and cooling conditions are summarized in Table 7 and shown in Figure 32, Figure 33, Figure 34.

The numbering of baby slabs represents the order they were rolled.

Table 7 Rolling and cooling conditions of the baby slabs

Slab No:	**TCR Thickness**	**TCR Temperature**	**Accelerated Cooling**
B-Slab1	Conventional plate production		No
B-Slab7	Conventional plate production		Yes, starting from 800°C
B-Slab2	3T (60mm)	950°C	No
B-Slab8	3T (60mm)	950°C	Yes
B-Slab3	3T (60mm)	900°C	No
B-Slab4	3T (60mm)	850°C	No
B-Slab9	3T (60mm)	850°C	Yes
B-Slab5	3T (60mm)	800°C	No
B-Slab6	3T (60mm)	800°C	Yes
B-Slab10	3T (60mm)	800°C	Yes
B-Slab11	3T (60mm)	750°C	Yes
B-Slab14	4T (80mm)	800°C	No
B-Slab13	4T (80mm)	800°C	Yes
B-Slab12	2T (40mm)	800°C	Yes

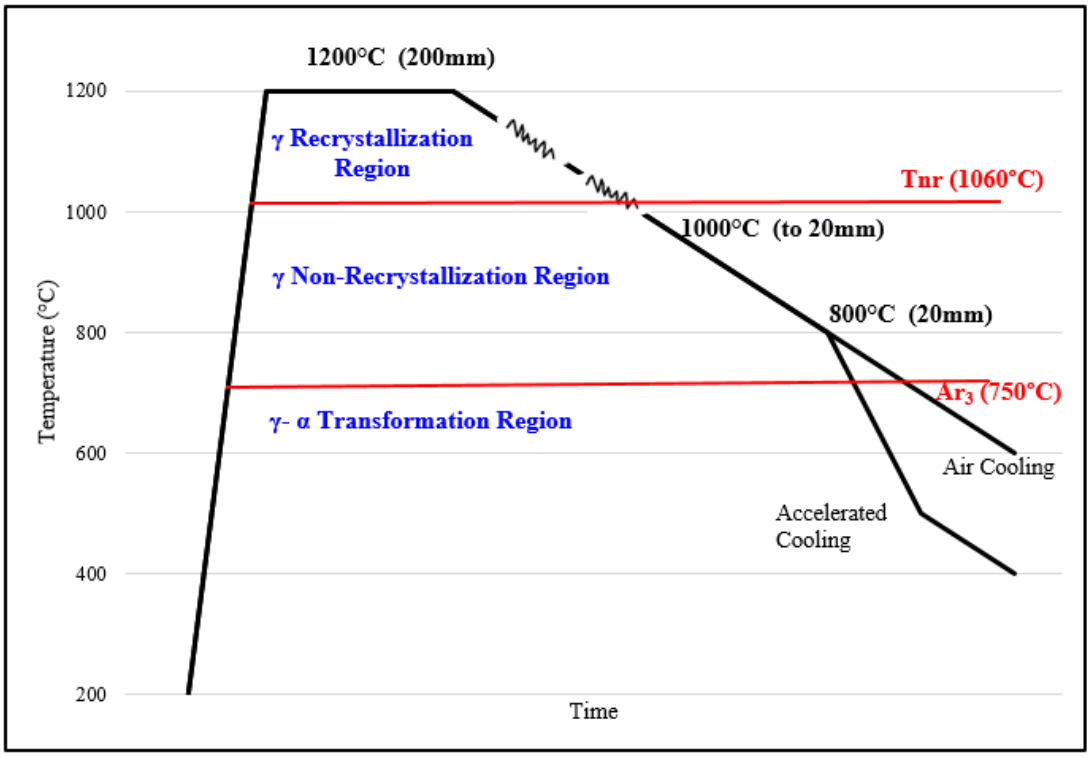

Figure 32 Rolling and cooling conditions of conventional plate production

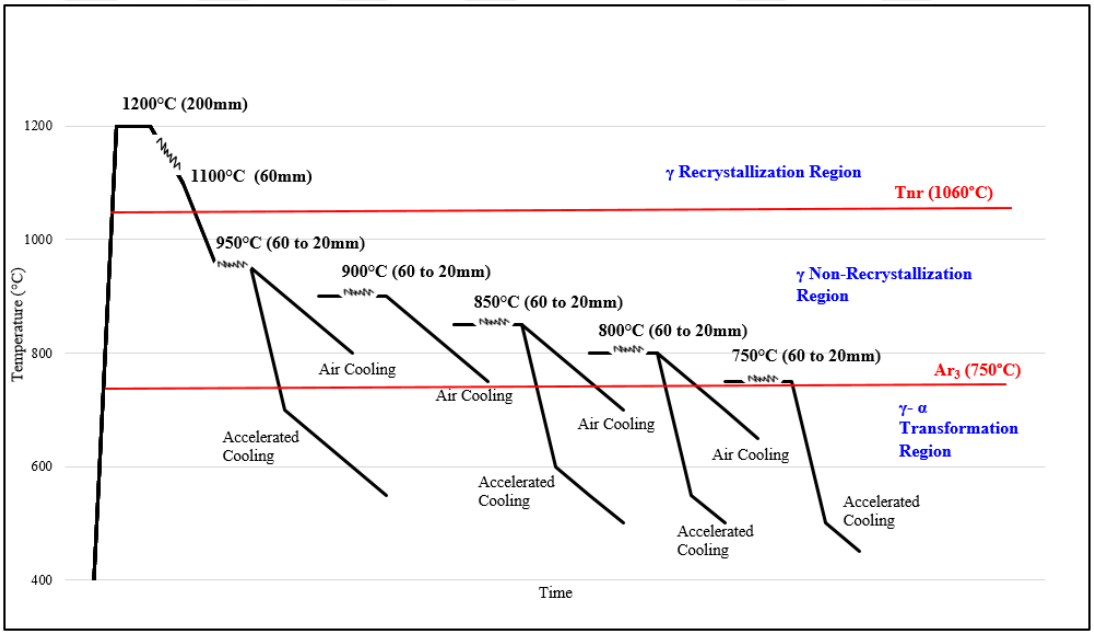

Figure 33 Rolling and cooling conditions of plate production with TCR at 3T

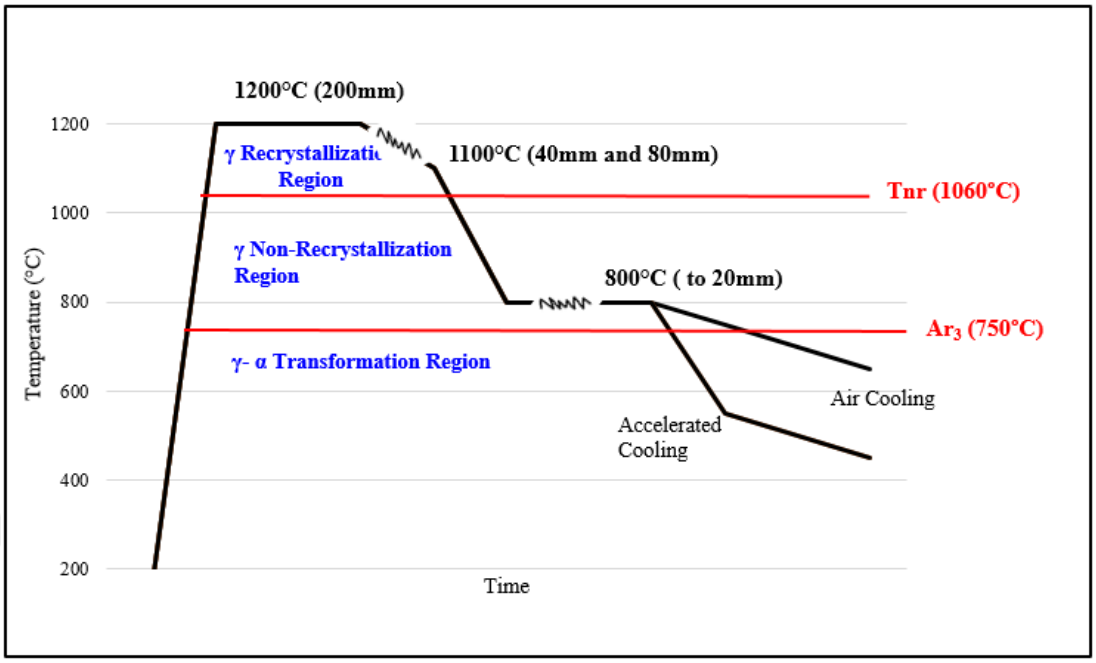

Figure 34 Rolling and cooling conditions of plate production with TCR at 2T&4T

3.2. Characterization of the Trial Production Plates

Mechanical tests and DWTT (Drop Weight Tear Test) were carried out in order to evaluate the strength, toughness and ductility of the steel plates. Mechanical tests were performed on samples taken in the transverse direction from the rolled plates as specified in the API Specification 5L.

Three samples were taken from each trial production plate as head-middle-end and tensile and impact tests were performed according to the ASTM A370 Standard Test Methods and Definitions for Mechanical Testing of Steel Products and small samples cut from tensile test specimens were used for the microstructural examination. Grain size evaluations were interpreted according to ASTM E112 Standard Test Methods for Determining Average Grain Size standard. In addition, DWTTs were carried out according to API 5L3 Drop-Weight Tear Tests on Line Pipe.

3.2.1. Mechanical Tests

Test specimens were prepared from plates as head-middle-end parts. After sizing and then milling operations, the samples are machined to test specimens as in Figure 35.

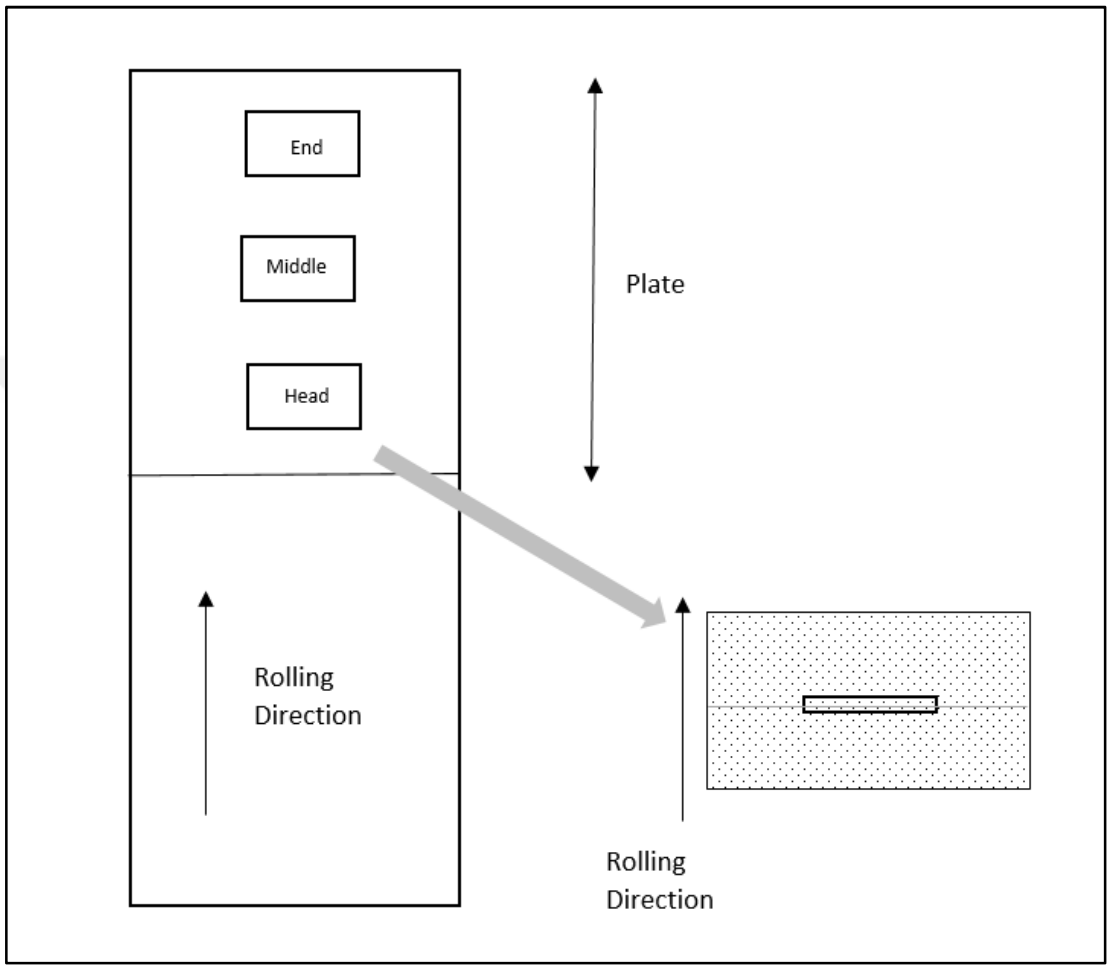

Figure 35 Sample preparation

In order to determine the strength of steel, mostly tensile test is performed and to determine toughness, impact test is carried out. The bending test can be performed for evaluating ductility, but it cannot be considered as a quantitative means of predicting performance. The specimens are prepared perpendicular to the rolling direction according to the API Specification 5L (Figure 36) [37].

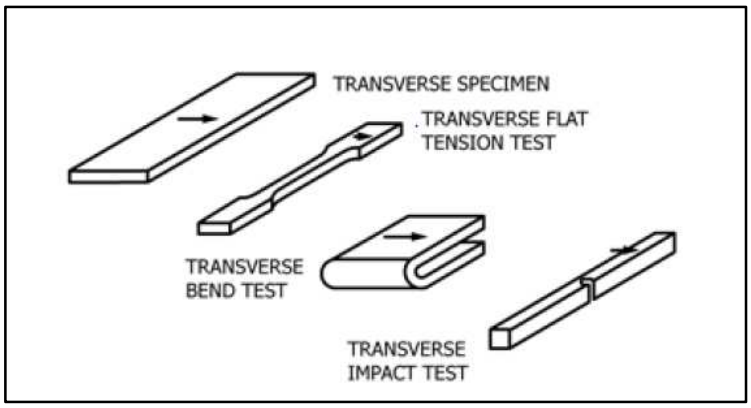

Figure 36 Relation of test specimens and rolling direction [37]

Test coupon dimensions for tensile test are 38 mm, 50 mm and 250 mm as width, gauge length and total length. The thickness of the test coupon is the material thickness as 20 mm and the radius of fillet is 13 mm. as shown in Figure 37. Test specimens were prepared from plates as head-middle-end parts, thus the stress-strain diagrams show the three properties which are similar to each other for each plate. Tensile tests were done using Zwick/Roell Z1200 Tensile Test Machine (Figure 38).

For impact tests, 10 mm*10 mm*55 mm are the dimensions of test coupons and notch depth is 2 mm (Figure 37). The impact test was repeated three times for each specified condition on V-notch test samples. Although the minimum specified test temperature is given as 0°C for impact test at the API Specification 5L, some tests were performed at minus 20°C. Impact tests were done using Zwick/Roell Charpy Impact Test Machine (Figure 39).

The ductility property of steel is interpreted according to Drop Weight Tear Test (DWTT). The DWTT is a kind of material characterization test which is aimed for avoiding brittle fracture. The dimensions of test specimen for DWTT are approximately 20 mm*75 mm*300 mm as thickness, width and length respectively in a rectangular form. The detail dimensions are given in Figure 37. The samples were kept in a liquid at a specified temperature at least 20 minutes, then a heavy weight is dropped from a distance onto the specimen.

Although the minimum specified test temperatures are given 0°C for DWTT at the API Specification 5L, in this trial the test temperatures were selected 0°C and minus 20°C. Finally, the fracture area is analyzed for finding the ratio of ductile area. DWTTs were done using Pradya DWTT machine (Figure 40) [38, 39].

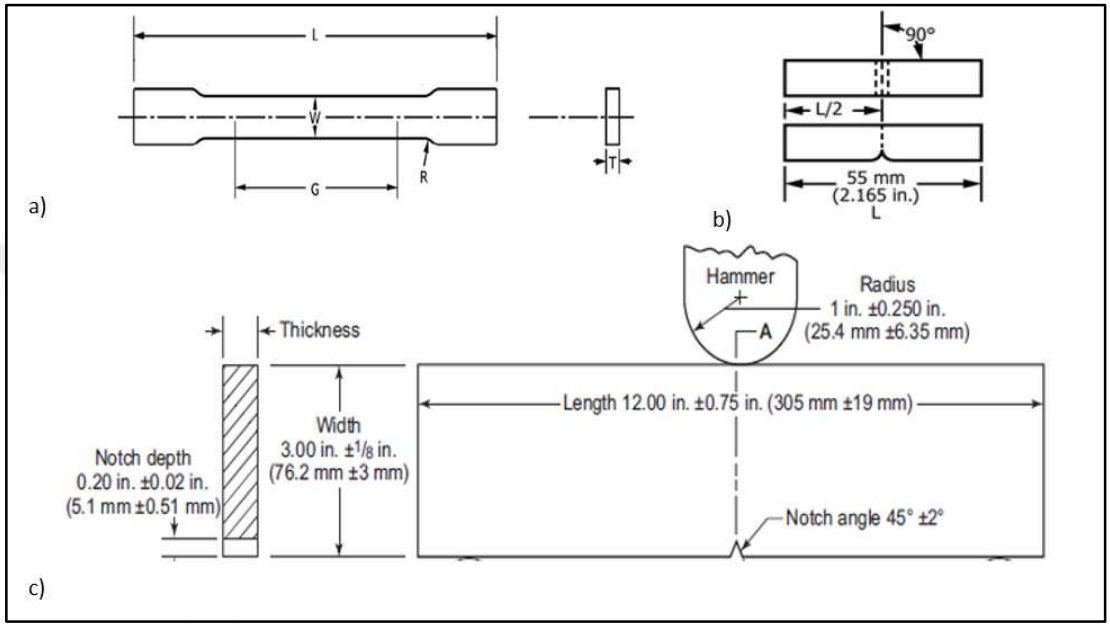

Figure 37 Figure of a) Tensile test sample, b) Impact test sample and c) DWTT sample

Figure 38 Zwick tensile test machine

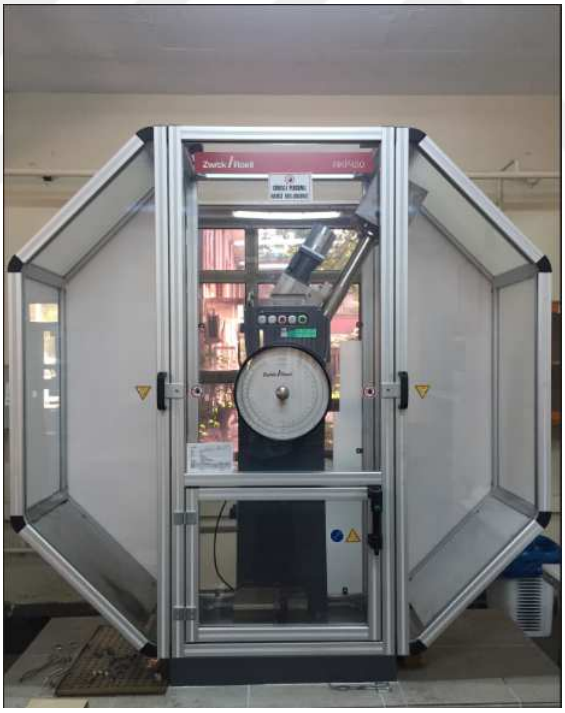

Figure 39 Zwick impact test machine

Figure 40 Pradya DWTT machine

3.2.2. Microstructural Examinations

Since API line-pipe steels are most widely used in worldwide as high strength low alloyed steels, they may have different and complex microstructures depending on their chemical compositions and production routes. It is well-known that the microstructure developed during the manufacturing process plays a crucial role in the mechanical properties.

The requirement of high strength with good fracture toughness and good weldability implies thermomechanical processing and the ultimate aim is to obtain a microstructure with the presence of appropriate phases and refined grain size. In microstructure, ferrite-pearlite combination and bainite phase is obtained in API grades. As the mechanical properties get better with adjustments in thermomechanical processing, reduction of pearlite content return in acicular ferrite and bainite phases.

Grain refinement is the other mechanism to increase strength and toughness at the same time. The reason for thermomechanical controlled process is to maximize grain refinement. The deformed austenite provides more nuclei while the austenite to ferrite transformation and ferrite nucleates predominantly.

Microstructural analysis and grain size determination were applied on each specimen that are prepared from head-middle-end samples (Figure 41).

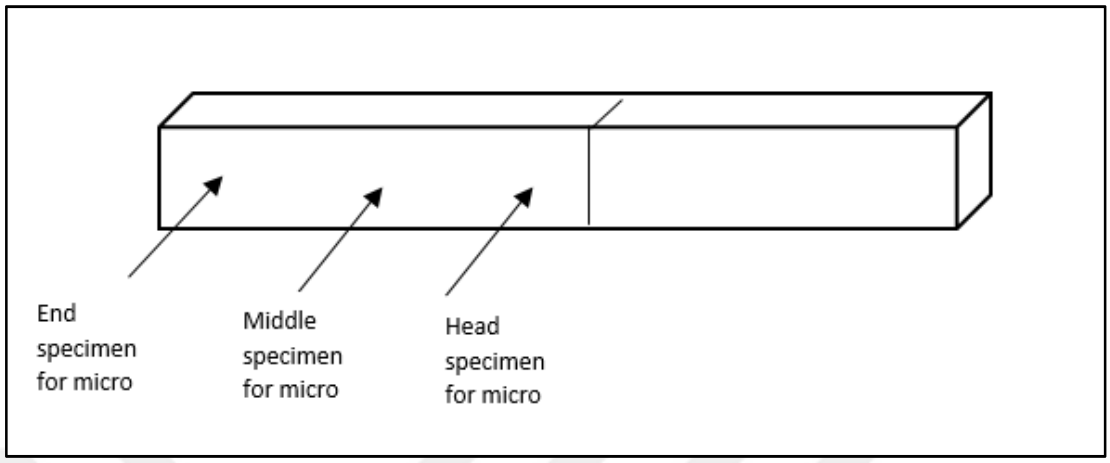

Figure 41 Sample preparation for microstructural examination

Sectioning, mounting, grinding, polishing and etching are performed for specimen preparation. Samples that are prepared for microstructural examinations are shown in Figure 42.

Figure 42 Microstructural examination samples

3.2.2.1. Sample Preparation and Tools for Microstructural Analysis

For sectioning, the materials are prepared by Struers Discotom-65 rough cutting device (Figure 43). Struers CitoPress-20 hot molding device was used for mounting (Figure 44). It does not influence the specimen as a result of chemical reaction or mechanical stress and mounting material ‘polyfast’ is electrically conducting.

Figure 43 Struers Discotom-65 rough cutting device

Figure 44 Struers CitoPress-20 hot molding device

Damaged surface layers can be removed by grinding. Mounted specimens were ground with rotating discs of abrasive paper. The coarseness of the paper is 120, 240, 500, 800, and 1200. Between each grade, the specimen is washed with water to prevent contamination from coarser grit present on the specimen surface. Struers TegraPol-21 grinding and polishing device is used for grinding process (Figure 45). Polishing discs are covered with soft cloth impregnated with abrasive diamond particles and oily lubricant. Scratches produced from the finest grinding stage are removed by polishing with diamond particles 6 microns in diameter to 1 micron in diameter in order to produce a smooth surface.

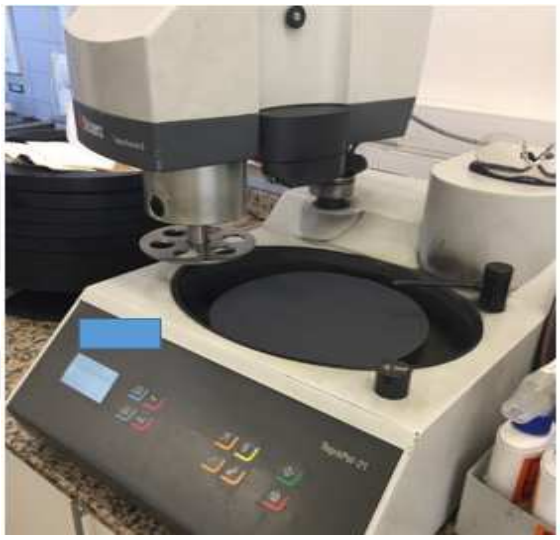

Figure 45 Struers TegraPol-21 grinding and polishing device

Etching is used to reveal the microstructure of the samples and Nital is used for etching of specimen which is a solution of 96 ml ethanol and 4 ml nitric acid.

Polished samples were examined by Nikon Epiphot 200 optical microscope. Inclusion rating and grain size measurements were done by Clemex Vision Program (Figure 46) [40]. JEOL JSM 5600 scanning electron microscope (SEM) was used for the electron microscopy studies (Figure 47).

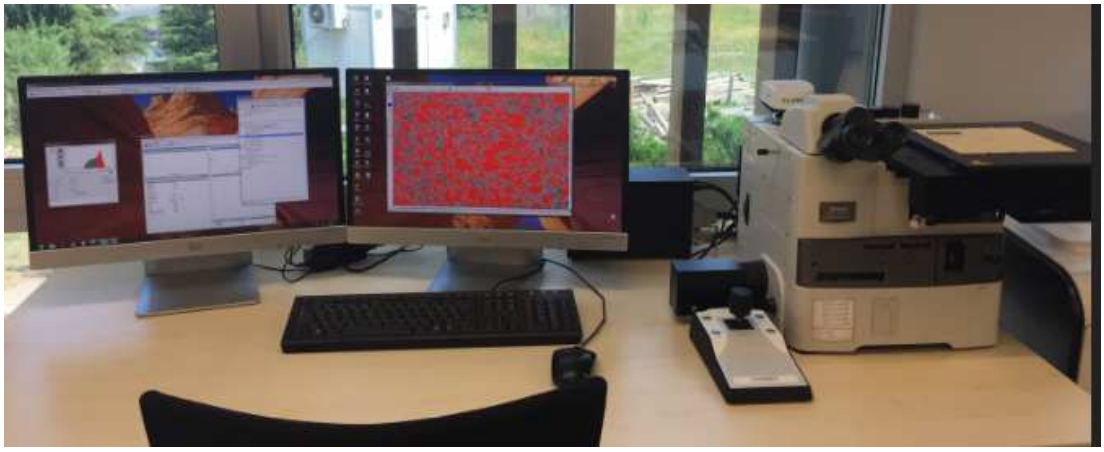

Figure 46 Clemex Vision Program

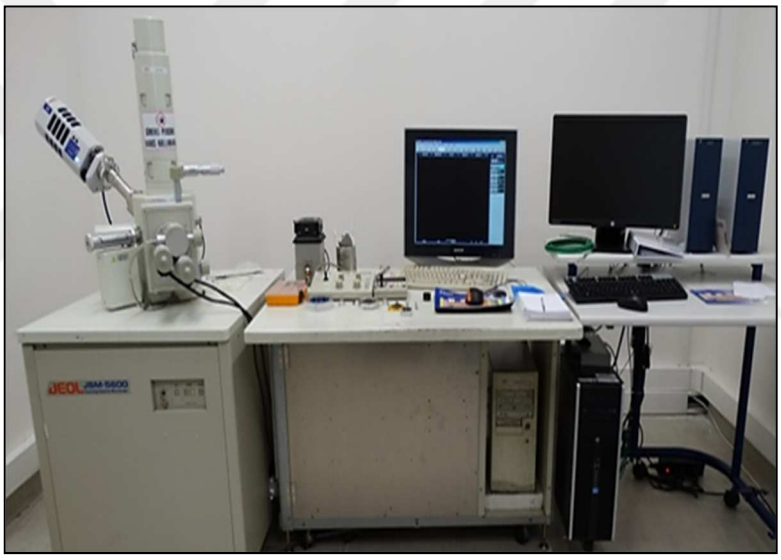

Figure 47 JEOL JSM 5600 SEM

CHAPTER 4

RESULTS AND DISCUSSION

4.1. Rolling Data of B-Slabs

Conventional plate rolling practice was applied to the slabs B-Slab1 and B-Slab7. The number of passes needed to decrease slab thickness to final plate thickness was 9 in these cases. Approximate temperatures, reduction ratio values, durations and applied force are given in Table 8. After rolling, B-Slab1 was cooled in air, but B-Slab7 was waited till the temperature decreased to 800°C, then cooled with water shower.

Table 8 Rolling data of B-Slab1 and B-Slab7

Rough Rolling								
		R. Roll #1	R. Roll #2	R. Roll #3	R. Roll #4	R. Roll #5	R. Roll #6	
Enter Temp. (°C)	Initial thickness (mm)	Thickness after each pass (mm)						Exit Temp. (°C)
1140	205	180	155	129	104	78	55	1100
	% RA	12	14	17	19	25	29	
	Time	Duration Time (sec)						Time
	0	50	70	90	100	110	120	120
		Force Mean (N)						
		9000	10000	11000	12000	13000	14000	

Finish Rolling				
	F. Roll #1	F.Roll #2	F. Roll #3	
Entering Temp. (°C)	Thickness after each pass (mm)			Exit Temp. (°C)
1090	38	27	20	1040
	31	29	26	
Time	Duration Time (sec)			Time
120	130	140	160	160
	Force Mean (N)			
	14000	13000	10000	

B-Slab2 and B-Slab8 were rolled with TCR and TMCP respectively. The controlled temperature was selected as 950°C for the last three passes. The beginning of temperature controlled thickness was 60 mm as three times of final thickness (3T). The number of passes needed to decrease slab thickness to final plate thickness was 10. Approximate temperatures, reduction ratio values, duration time and applied forces are given in Table 9. After rolled, B-Slab2 was cooled in air and B-Slab8 was cooled with water shower.

Table 9 Rolling data of B-Slab2 and B-Slab8

Rough Rolling										
		R. Roll #1	R. Roll #2	R. Roll #3	R. Roll #4	R. Roll #5	R. Roll #6	R. Roll #7	R. Roll #8	
Enter Temp. (°C)	Initial thickness (mm)	Thickness after each pass (mm)								Exit Temp. (°C)
1140	205	180	157	134	113	94	77	60	60	1090
	% RA	12	13	15	16	17	18	22	0	
	Time	Duration Time (sec)								Time
	0	50	70	80	90	100	110	130	140	140
		Force Mean (N)								
		9000	10000	10000	10000	11000	11000	12000	0	

Finish Rolling				
	F. Roll #1	F.Roll #2	F. Roll #3	
Enter Temp. (°C)	Thickness after each pass (mm)			Exit Temp. (°C)
950	37	27	20	930
	30	27	26	
Time	Duration Time (sec)			Time
270	280	290	310	310
	Force Mean (N)			
	25000	17000	14000	

B-Slab3 were rolled with TCR. The controlled temperature was selected as 900°C for the last three passes. The beginning of temperature controlled thickness was 60 mm as three times of final thickness (3T). The number of passes needed to decrease slab thickness to final plate thickness was 10. Approximate temperatures, reduction ratio values, durations and applied forces are given in Table 10. After being rolled, B-Slab3 was cooled in air.

Table 10 Rolling data of B-Slab3

Rough Rolling										
		R. Roll #1	R. Roll #2	R. Roll #3	R. Roll #4	R. Roll #5	R. Roll #6	R. Roll #7	R. Roll #8	
Enter Temp. (°C)	Initial thickness (mm)	Thickness after each pass (mm)								Exit Temp. (°C)
1140	205	180	156	134	113	94	76	60	60	1090
	% RA	12	13	14	16	17	19	21	0	
	Time	Duration Time (sec)								Time
	0	50	80	90	100	120	130	140	150	150
		Force Mean (N)								
		9000	9000	10000	10000	10000	11000	11000	0	

Finish Rolling				
	F. Roll #1	F.Roll #2	F. Roll #3	
Enter Temp. (°C)	Thickness after each pass (mm)			Exit Temp. (°C)
910	37	27	20	900
	30	27	26	
Time	Duration Time (sec)			Time
400	410	420	430	430
	Force Mean (N)			
	28000	20000	16000	

B-Slab4 and B-Slab9 were rolled with TCR and TMCP respectively. The controlled temperature was selected as 850°C for the last three passes. The increase in exit temperature after rolling was due to the heat evolved during deformation that cannot be removed fast enough. The beginning of temperature controlled thickness was 60 mm as three times of final thickness (3T). The number of passes needed to decrease slab thickness to final plate thickness was 10. Approximate temperatures, reduction ratio values, durations and applied forces are given in Table 11. After rolled, B-Slab4 was cooled in air and B-Slab9 was cooled with water shower.

Table 11 Rolling data of B-Slab4 and B-Slab9

Rough Rolling										
		R. Roll #1	R. Roll #2	R. Roll #3	R. Roll #4	R. Roll #5	R. Roll #6	R. Roll #7	R. Roll #8	
Enter Temp. (°C)	Initial thickness (mm)	Thickness after each pass (mm)								Exit Temp. (°C)
1140	205	180	157	134	113	94	76	60	60	1080
	% RA	12	13	15	16	17	19	21	0	
	Time	Duration Time (sec)								Time
	0	50	70	80	100	110	130	140	150	150
		Force Mean (N)								
		9000	9000	9000	10000	10000	10000	11000	0	

Finish Rolling				
	F. Roll #1	F.Roll #2	F. Roll #3	
Entering Temp. (°C)	Thickness after each pass (mm)			Exit Temp. (°C)
860	38	27	20	870
	29	29	26	
Time	Duration Time (sec)			Time
500	510	520	540	540
	Force Mean (N)			
	30000	24000	20000	

B-Slab5 was rolled with TCR. B-Slab6 and B-Slab10 were rolled with TMCP. In fact, B-Slab10 was the verification of the production of B-Slab6. The controlled temperature was selected as 800°C for the last three passes. The increase in exit temperature after rolling was depend on the heat exit during phase transformation at that time and the heat that cannot be removed fast enough. The beginning of temperature controlled thickness was 60 mm as three times of final thickness (3T). The number of passes needed to decrease slab thickness to final plate thickness was 10. Approximate temperatures, reduction ratio values, durations and applied forces are given in Table 12. After being rolled, B-Slab5 was cooled in air and B-Slab6 and B-Slab10 were cooled with water shower.

Table 12 Rolling data of B-Slab5, B-Slab6 and B-Slab10

Rough Rolling										
		R. Roll #1	R. Roll #2	R. Roll #3	R. Roll #4	R. Roll #5	R. Roll #6	R. Roll #7	R. Roll #8	
Entering Temp. (°C)	Initial thickness (mm)	Thickness after each pass (mm)								Exit Temp. (°C)
1140	205	180	156	134	113	94	76	60	60	1090
	% RA	12	13	14	16	17	19	21	0	
	Time	Duration Time (sec)								Time
	0	50	70	80	90	100	110	130	140	140
		Force Mean (N)								
		9000	9000	9000	9000	10000	10000	11000	0	

Finish Rolling				
	F. Roll #1	F.Roll #2	F. Roll #3	
Entering Temp. (°C)	Thickness after each pass (mm)			Exit Temp. (°C)
810	41	28	20	830
	25	32	29	
Time	Duration Time (sec)			Time
620	630	640	660	660
	Force Mean (N)			
	30000	27000	23000	

B-Slab11 was rolled with TCR. The controlled temperature was selected as 750°C for the last three passes. Since the loads increased too much, B-slab was started to be rolled at 770°C. The increase in exit temperature after rolling was due to the deformation heating that cannot be removed fast enough. The beginning of temperature controlled thickness was 60 mm as three times of final thickness (3T). The number of passes needed to decrease slab thickness to final plate thickness was 10. Approximate temperatures, reduction ratio values, durations and applied forces are given in Table 13. After being rolled, B-Slab11 was cooled with water shower.

Table 13 Rolling data of B-Slab11

Rough Rolling										
		R. Roll #1	R. Roll #2	R. Roll #3	R. Roll #4	R. Roll #5	R. Roll #6	R. Roll #7	R. Roll #8	
Enter Temp. (°C)	Initial thickness (mm)	Thickness after each pass (mm)								Exit Temp. (°C)
1140	205	180	156	134	113	94	76	60	60	1090
	% RA	12	13	14	16	17	19	21	0	
	Time	Duration Time (sec)								Time
	0	50	70	80	90	100	110	120	130	130
		Force Mean (N)								
		9000	9000	9000	9000	10000	10000	11000	0	

Finish Rolling				
	F. Roll #1	F.Roll #2	F. Roll #3	
Enter Temp. (°C)	Thickness after each pass (mm)			Exit Temp. (°C)
770	42	29	20	790
	24	31	31	
Time	Duration Time (sec)			Time
680	690	720	750	750
	Force Mean (N)			
	31000	32000	33000	

B-Slab14 and B-Slab13 were rolled with TCR and TMCP respectively. The controlled temperature was selected as 800°C for the last three passes. At this time, the beginning of temperature controlled thickness was 80 mm as four times of final thickness (4T).

The purpose of TCR at 4T was to provide more reduction ratio and later finer grain size, yet the works did not go as planned. The number of passes in rough rolling decreased from 7 to 5 but the last three passes increased from 3 to 5. Although the total number of passes needed to decrease slab thickness to final plate thickness did not change, the change in number of controlled temperature passes resulted in deterioration of TCR. Approximate temperatures, reduction ratio values, durations and applied forces are given in Table 14. After rolling, B-Slab14 was cooled in air and B-Slab13 were cooled with water shower .

Table 14 Rolling data of B-Slab14 and B-Slab13

Rough Rolling								
		R. Roll #1	R. Roll #2	R. Roll #3	R. Roll #4	R. Roll #5	R. Roll #6	
Enter Temp. (°C)	Initial thickness (mm)	Thickness after each pass (mm)						Exit Temp. (°C)
1140	205	180	154	129	104	80	80	1110
	% RA	12	14	16	19	23	0	
	Time	Duration Time (sec)						Time
	0	50	70	90	100	110	120	120
		Force Mean (N)						
		9000	9000	10000	11000	11000	0	

Finish Rolling						
	F. Roll #1	F.Roll #2	F. Roll #3	F. Roll #4	F. Roll #5	
Entering Temp. (°C)	Thickness after each pass (mm)					Exit Temp. (°C)
810	57	42	32	25	20	810
	29	26	24	22	20	
Time	Duration Time (sec)					Time
770	780	800	830	850	880	880
	Force Mean (N)					
	30000	27000	24000	22000	20000	

B-Slab12 was rolled with TMCP. The controlled temperature was selected as 800°C for the last three passes. At this time, the beginning of temperature controlled thickness was 40 mm as two times of final thickness (2T). The purpose of TCR at 2T was to work out reduction ratio effects on grain size. The number of passes needed to decrease slab thickness to final plate thickness was 10. Approximate temperatures, reduction ratio values, duration and applied forces are given in Table 15. After rolling, B-Slab12 was cooled with water shower.

Table 15 Rolling data of B-Slab12

Rough Rolling									
		R. Roll #1	R. Roll #2	R. Roll #3	R. Roll #4	R. Roll #5	R. Roll #6	R. Roll #7	R. Roll #8	
Enter Temp. (°C)	Initial thickness (mm)	Thickness after each pass (mm)								Exit Temp. (°C)
1133	205	180	155	129	103	78	56	40	40	1088
	% RA	12	14	17	20	24	28	29	0	
	Time	Duration Time (sec)								Time
	0	60	70	90	100	110	120	130	140	140
		Force Mean (N)								
		9000	9000	10000	11000	12000	14000	15000	0	

Finish Rolling				
	F. Roll #1	F.Roll #2	F. Roll #3	
Enter Temp. (°C)	Thickness after each pass (mm)			Exit Temp. (°C)
810	32	25	20	805
	14	22	20	
Time	Duration Time (sec)			Time
440	450	460	480	480
	Force Mean (N)			
	24000	21000	19000	

4.2. The Tensile and Impact Tests Results

As mentioned before, the tensile strength requirements for API X60 and X70 grades are 520-760 MPa and 570-760 MPa, respectively. For the yield strength, the requirements are 415-565 MPa and 485-635 MPa with respective minimum percent elongations of 24% and 22%. In addition, for both grades the maximum allowed Yield strength / Tensile strength ratio is 0.93. The tensile test results of all samples are given in Table 16.

Table 16 Tensile test results of trials

B-Slabs	Heat Treatment	TCR Thickness (mm)	Yield Strength (MPa)	Tensile Strength (MPa)	Yield / Tensile Ratio	% EL
B-Slab1	Conventionally Rolled	-	427	579	0.74	35
B-Slab7	Conventionally Rolled + Cooling from 800°C	-	547	651	0.84	32
B-Slab2	950°C TCR	3T	444	585	0.76	34
B-Slab8	950°C TMCP	3T	511	638	0.80	33
B-Slab3	900°C TCR	3T	387	548	0.71	35
B-Slab4	850°C TCR	3T	424	550	0.77	34
B-Slab9	850°C TMCP	3T	502	617	0.81	34
B-Slab5	800°C TCR	3T	512	614	0.83	33
B-Slab6	800°C TMCP	3T	456	562	0.81	34
B-Slab10	800°C TMCP	3T	528	633	0.83	33
B-Slab11	750°C TMCP	3T	534	623	0.86	33
B-Slab14	800°C TCR	4T	531	662	0,80	33
B-Slab13	800°C TMCP	4T	392	550	0.72	35
B-Slab12	800°C TMCP	2T	491	580	0.84	34

As mentioned before, the impact test requirements of API X60 and X70 grade is minimum 40 joules and 68 joules at 0°C, respectively. The impact test results are given in Table 17.

Table 17 Impact test results of trials

B-Slabs	Heat Treatment	TCR Thickness (mm)	Impact Test Temp.	Impact Test (J)
B-Slab1	Conventionally Rolled	-	-20°C	76
B-Slab7	Conventionally Rolled + Cooling from 800°C	-	0°C	188
B-Slab2	950°C TCR	3T	-20°C	19
B-Slab8	950°C TMCP	3T	0°C	214
B-Slab3	900°C TCR	3T	-20°C	221
B-Slab4	850°C TCR	3T	-20°C	250
B-Slab9	850°C TMCP	3T	0°C	234
B-Slab5	800°C TCR	3T	-20°C	213
B-Slab6	800°C TMCP	3T	-20°C	241
B-Slab10	800°C TMCP	3T	0°C	213
B-Slab11	750°C TMCP	3T	0°C	215
B-Slab14	800°C TCR	4T	0°C	111
B-Slab13	800°C TMCP	4T	0°C	224
B-Slab12	800°C TMCP	2T	0°C	226

4.3. The Drop Weight Tear Tests Results

According to the API Specification 5L, for both X60 and X70 grade, the average shear fracture area shall be ≥ 85 % at a test temperature of maximum 0°C or lower (if agreed). The shear fracture dull, gray and silky appearance is to be rated by the percent of shear fracture have cleavage fracture that is bright and crystalline in appearance. The shear areas in the region of intermittent shear and cleavage fracture is to be neglected in rating [4,38].

B-Slab1 which was conventionally rolled, has no ductile fracture on complete fracture surface that means 0% ductile fracture as seen in Figure 48.

Figure 48 DWTT Result for B-Slab1

B-Slab7 which was conventionally rolled, and cooled when its temperature decreases to 800°C has %90 ductile fracture on complete fracture surface at 0˚C as seen in Figure 49. The shear areas in the region of intermittent shear and cleavage fracture is neglected in rating. The DWTT result is successful according to API 5L specification.

Figure 49 DWTT Result for B-Slab7

B-Slab2 which was rolled with TCR (3T) at 950°C, has no ductile fracture on complete fracture surface at minus 20˚C. The DWTT result is not successful with 0% ductile fracture (Figure 50).

Figure 50 DWTT Result for B-Slab2

B-Slab8 which was rolled with TMCP (3T) at 950°C, has 90% ductile fracture on complete fracture surface at 0°C as seen in Figure 51. The shear areas in the region of intermittent shear and cleavage fracture is neglected in rating. The DWTT result is successful according to API Specification 5L.

Figure 51 DWTT Result for B-Slab8

B-Slab3 which was rolled with TCR (3T) at 900°C, has 80% ductile fracture on complete fracture surface at minus 20°C. The shear areas in the region of intermittent shear and cleavage fracture is neglected in rating. The DWTT result is not in the safe zone but test temperature is minus 20°C. The DWTT result is expected to be more successful at 0°C. For the present, it can be said that "not successful" according to API Specification 5L (Figure 52).

Figure 52 DWTT Result for B-Slab3

B-Slab4 which was rolled with TCR (3T) at 850°C, has 90% ductile fracture on complete fracture surface at minus 20°C. The shear areas in the region of intermittent shear and cleavage fracture is neglected in rating. The DWTT result is expected to be more successful at 0°C (Figure 53).

Figure 53 DWTT Result for B-Slab4

B-Slab9 which was rolled with TMCP (3T) at 850°C, has 100% ductile fracture on complete fracture surface at 0°C (Figure 54). The shear areas in the region of intermittent shear and cleavage fracture can be neglected in rating. This DWTT result is the best result according to API Specification 5L.

Figure 54 DWTT Result for B-Slab9

B-Slab5 which was rolled with TCR (3T) at 800°C, has 90% ductile fracture on complete fracture surface at minus 20°C. The shear areas in the region of intermittent shear and cleavage fracture is neglected in rating. The DWTT result is expected to be more successful at 0°C (Figure 55).

Figure 55 DWTT Result for B-Slab5

B-Slab6 and B-Slab10 which were rolled with TMCP (3T) at 800°C, has 90% and 95% ductile fracture on complete fracture surface at minus 20°C and at 0°C, respectively (Figure 56). The shear areas in the region of intermittent shear and cleavage fracture is neglected. The DWTT of B-Slab10 is more successful than B-Slab6 due to the test temperature.

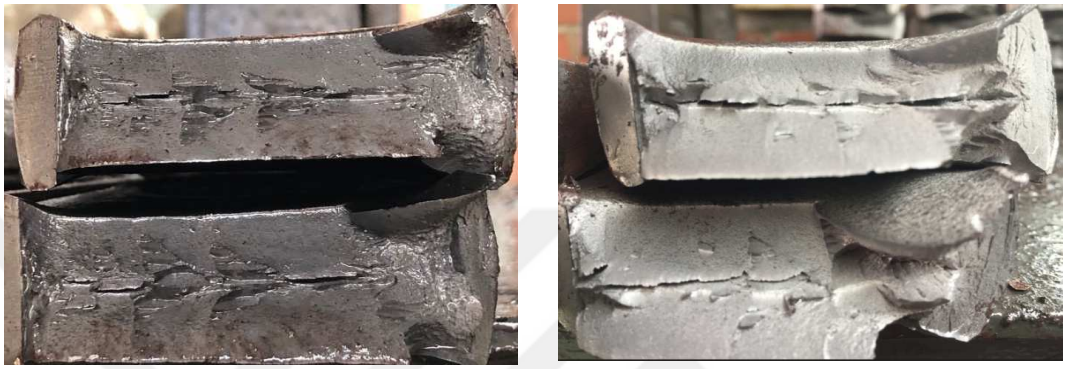

Figure 56 DWTT Result for B-Slab6 & B-Slab10

B-Slab11 which was rolled with TMCP (3T) at 750°C, has 95% ductile fracture on complete fracture surface at 0°C. The shear areas in the region of intermittent shear and cleavage fracture is neglected in rating. The DWTT result is successful according to API Specification 5L (Figure 57).

Figure 57 DWTT Result for B-Slab11

B-Slab14 which was rolled with TCR (4T) at 800°C has 0% ductile fracture on complete fracture surface at 0°C (Figure 58). The DWTT result is not successful according to API Specification 5L.

Figure 58 DWTT Result for B-Slab14

B-Slab13 which was rolled with TMCP (4T) at 800°C, has a 50% ductile fracture on complete fracture surface at 0°C (Figure 59). TCR application was disabled but rapid cooling has shown some effect on ductility. This DWTT result is not successful according to API Specification 5L.

Figure 59 DWTT Result for B-Slab13

B-Slab12 which was trying to rolled with TMCP (2T) at 800°C, has 90% ductile fracture on complete fracture surface at 0°C. The shear areas in the region of intermittent shear and cleavage fracture is neglected in rating. The DWTT is successful according to API Specification 5L (Figure 60).

Figure 60 DWTT Result for B-Slab12

Summary of the DWTT results are given by the Table 18.

Table 18 Summary of DWTT Results

B-Slabs	**Heat Treatment**	**TCR Thickness (mm)**	**DWTT (%)**
B-Slab1	Conventionally Rolled	-	0
B-Slab7	Conventionally Rolled + Cooling from 800°C	-	90
B-Slab2	950°C TCR	3T	0
B-Slab8	950°C TMCP	3T	90
B-Slab3	900°C TCR	3T	80
B-Slab4	850°C TCR	3T	90
B-Slab9	850°C TMCP	3T	100
B-Slab5	800°C TCR	3T	90
B-Slab6	800°C TMCP	3T	90
B-Slab10	800°C TMCP	3T	95
B-Slab11	750°C TMCP	3T	95
B-Slab14	800°C TCR	4T	0
B-Slab13	800°C TMCP	4T	50
B-Slab12	800°C TMCP	2T	90

4.4. Evaluation of Mechanical Test and DWTT Results

In order to select the optimum processing conditions, the results should be considered as a whole (Table 19).

Table 19 Summary of mechanical test and DWTT results

B-Slabs	Yield Strength (MPa)	Tensile Strength (MPa)	YS / TS Ratio	% EL	Impact Test Temp.	Impact Test (J)	DWTT (%)
B-Slab1	427	579	0.74	35	-20°C	76	0
B-Slab7	547	651	0.84	32	0°C	188	90
B-Slab2	444	585	0.76	34	-20°C	19	0
B-Slab8	511	638	0.80	33	0°C	214	90
B-Slab3	387	548	0.71	35	-20°C	221	80
B-Slab4	424	550	0.77	34	-20°C	250	90
B-Slab9	502	617	0.81	34	0°C	234	100
B-Slab5	512	614	0.83	33	-20°C	213	90
B-Slab6	456	562	0.81	34	-20°C	241	90
B-Slab10	528	633	0.83	33	0°C	213	95
B-Slab11	534	623	0.86	33	0°C	215	95
B-Slab14	531	662	0,80	33	0°C	111	0
B-Slab13	392	550	0.72	35	0°C	224	50
B-Slab12	491	580	0.84	34	0°C	226	90

4.5. Microstructural Characterization by Optical Microscope

Generally, ferrite phase dominates in API grades X60 and X70 with low carbon content. Grain size calculation of ferrite grains is based on ASTM E112.

4.5.1. Grain Size Calculation

According to the analysis of grain size distribution due to the specimens that are taken from the head-middle-end of plates demonstrate a lower ferritic grain size according to ASTM E112. In Clemex Vision program, all grains are colored and calculated due to number of grains per unit area, average grain area, average diameter, mean intercept and number of intercepts per unit length of test line with the help of "Routines" [40].

Grain Size Number(G) is found by Intersection Count Method method according to "Grain Size Relationships Computed for Uniform, Randomly Oriented, Equiaxed Grains Table placed in standard. The microscopic image is intersected by vertical and horizontal lines, then the intersection of lines and grain boundaries are counted as tangent hits 0.5 point, grain boundary intersections 1 point, triple-point intersections 1.5 point. After calculations, average grain diameters are estimated. At last, calculations are compared with results of Clemex Program. As it is known, one important thing is that with the G number increases, grain size and grain diameter decrease inversely according to ASTM E112 [27].

B-Slab1

B-Slab1 consist of mostly ferrite phase, but some pearlitic microstructure is also obtained. The grain size distribution is generally homogeneous as G-11.5 along the plate when head-middle-end specimens are calculated averagely. The microstructure and the grain size images are given in Figure 61 and Figure 62. The grain size calculation by intersection count method is given in Table 20 briefly.

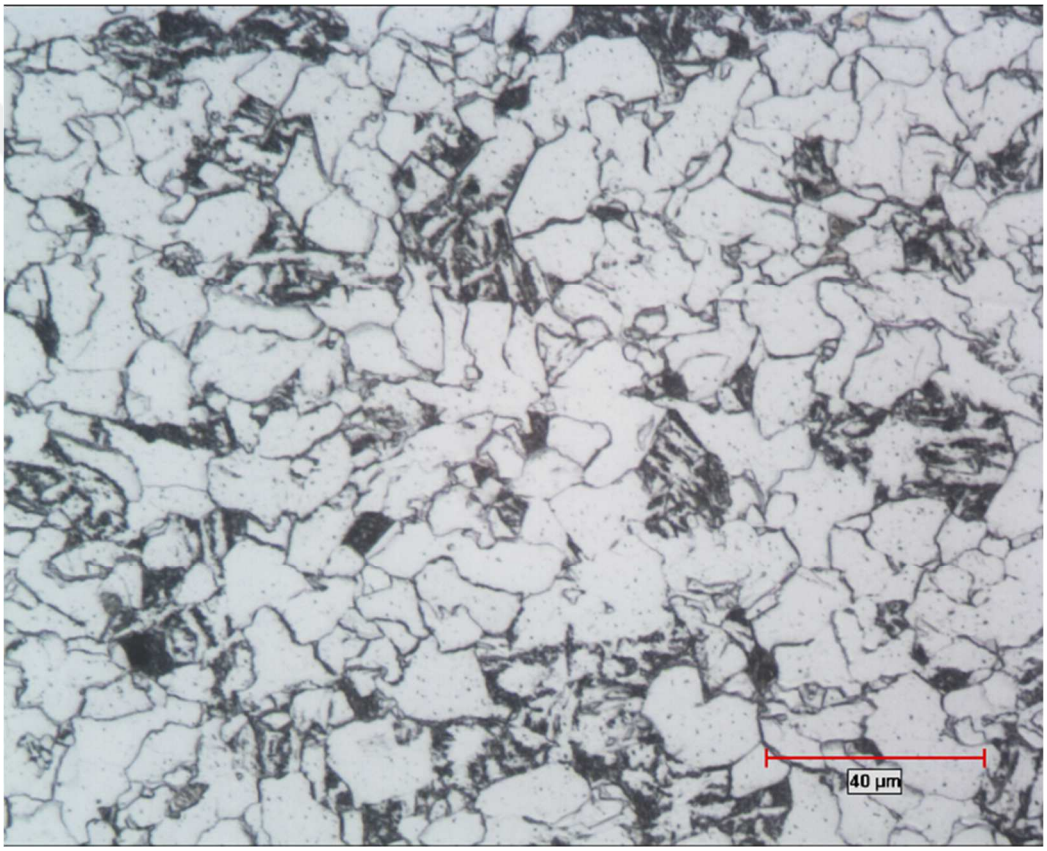

Figure 61 Microstructure of B-Slab1 (x500)

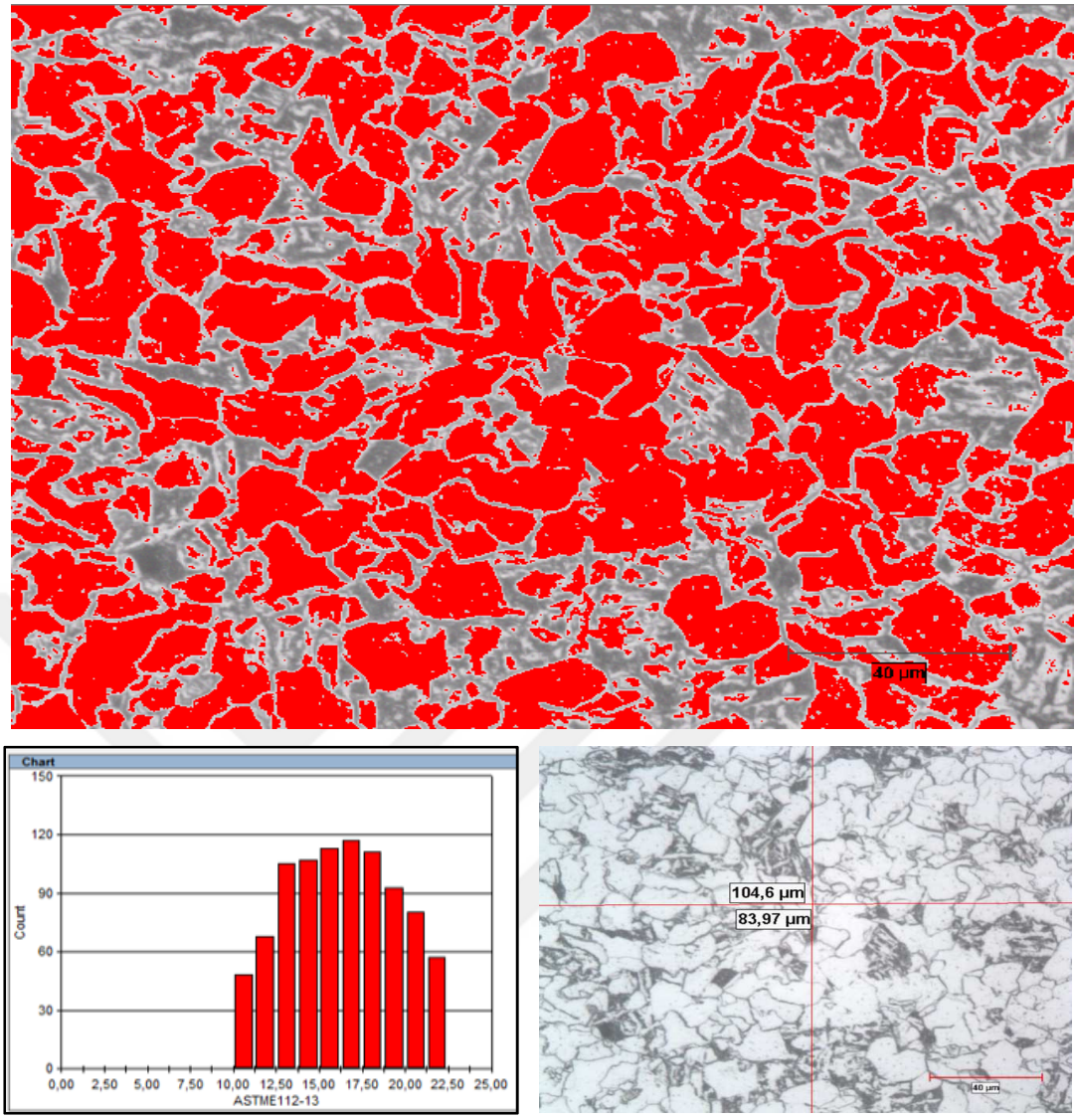

Figure 62 Grain size image of B-Slab1 (x500)

Table 20 Grain size calculation of B-Slab1

Horizontal Line (A)	104.60
Horizontal #grain (C1)	32.50
Vertical Line (B)	83.97
Vertical #grain (C2)	23.00
A / C1 = D1	3.2185
B / C2 = D2	3.6509
Average Value = (D1 + D2)/2 = D3	3.4347
Diameter (µm)	6.87
ASTM E112	**11.5**

B-Slab7

B-Slab7 consist of mostly ferrite phase, but some pearlitic microstructure is also obtained. The grain size distribution is generally homogeneous as G-13.5 along the plate when head-middle-end specimens are calculated averagely. The microstructure and the grain size images are given in Figure 63 and Figure 64. The grain size calculation by intersection count method is given in Table 21 briefly.

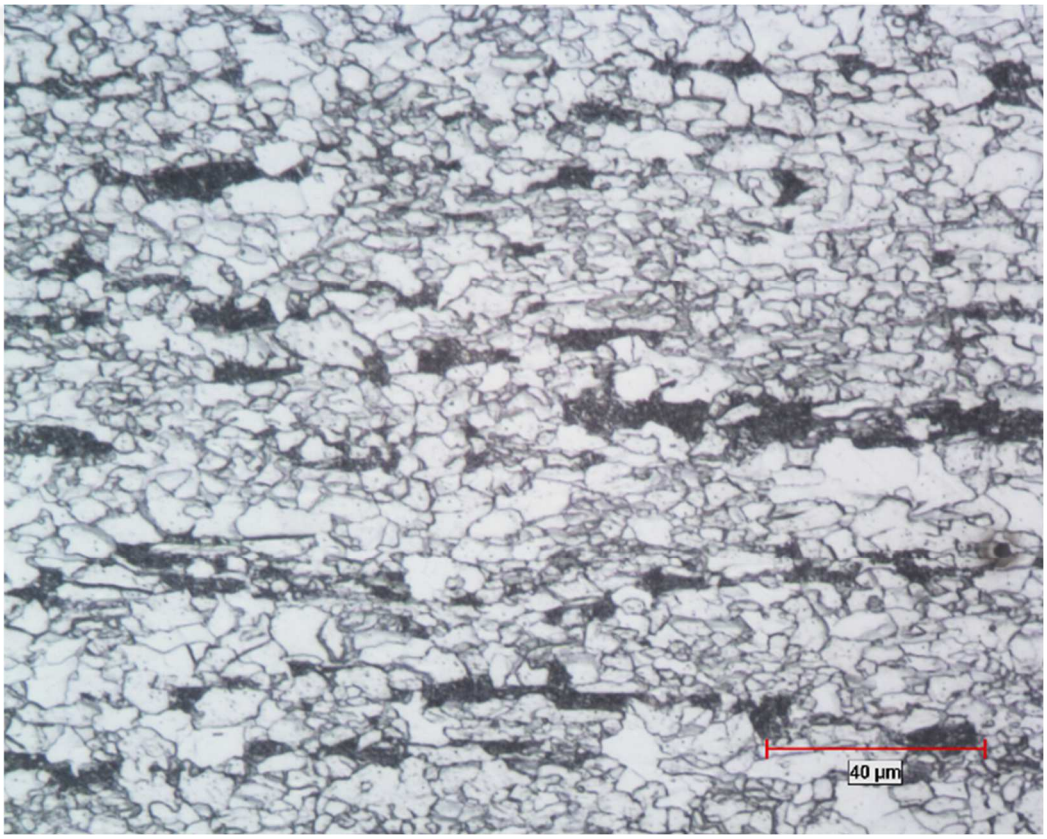

Figure 63 Microstructure of B-Slab7 (x500)

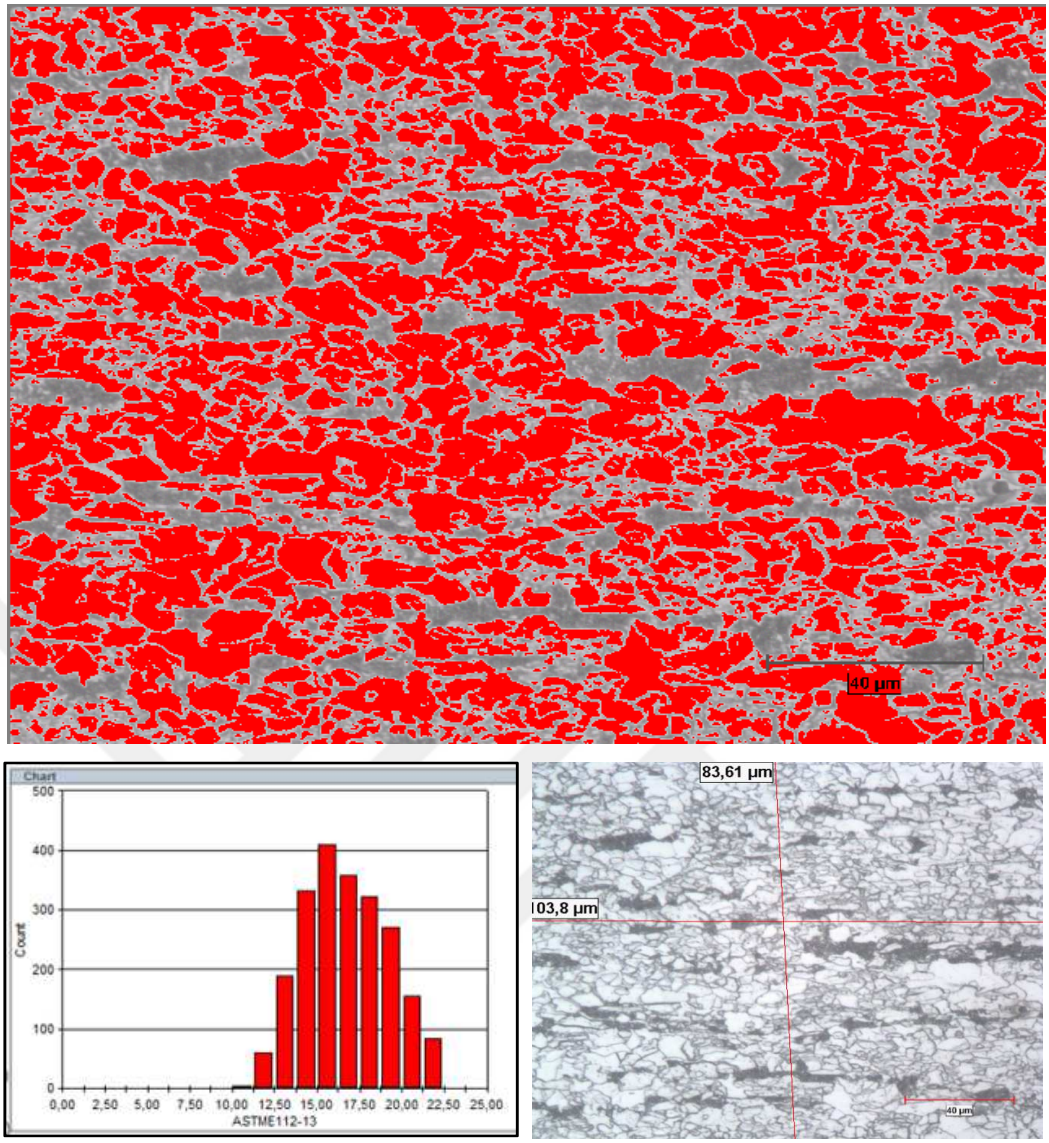

Figure 64 Grain size image of B-Slab7 (x500)

Table 21 Grain size calculation of B-Slab7

Horizontal Line (A)	103.80
Horizontal #grain (C1)	58.50
Vertical Line (B)	83.61
Vertical #grain (C2)	48.00
A / C1 = D1	1.7744
B / C2 = D2	1.7419
Ave. Value = (D1 + D2)/2 = D3	1.7581
Diameter (µm)	3.52
ASTM E112	**13.5**

B-Slab2

B-Slab2 consist of mostly ferrite phase, but some pearlitic microstructure is also obtained. The grain size distribution is generally homogeneous as G-11.5 along the plate when head-middle-end specimens are calculated averagely. The microstructure and the grain size images are given in Figure 65 and Figure 66. The grain size calculation by intersection count method is given in Table 22 briefly.

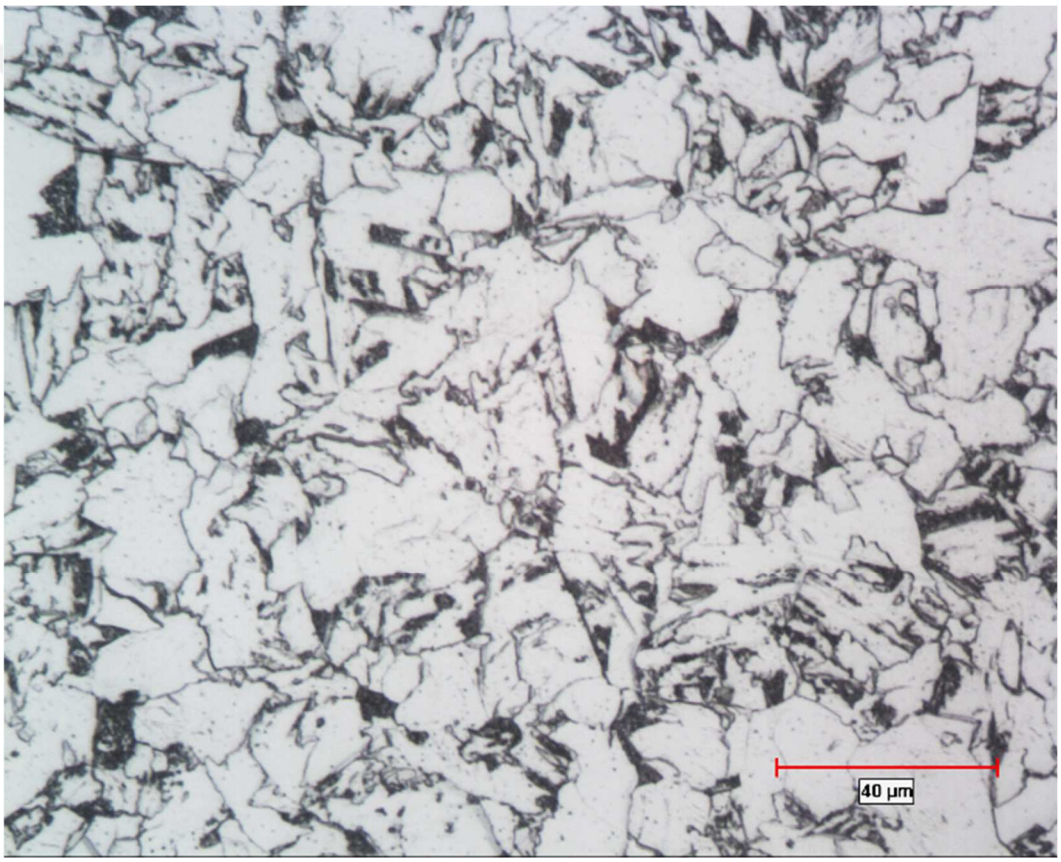

Figure 65 Microstructure of B-Slab2 (x500)

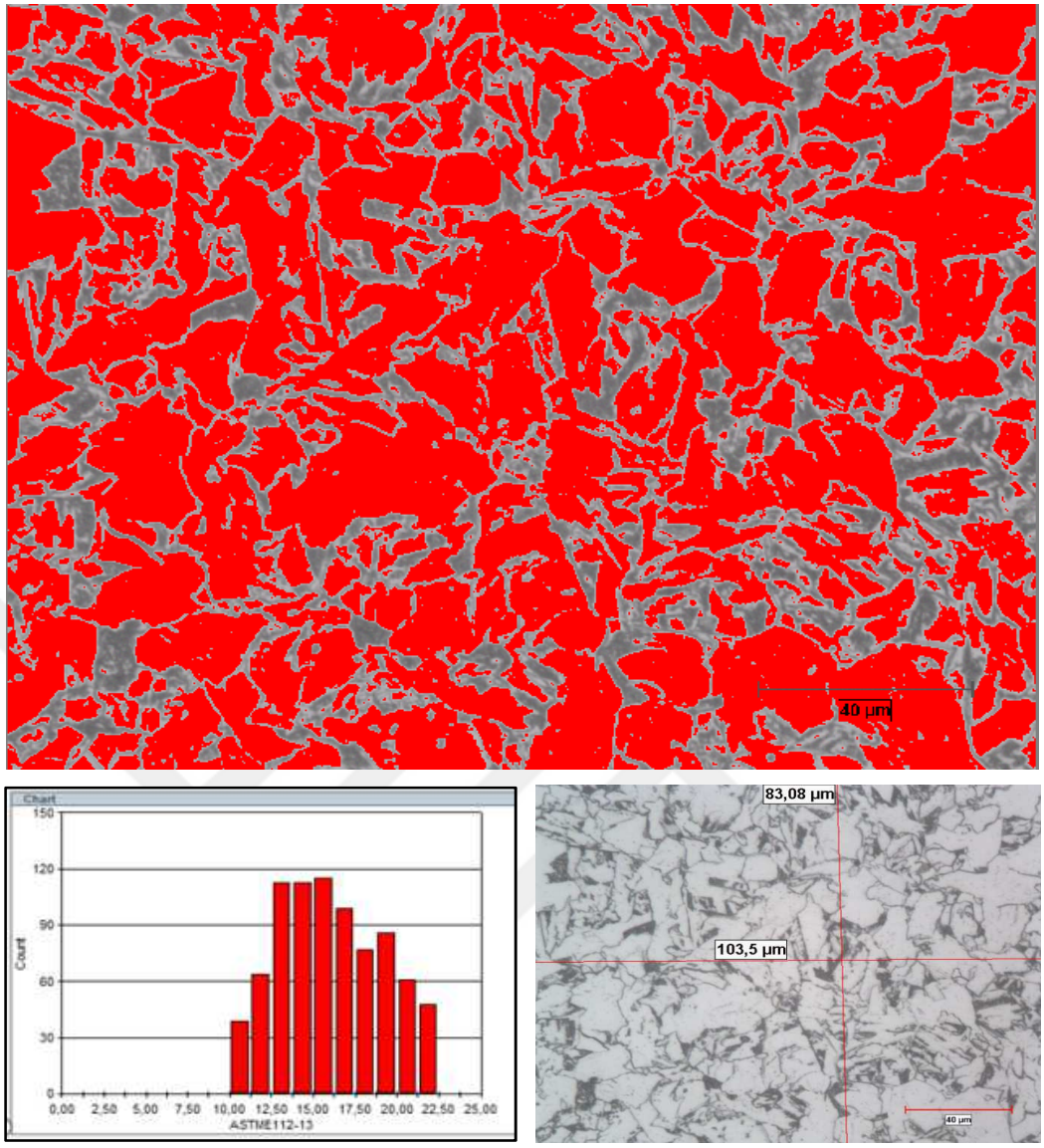

Figure 66 Grain size image of B-Slab2 (x500)

Table 22 Grain size calculation of B-Slab2

Horizontal Line (A)	103.50
Horizontal #grain (C1)	36.50
Vertical Line (B)	83.08
Vertical #grain (C2)	23.50
A / C1 = D1	2.8356
B / C2 = D2	3.5353
Ave. Value = (D1 + D2)/2 = D3	3.1855
Diameter (µm)	6.37
ASTM E112	**11.5**

B-Slab8

B-Slab8 consist of mostly ferrite phase, but some pearlitic microstructure is also obtained. The grain size distribution is generally homogeneous as G-13.0 along the plate when head-middle-end specimens are calculated averagely. The microstructure and the grain size images are given in Figure 67 and Figure 68. The grain size calculation by intersection count method is given in Table 23 briefly.

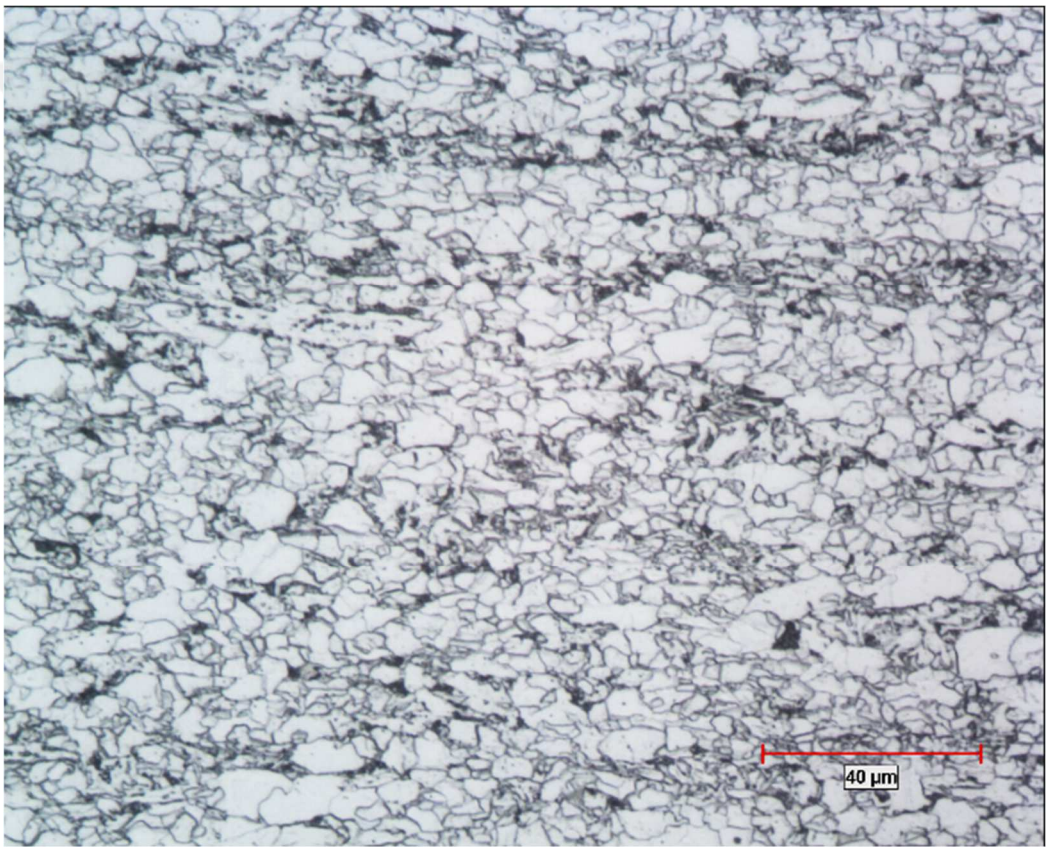

Figure 67 Microstructure of B-Slab8 (x500)

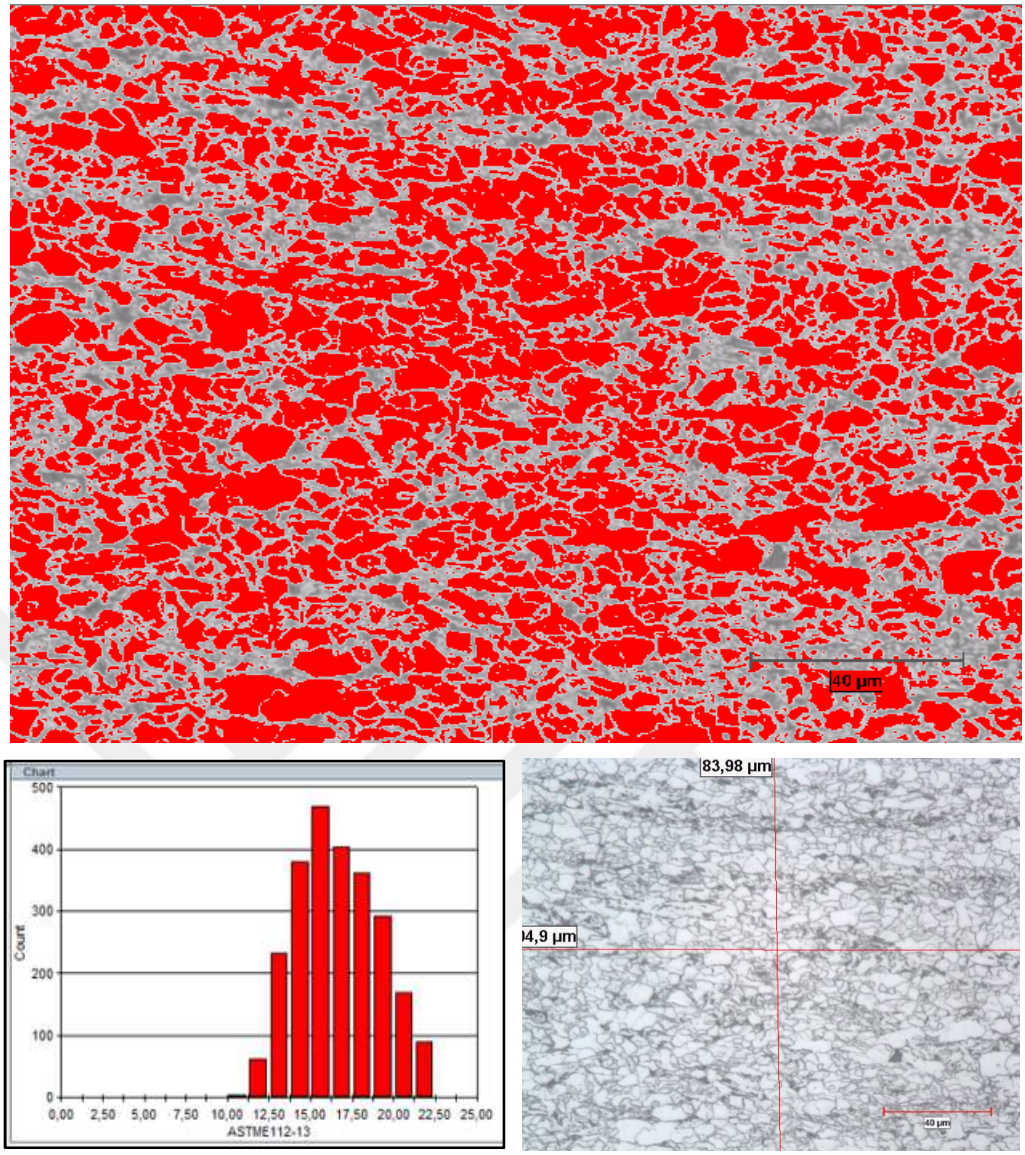

Figure 68 Grain size image of B-Slab8 (x500)

Table 23 Grain size calculation of B-Slab8

Horizontal Line (A)	104.90
Horizontal #grain (C1)	50.00
Vertical Line (B)	83.98
Vertical #grain (C2)	45.50
A / C1 = D1	2.0980
B / C2 = D2	1.8457
Ave. Value = (D1 + D2)/2 = D3	1.9719
Diameter (µm)	3.94
ASTM E112	**13.0**

B-Slab3

B-Slab3 consist of mostly ferrite phase, but some pearlitic microstructure is also obtained. The grain size distribution is generally homogeneous as G-12.0 along the plate when head-middle-end specimens are calculated averagely. The microstructure and the grain size images are given in Figure 69 and Figure 70. The grain size calculation by intersection count method is given in Table 24 briefly.

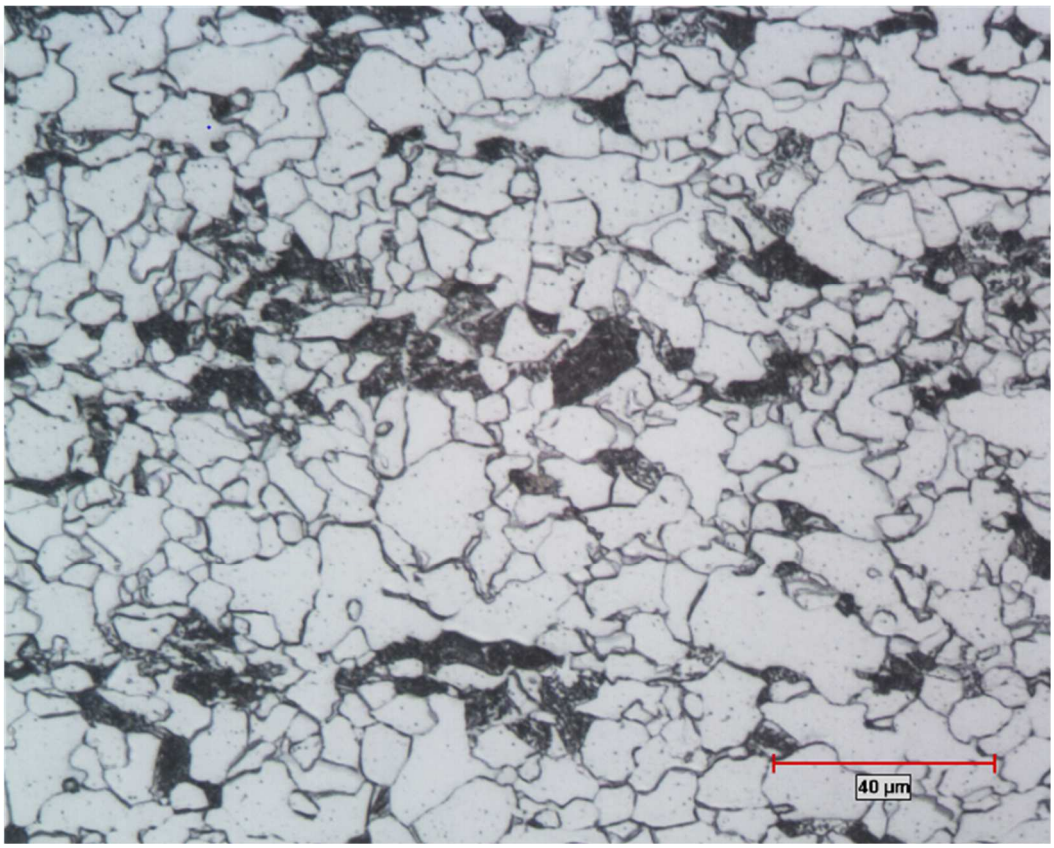

Figure 69 Microstructure of B-Slab3 (x500)

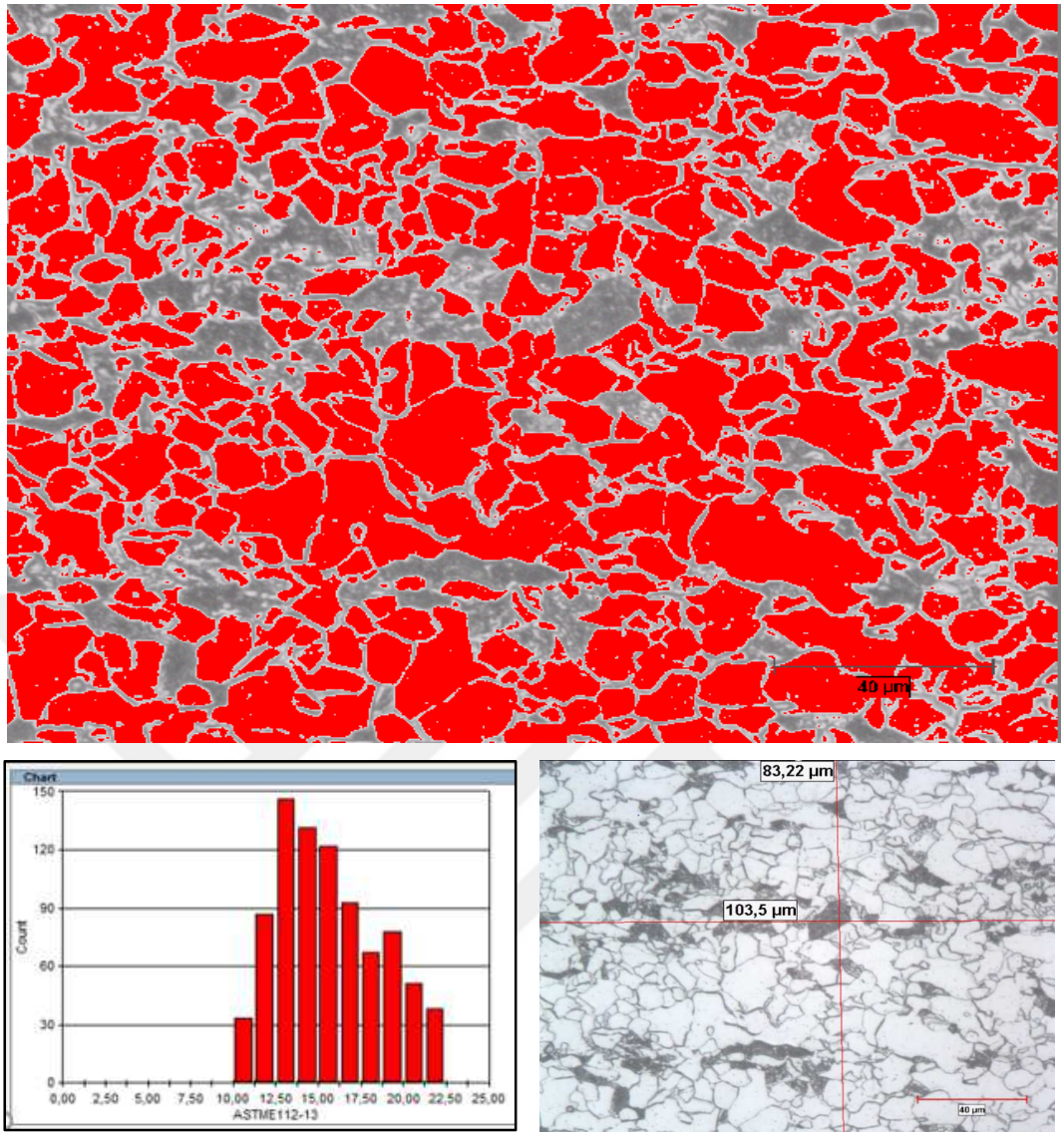

Figure 70 Grain size image of B-Slab3 (x500)

Table 24 Grain size calculation of B-Slab3

Horizontal Line (A)	103.50
Horizontal #grain (C1)	35.00
Vertical Line (B)	83.22
Vertical #grain (C2)	29.00
A / C1 = D1	2.9571
B / C2 = D2	2.8697
Ave. Value = (D1 + D2)/2 = D3	2.9134
Diameter (µm)	5.83
ASTM E112	**12.0**

B-Slab4

B-Slab4 consist of mostly ferrite phase, but some pearlitic microstructure is also obtained. The grain size distribution is generally homogeneous as G-12.0 along the plate when head-middle-end specimens are calculated averagely. The microstructure and the grain size images are given in Figure 71 and Figure 72. The grain size calculation by intersection count method is given in Table 25 briefly.

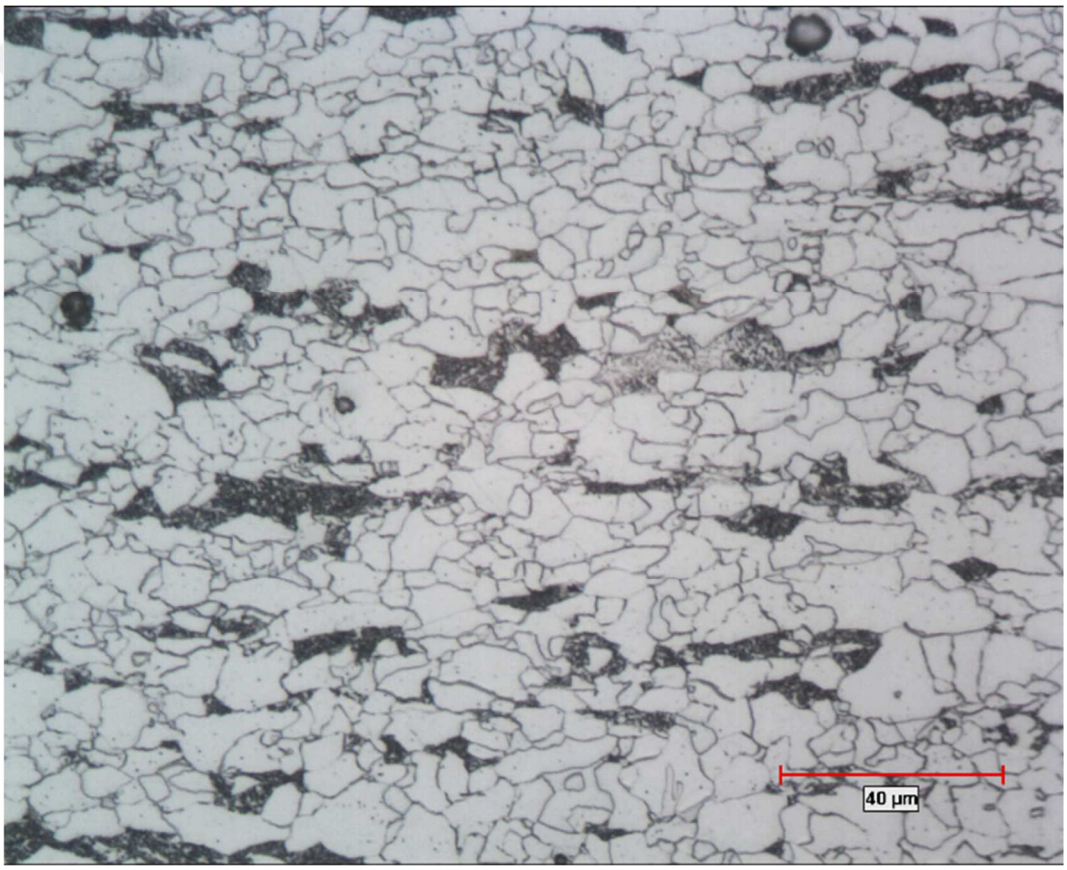

Figure 71 Microstructure of B-Slab4 (x500)

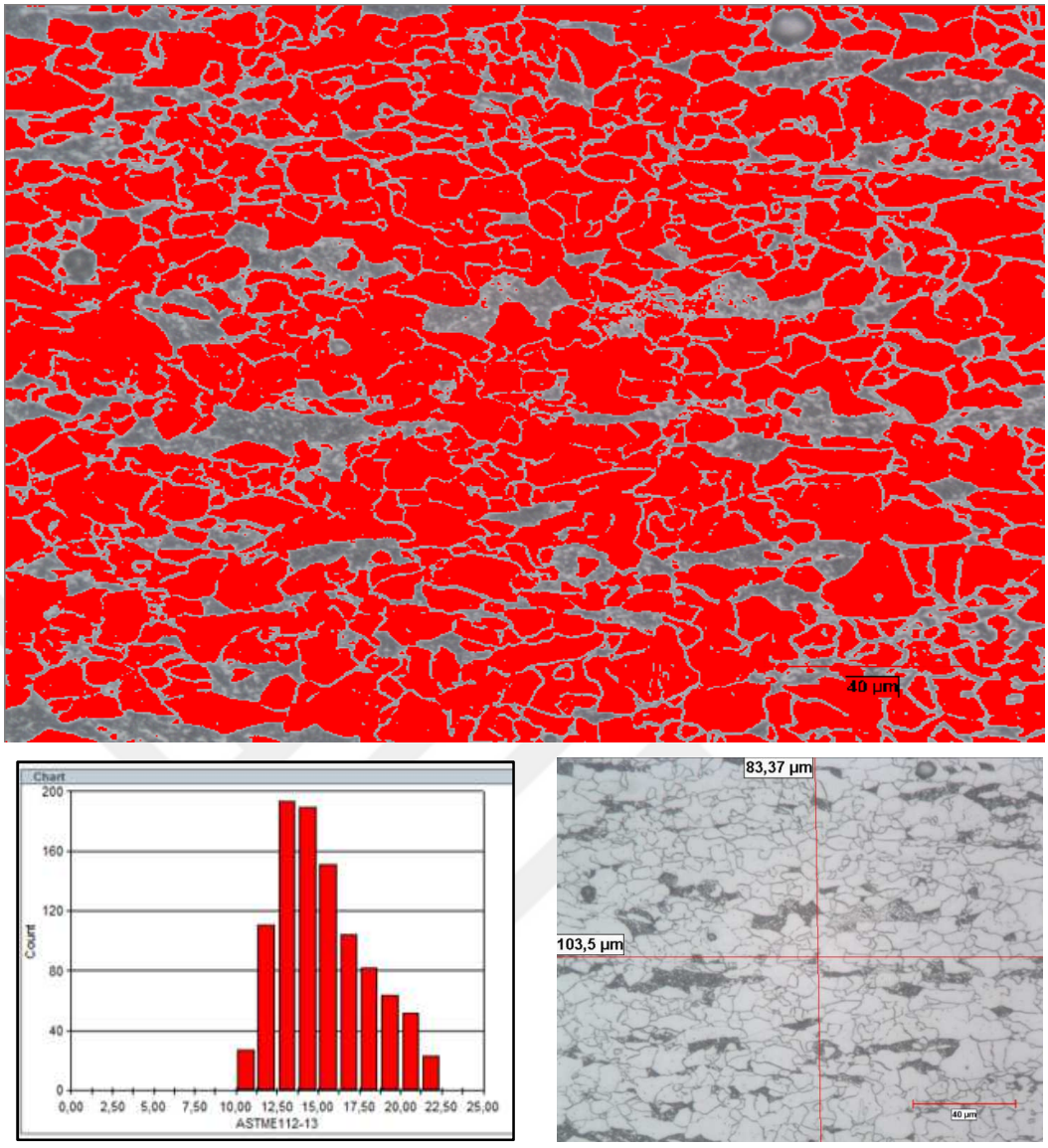

Figure 72 Grain size image of B-Slab4 (x500)

Table 25 Grain size calculation of B-Slab4

Horizontal Line (A)	103.50
Horizontal #grain (C1)	35.00
Vertical Line (B)	83.37
Vertical #grain (C2)	30.00
A / C1 = D1	2.9571
B / C2 = D2	2.7790
Ave. Value = (D1 + D2)/2 = D3	2.8681
Diameter (µm)	5.74
ASTM E112	**12.0**

B-Slab9

B-Slab9 consist of mostly ferrite phase, but some pearlitic microstructure is also obtained. The grain size distribution is generally homogeneous as G-13.0 along the plate when head-middle-end specimens are calculated averagely. The microstructure and the grain size images are given in Figure 73 and Figure 74. The grain size calculation by intersection count method is given in Table 26 briefly.

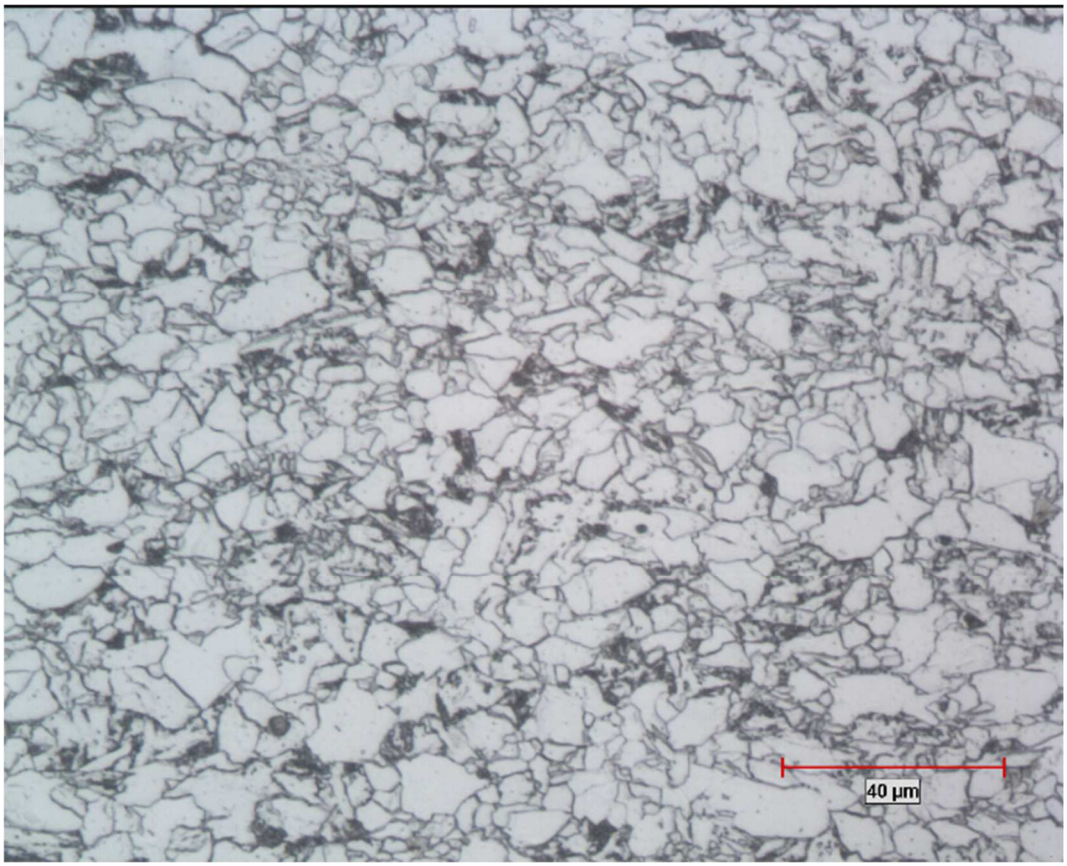

Figure 73 Microstructure of B-Slab9 (x500)

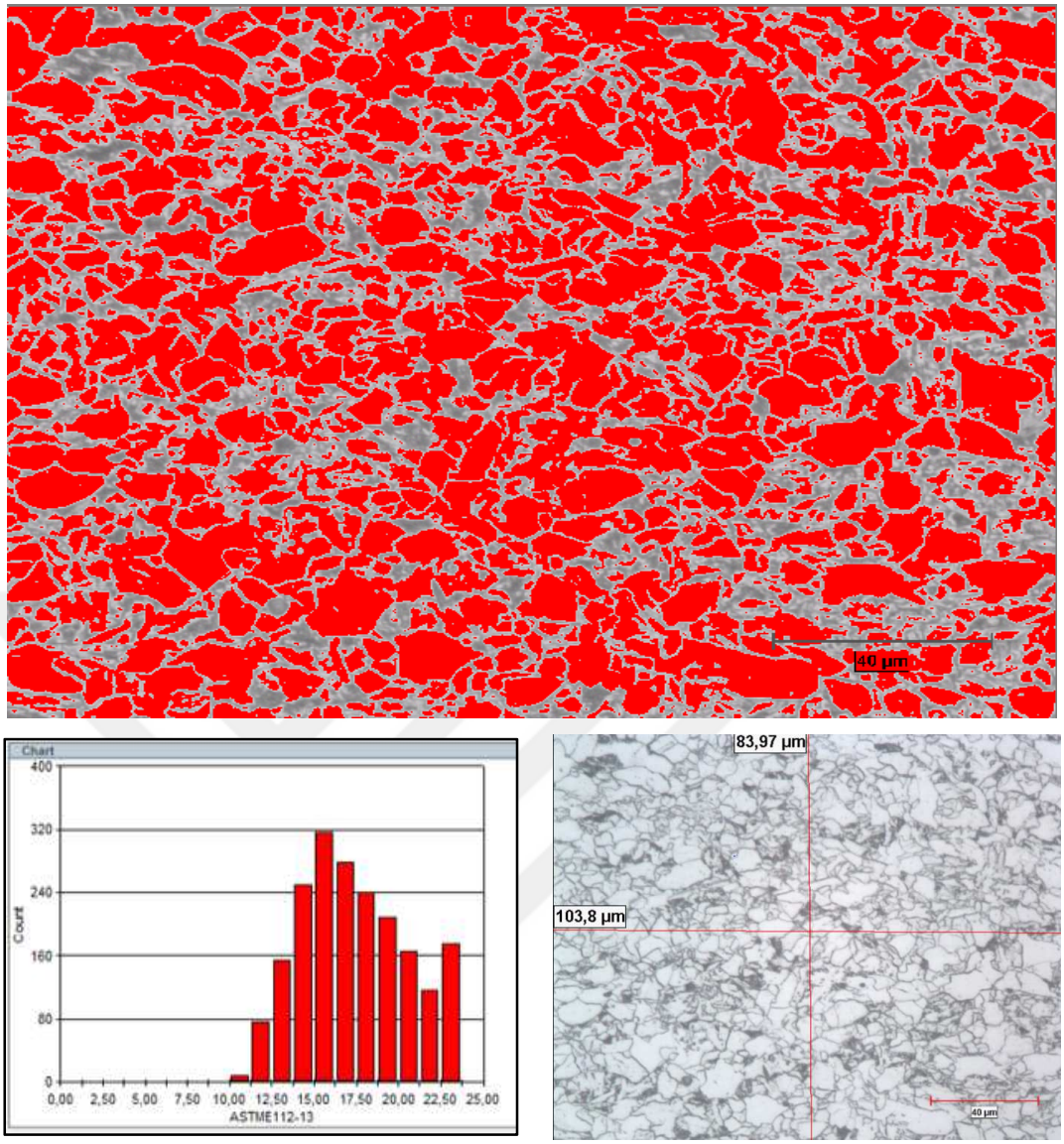

Figure 74 Grain size image of B-Slab9 (x500)

Table 26 Grain size calculation of B-Slab9

Horizontal Line (A)	103.80
Horizontal #grain (C1)	49.00
Vertical Line (B)	83.97
Vertical #grain (C2)	43.50
A / C1 = D1	2.1184
B / C2 = D2	1.9303
Ave. Value = (D1 + D2)/2 = D3	2.0244
Diameter (µm)	4.05
ASTM E112	**13.0**

B-Slab5

B-Slab5 consist of mostly ferrite phase, but some pearlitic microstructure is also obtained. The grain size distribution is generally homogeneous as G-12.5 along the plate when head-middle-end specimens are calculated averagely. The microstructure and the grain size images are given in Figure 75 and Figure 76. The grain size calculation by intersection count method is given in Table 27 briefly.

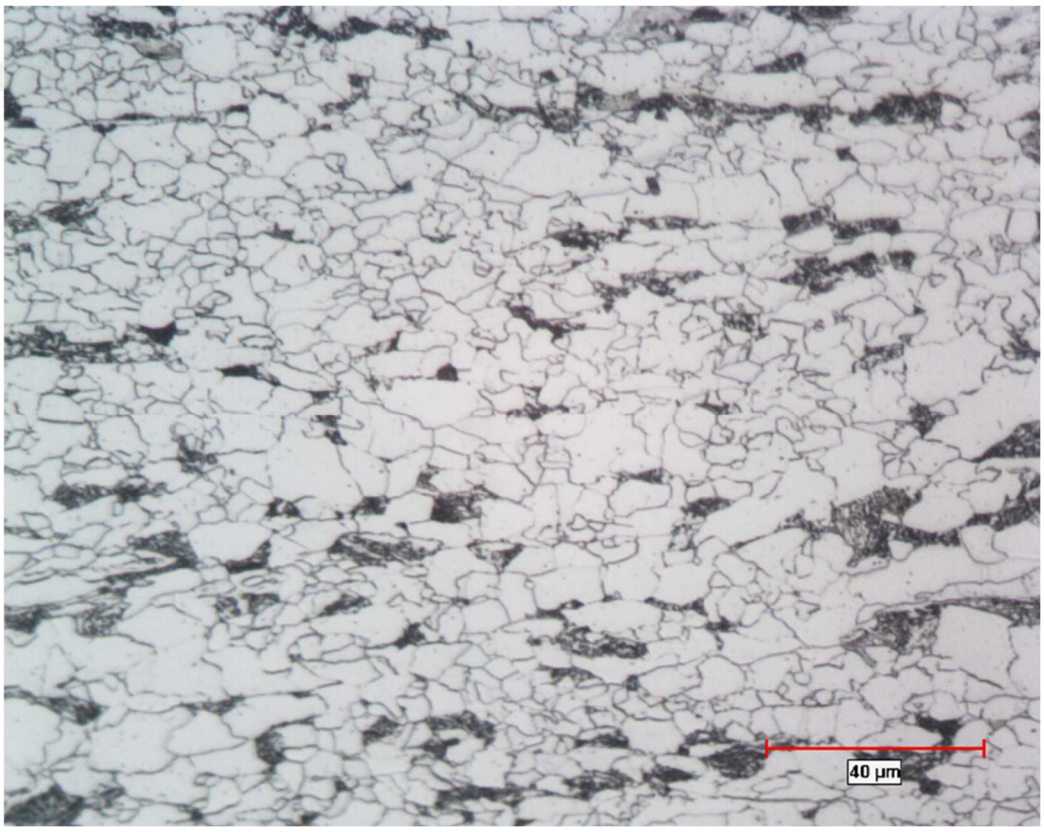

Figure 75 Microstructure of B-Slab5 (x500)

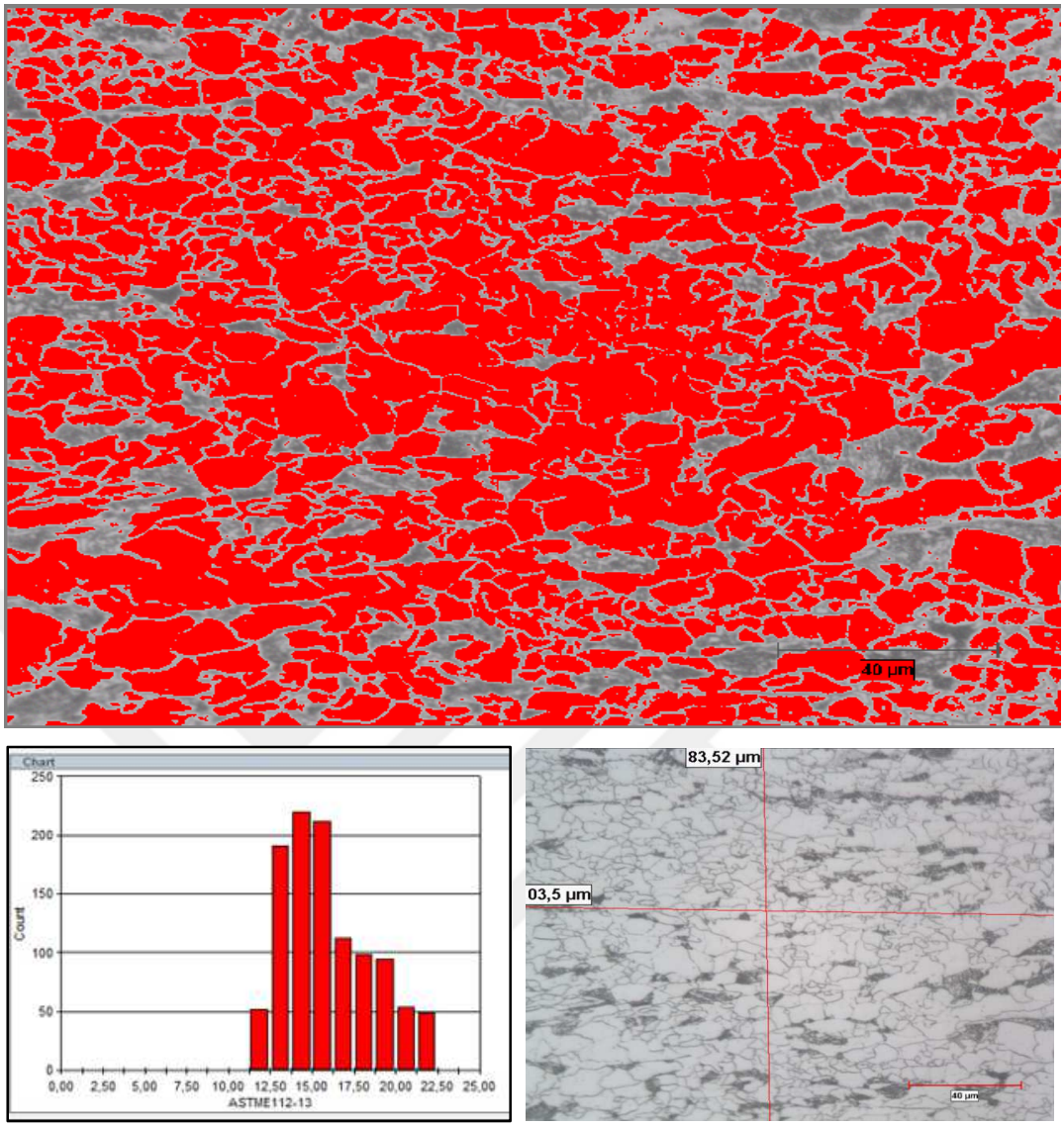

Figure 76 Grain size image of B-Slab5 (x500)

Table 27 Grain size calculation of B-Slab5

Horizontal Line (A)	103.50
Horizontal #grain (C1)	45.50
Vertical Line (B)	83.52
Vertical #grain (C2)	38.00
A / C1 = D1	2.2747
B / C2 = D2	2.1979
Ave. Value = (D1 + D2)/2 = D3	2.2363
Diameter (µm)	4.47
ASTM E112	**12.5**

B-Slab6

B-Slab6 consist of mostly ferrite phase, but some pearlitic microstructure is also obtained. The grain size distribution is generally homogeneous as G-12.5 along the plate when head-middle-end specimens are calculated averagely. The microstructure and the grain size images are given in Figure 77 and Figure 78. The grain size calculation by intersection count method is given in Table 28 briefly.

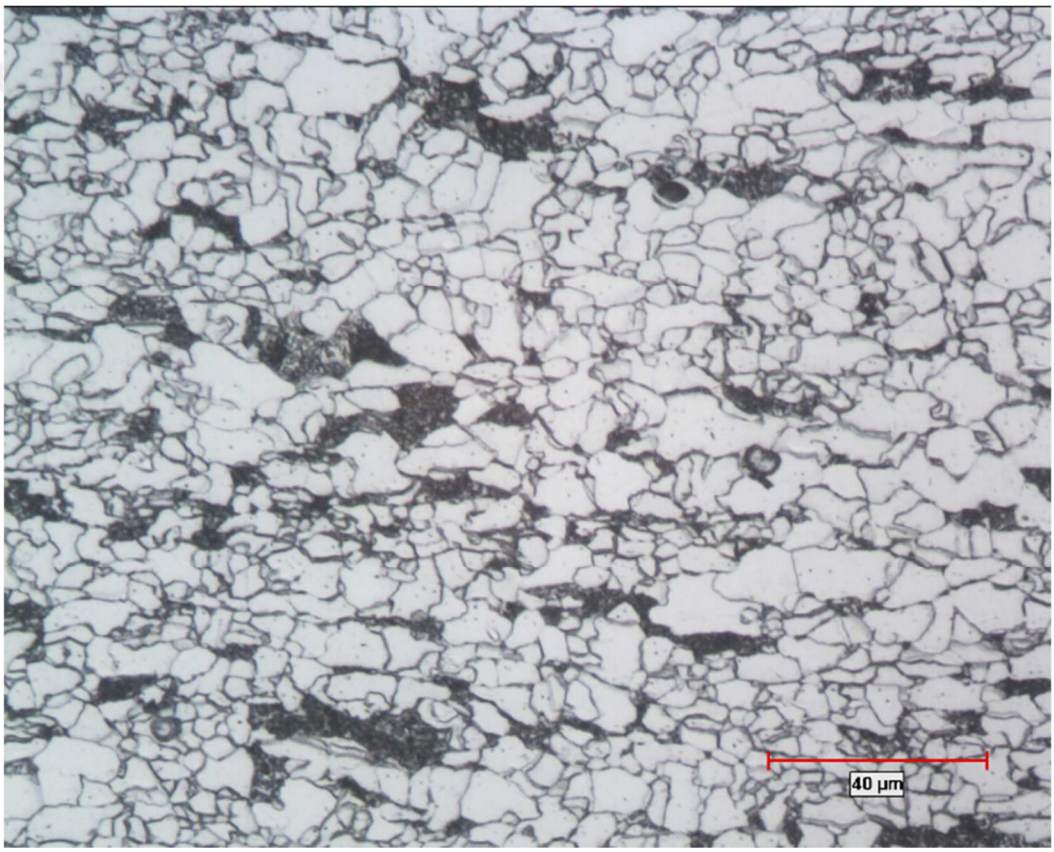

Figure 77 Microstructure of B-Slab6 (x500)

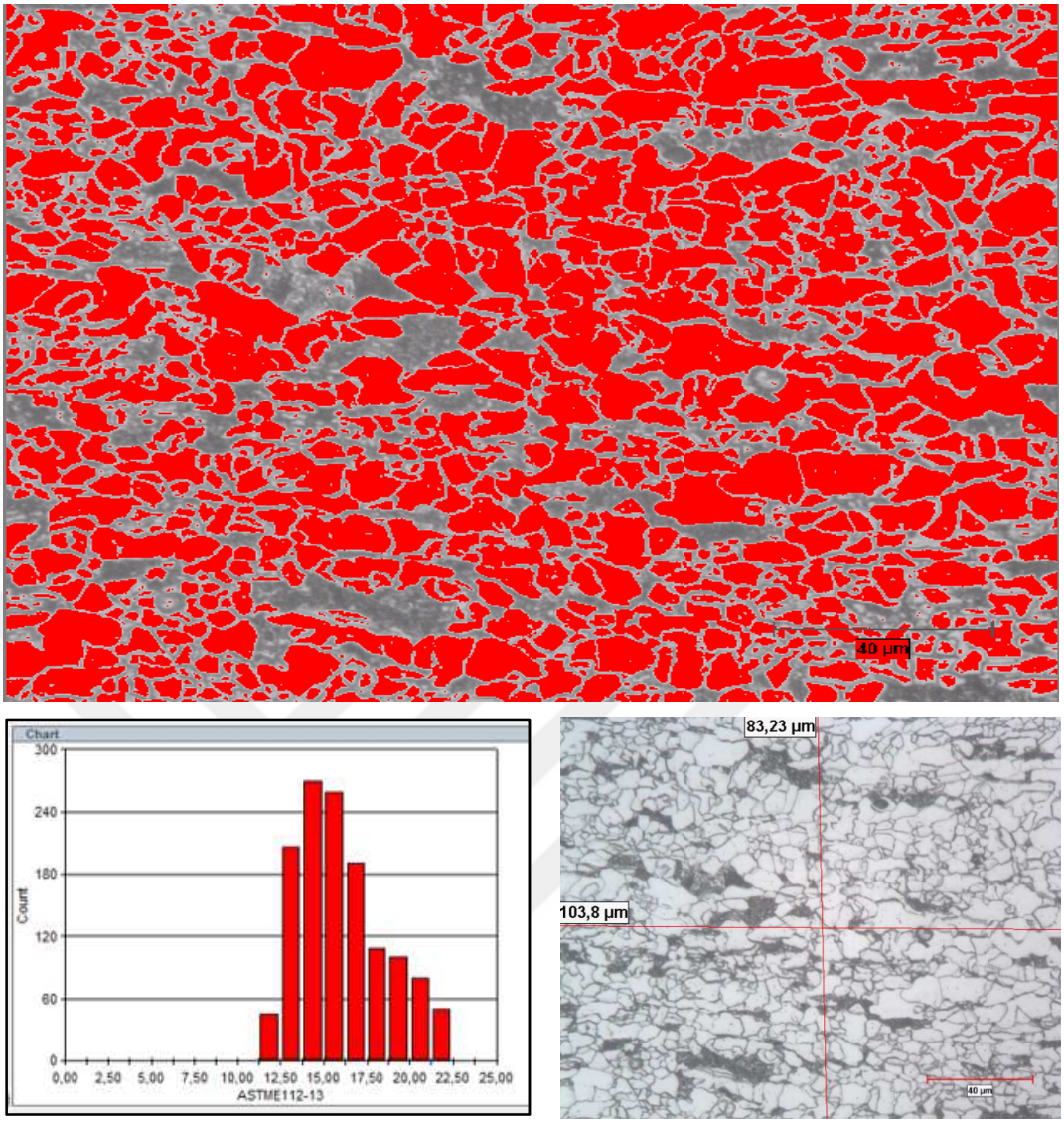

Figure 78 Grain size image of B-Slab6 (x500)

Table 28 Grain size calculation of B-Slab6

Horizontal Line (A)	103.80
Horizontal #grain (C1)	43.00
Vertical Line (B)	83.23
Vertical #grain (C2)	39.00
A / C1 = D1	2.4140
B / C2 = D2	2.1341
Ave. Value = (D1 + D2)/2 = D3	2.2740
Diameter (µm)	4.55
ASTM E112	**12.5**

B-Slab10

B-Slab10 consist of mostly ferrite phase, but some pearlitic microstructure is also obtained. The grain size distribution is generally homogeneous as G-13.0 along the plate when head-middle-end specimens are calculated averagely. The microstructure and the grain size images are given in Figure 79 and Figure 80. The grain size calculation by intersection count method is given in Table 29 briefly.

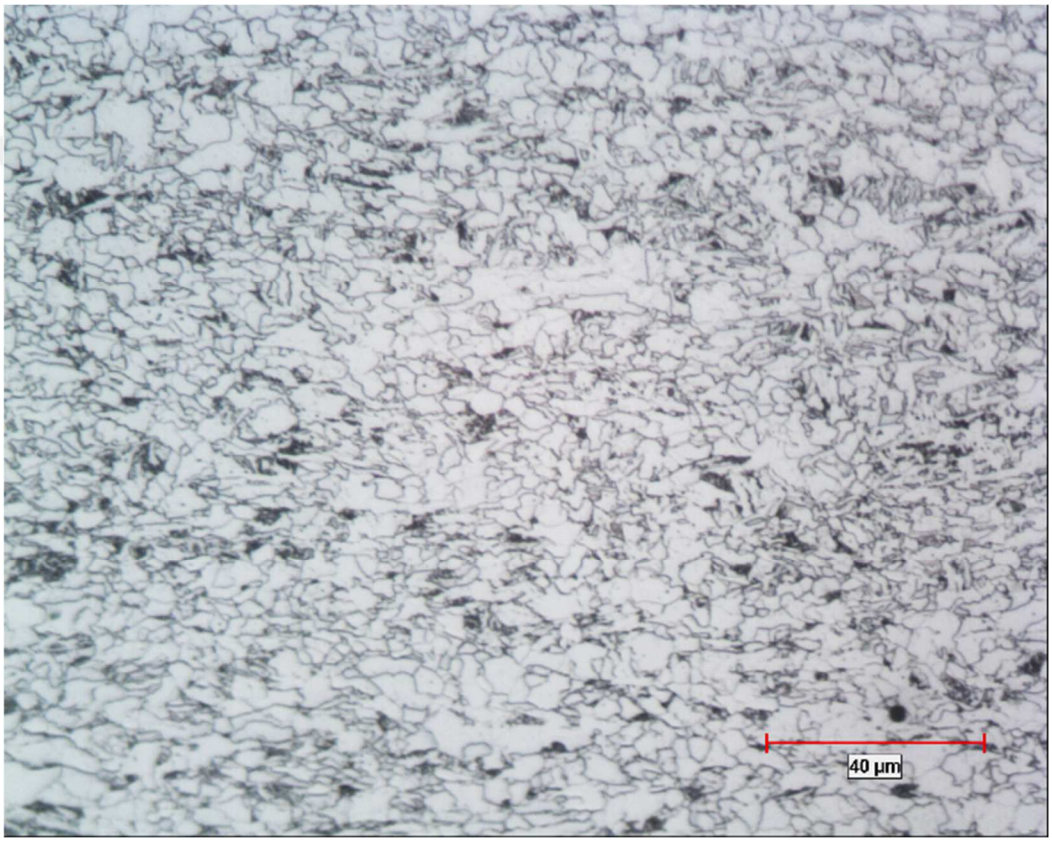

Figure 79 Microstructure of B-Slab10 (x500)

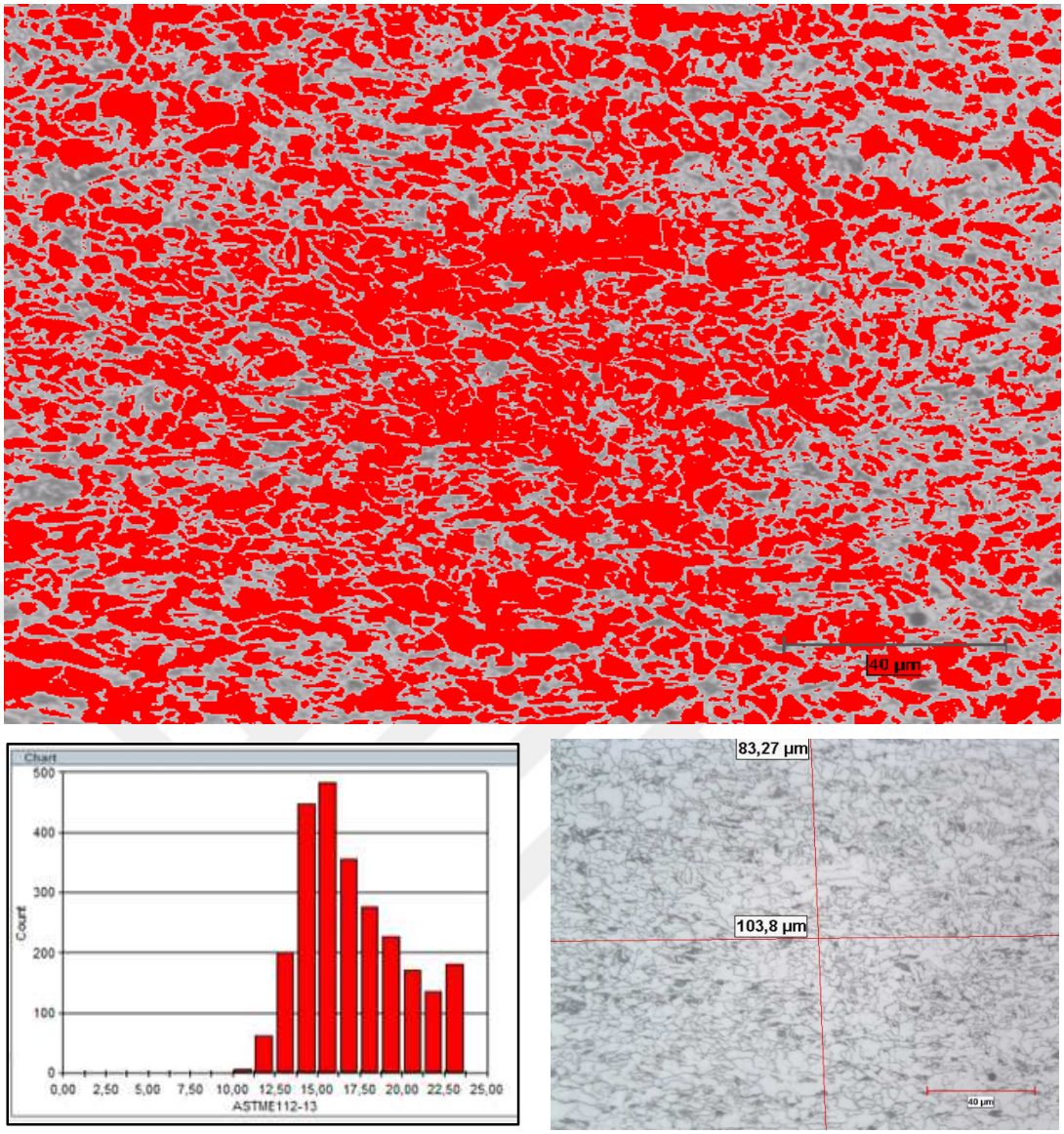

Figure 80 Grain size image of B-Slab10 (x500)

Table 29 Grain size calculation of B-Slab10

Horizontal Line (A)	103.80
Horizontal #grain (C1)	51.50
Vertical Line (B)	83.27
Vertical #grain (C2)	44.50
A / C1 = D1	2.0155
B / C2 = D2	1.8712
Ave. Value = (D1 + D2)/2 = D3	1.9434
Diameter (µm)	3.89
ASTM E112	**13.0**

B-Slab11

B-Slab11 consist of mostly ferrite phase, but some pearlitic microstructure is also obtained. The grain size distribution is generally homogeneous as G-13.0 along the plate when head-middle-end specimens are averaged. The microstructure and the grain size images are given in Figure 81 and Figure 82. The grain size calculation by intersection count method is given in Table 30 briefly.

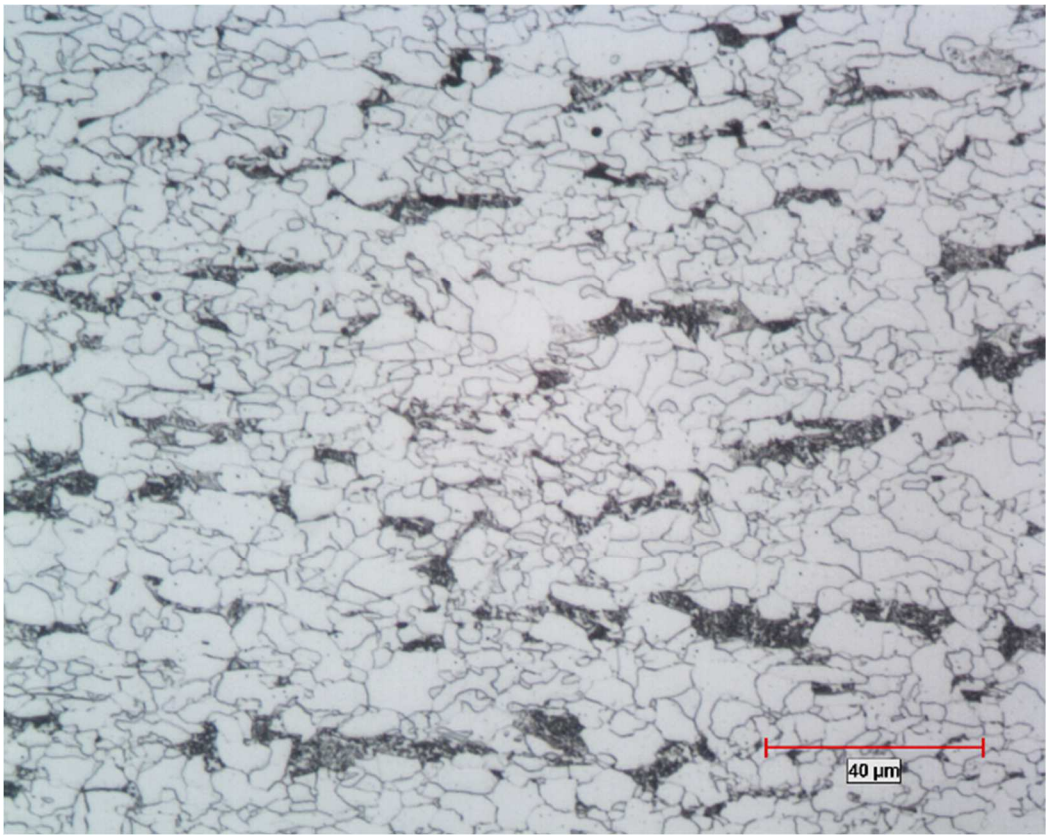

Figure 81 Microstructure of B-Slab11 (x500)

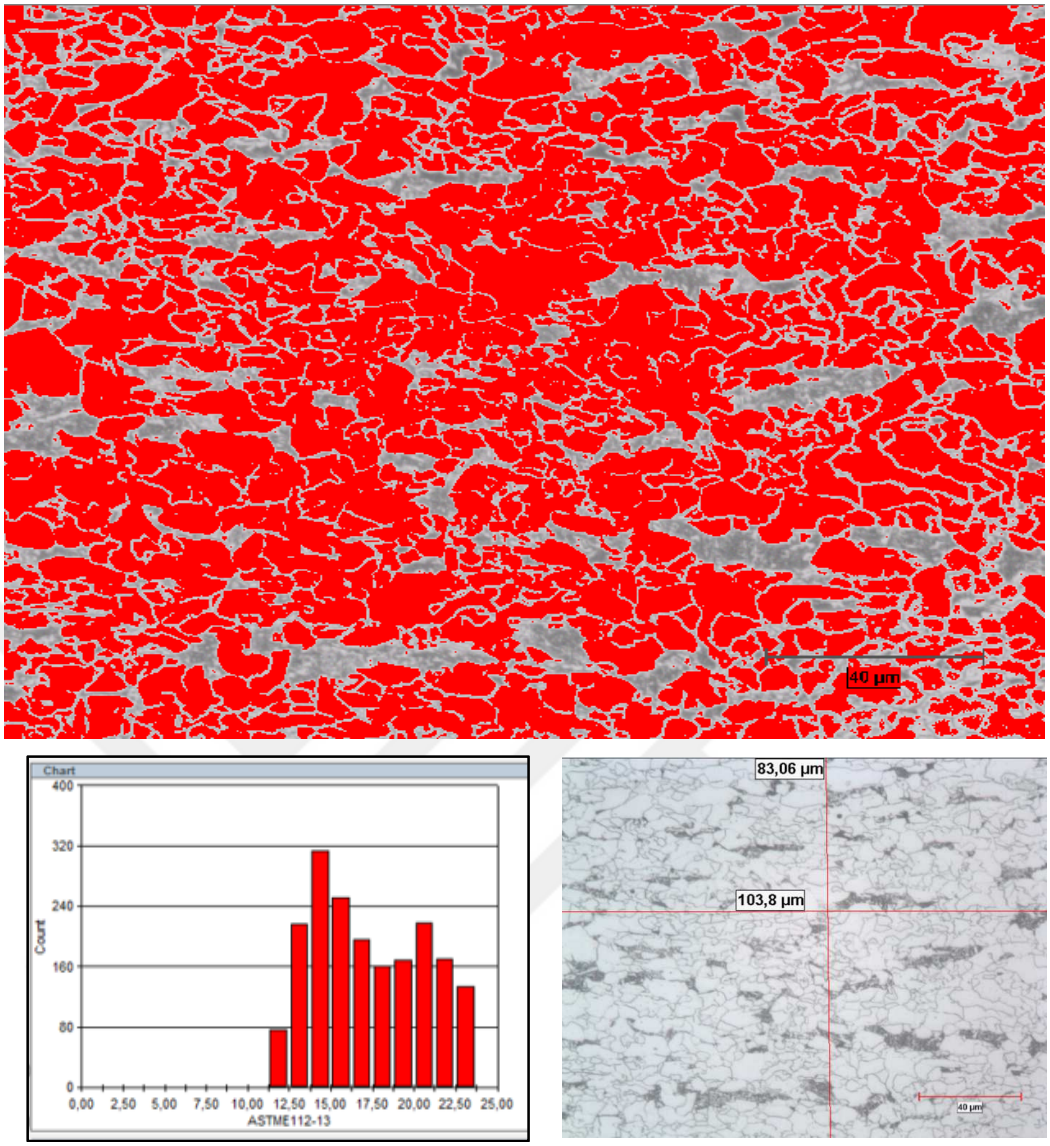

Figure 82 Grain size image of B-Slab11 (x500)

Table 30 Grain size calculation of B-Slab11

Horizontal Line (A)	103.80
Horizontal #grain (C1)	50.00
Vertical Line (B)	83.06
Vertical #grain (C2)	42.00
A / C1 = D1	2.0760
B / C2 = D2	1.9776
Ave. Value = (D1 + D2)/2 = D3	2.0268
Diameter (µm)	4.05
ASTM E112	**13.0**

B-Slab14

B-Slab14 consist of mostly acicular ferrite phase, but some pearlitic microstructure is also obtained. The grain size distribution is generally homogeneous as G-13.5 along the plate when head-middle-end specimens are calculated averagely. The microstructure and the grain size images are given in Figure 83 and Figure 84. The grain size calculation by intersection count method is given in Table 31 briefly.

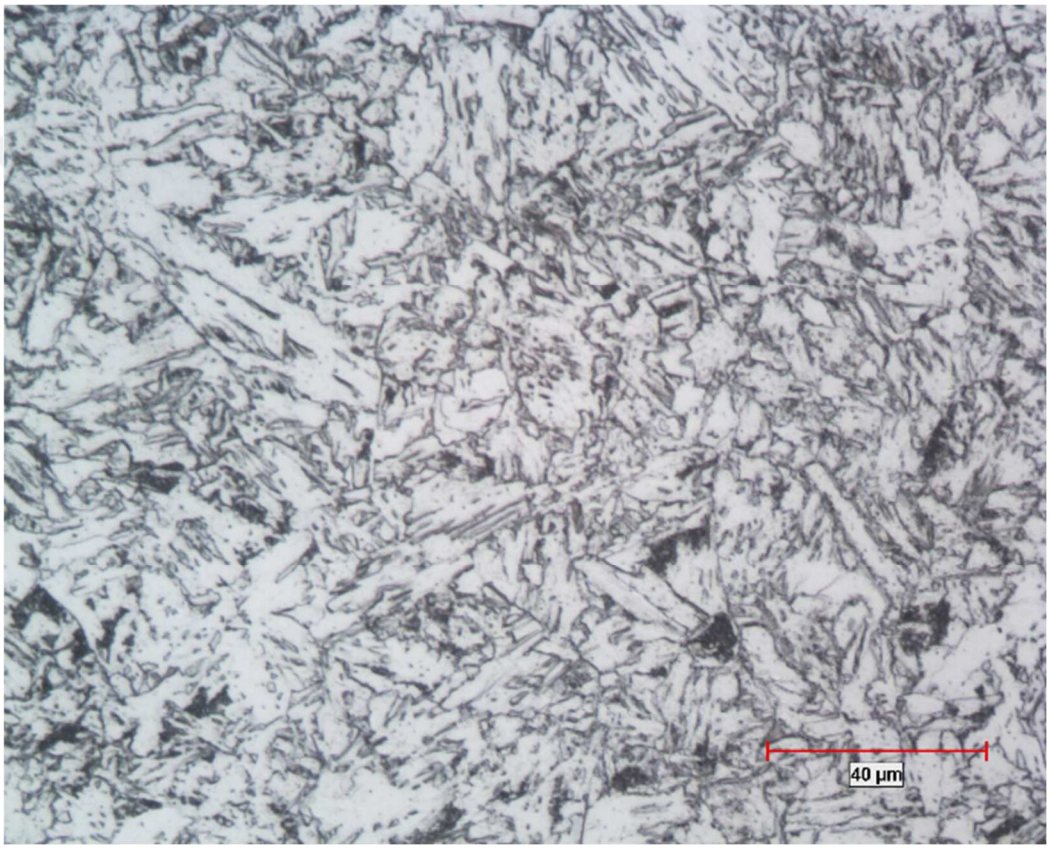

Figure 83 Microstructure of B-Slab14 (x500)

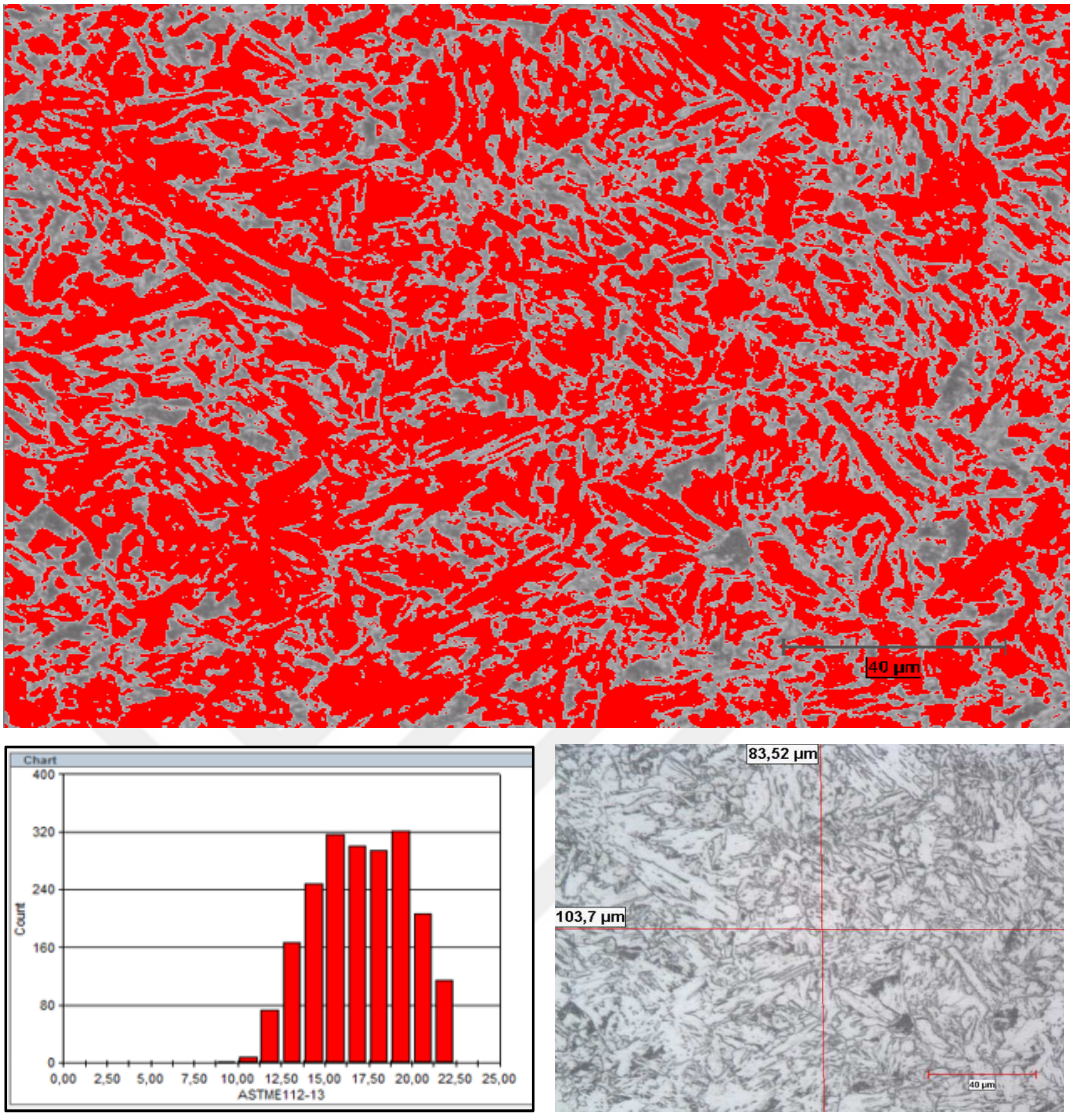

Figure 84 Grain size image of B-Slab14 (x500)

Table 31 Grain size calculation of B-Slab14

Horizontal Line (A)	103.70
Horizontal #grain (C1)	62.00
Vertical Line (B)	83.52
Vertical #grain (C2)	49.00
A / C1 = D1	1.6726
B / C2 = D2	1.7045
Ave. Value = (D1 + D2)/2 = D3	1.6885
Diameter (µm)	3.38
ASTM E112	**13.5**

B-Slab13

B-Slab13 consist of mostly ferrite phase, but some pearlitic microstructure is also obtained. The grain size distribution is generally homogeneous as G-12.0 along the plate when head-middle-end specimens are calculated averagely. The microstructure image and the grain size calculation is given in Figure 85 and Figure 86. The grain size calculation by intersection count method is given in Table 32 briefly.

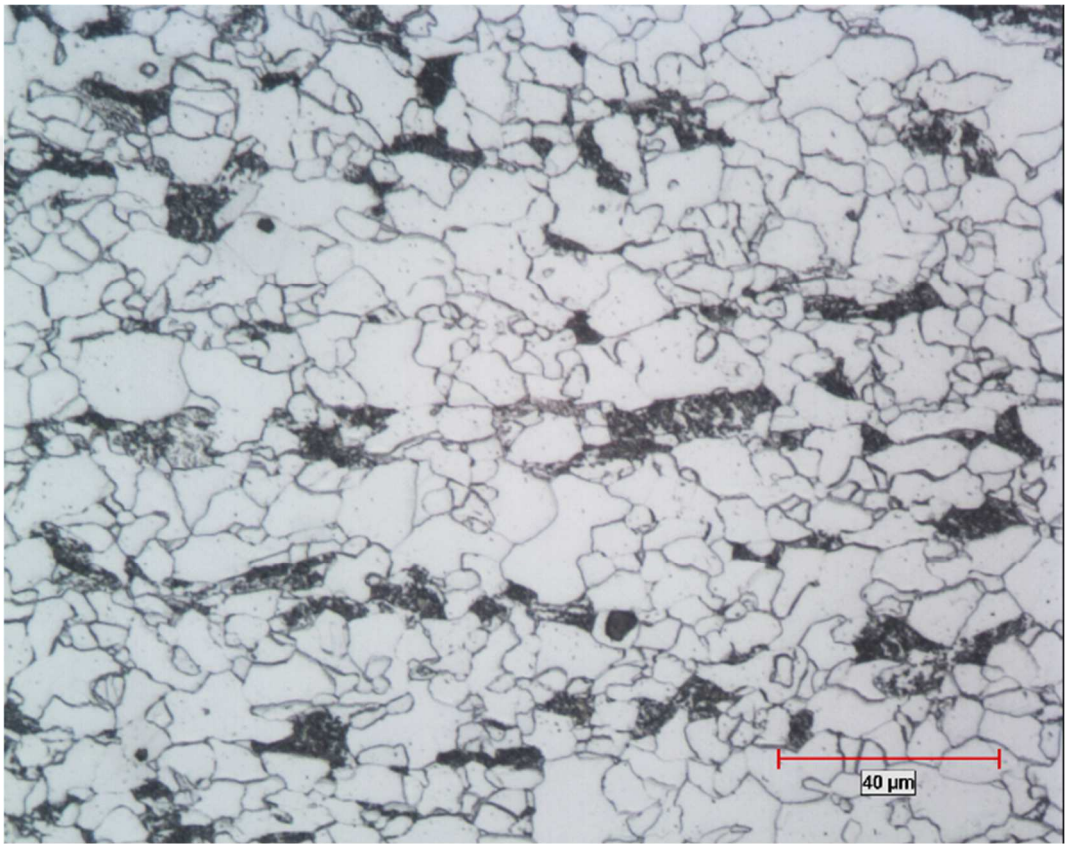

Figure 85 Microstructure of B-Slab13 (x500)

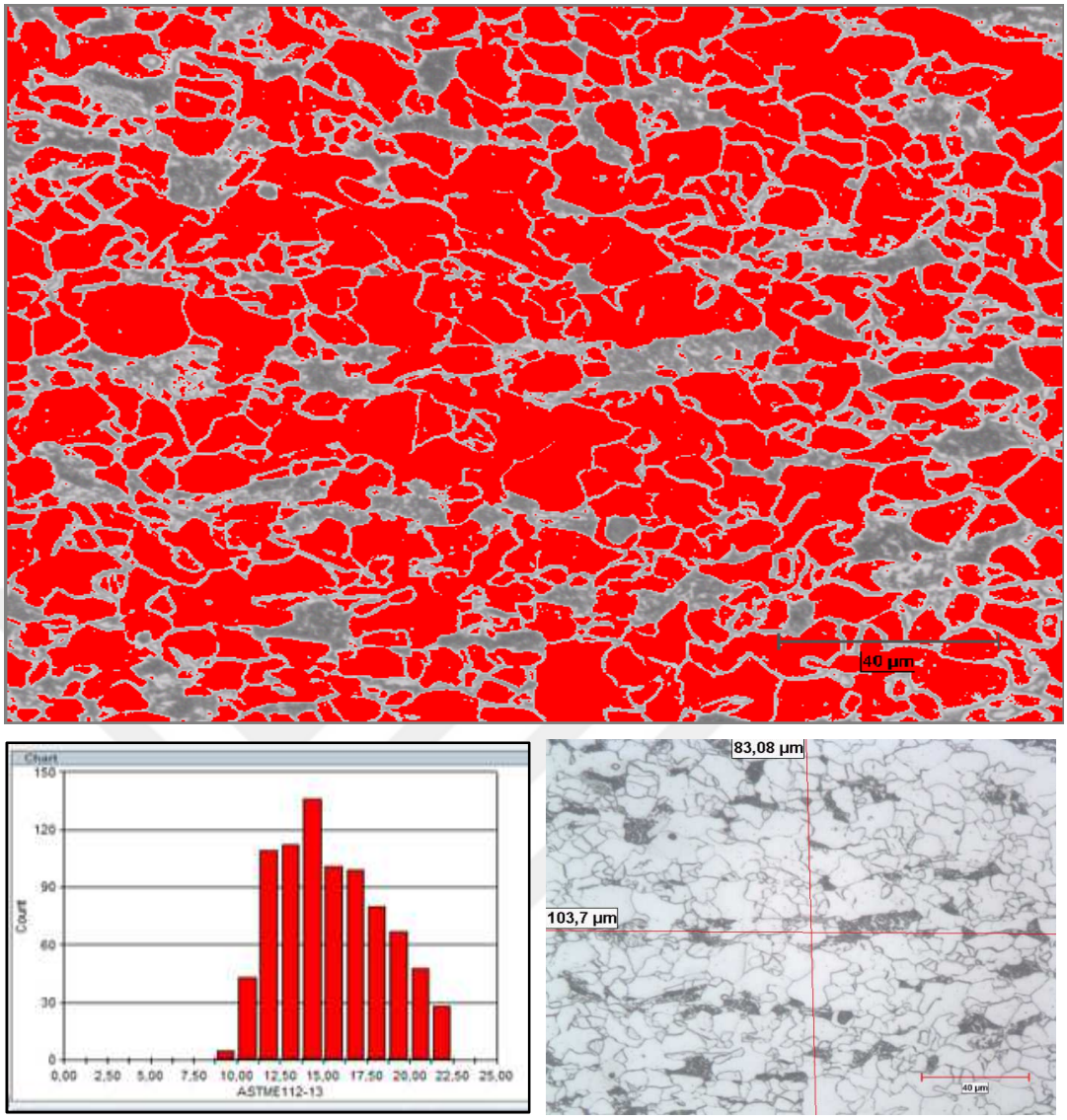

Figure 86 Grain size image of B-Slab13 (x500)

Table 32 Grain size calculation of B-Slab13

Horizontal Line (A)	103.70
Horizontal #grain (C1)	34.00
Vertical Line (B)	83.08
Vertical #grain (C2)	29.50
A / C1 = D1	3.0500
B / C2 = D2	2.8163
Ave. Value = (D1 + D2)/2 = D3	2.9331
Diameter (µm)	5.87
ASTM E112	**12.0**

B-Slab12

B-Slab12 consist of ferrite phase, but some pearlitic microstructure is also obtained. The grain size distribution is generally homogeneous as G-12.5 along the plate when head-middle-end specimens are calculated averagely. The microstructure and the grain size images are given in Figure 87 and Figure 88. The grain size calculation by intersection count method is given in Table 33 briefly.

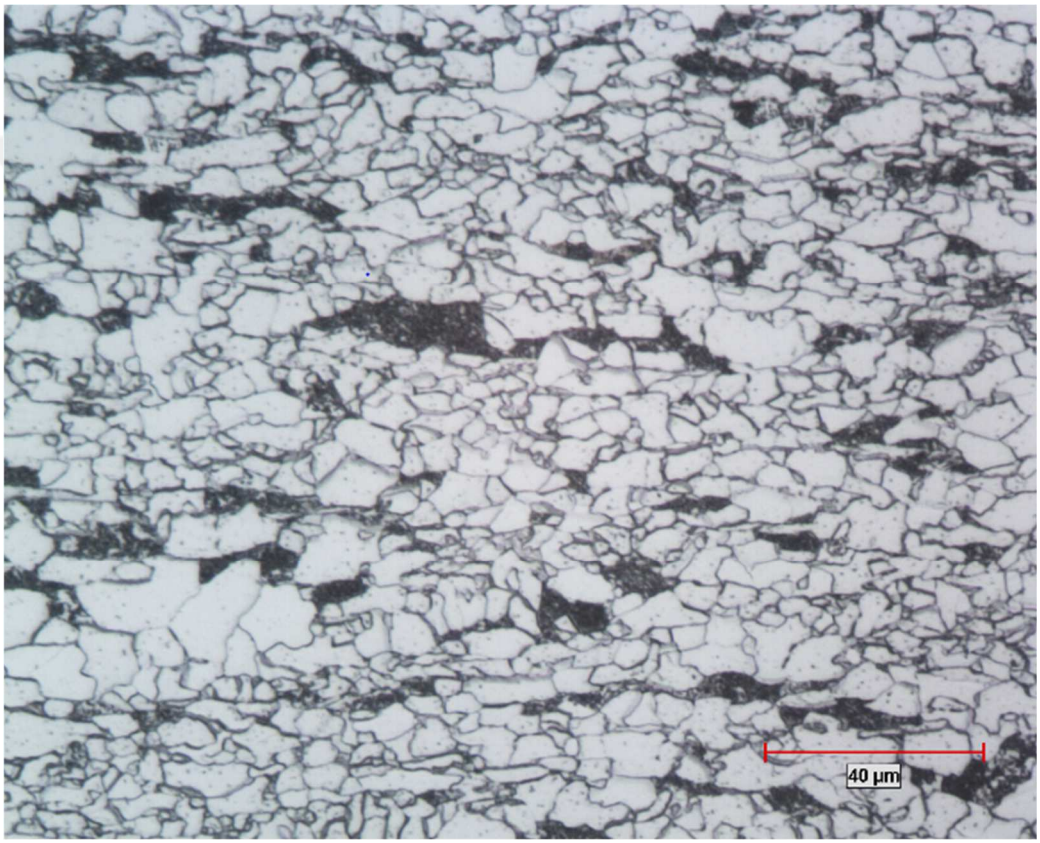

Figure 87 Microstructure of B-Slab12 (x500)

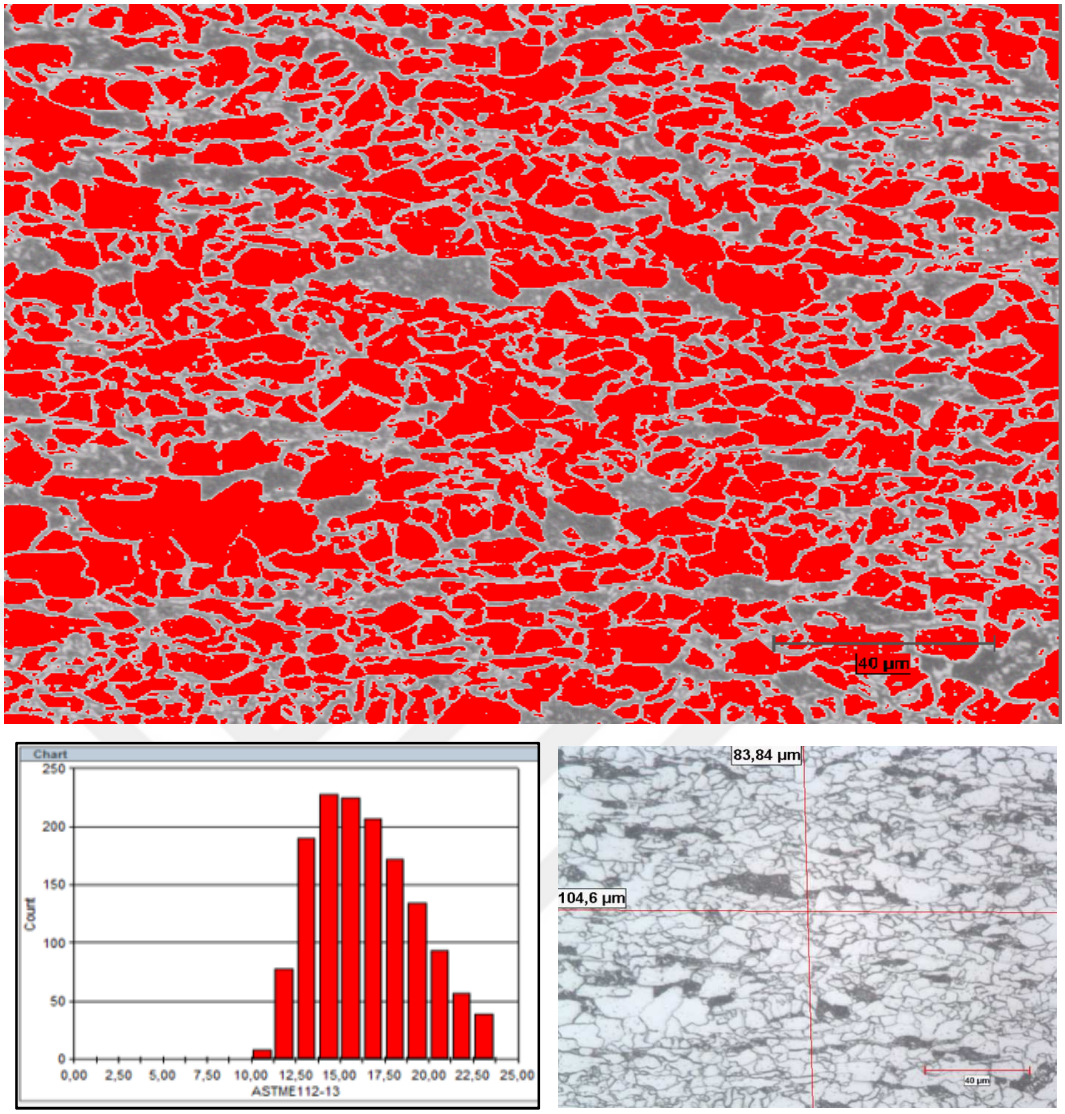

Figure 88 Grain size image of B-Slab12 (x500)

Table 33 Grain size calculation of B-Slab12

Horizontal Line (A)	103.50
Horizontal #grain (C1)	43.50
Vertical Line (B)	83.52
Vertical #grain (C2)	37.50
A / C1 = D1	2.3793
B / C2 = D2	2.2272
Ave. Value = (D1 + D2)/2 = D3	2.3033
Diameter (µm)	4.61
ASTM E112	**12.5**

4.5.2. Grain Size Analysis

The equivalent of as grain diameter according to ASTM E112 Microscopic Grain Size Relationships is given in the Table 34 [27].

The microstructure of head-middle-end specimens respectively are examined and approximate average grain size values of all samples are listed in Table 35.

Table 34 ASTM Grain Size Numbers and corresponding average grain diameters

ASTM Grain Size No	Average Grain Diameter (μm)
6.0	44.9
6.5	37.8
7.0	31.8
7.5	26.7
8.0	22.5
8.5	18.9
9.0	15.9
9.5	13.3
10.0	11.2
10.5	9.4
11.0	7.9
11.5	6.7
12.0	5.6
12.5	4.7
13.0	4.0
13.5	3.3
14.0	2.8

Table 35 Average grain size values of the samples

	Heat Treatment	ASTM Grain Size No	Average Grain Diameter (μm)
B-Slab1	Conventionally Rolled	11.5	6.9
B-Slab7	Conventionally Rolled + Cooling from 800°C	13.5	3.5
B-Slab2	950°C TCR	11.5	6.4
B-Slab8	950°C TMCP	13.0	3.9
B-Slab3	900°C TCR	12.0	5.8
B-Slab4	850°C TCR	12.0	5.7
B-Slab9	850°C TMCP	13.0	4.1
B-Slab5	800°C TCR	12.5	4.5
B-Slab6	800°C TMCP	12.5	4.6
B-Slab10	800°C TMCP	13.0	3.9
B-Slab11	750°C TMCP	13.0	4.1
B-Slab14	800°C TCR	13.5	3.4
B-Slab13	800°C TMCP	12.0	5.9
B-Slab12	800°C TMCP	12.5	4.6

4.5.3. Effects of Grain Size on Mechanical Properties

The graphs are based on the result of measurement of grain size refinement versus mechanical properties and the values are depended on consideration of industrial production conditions.

Tensile and yield strengths vs grain size is shown in Figure 89, elongation vs grain size is shown in Figure 90, impact test vs grain size is shown in Figure 91.

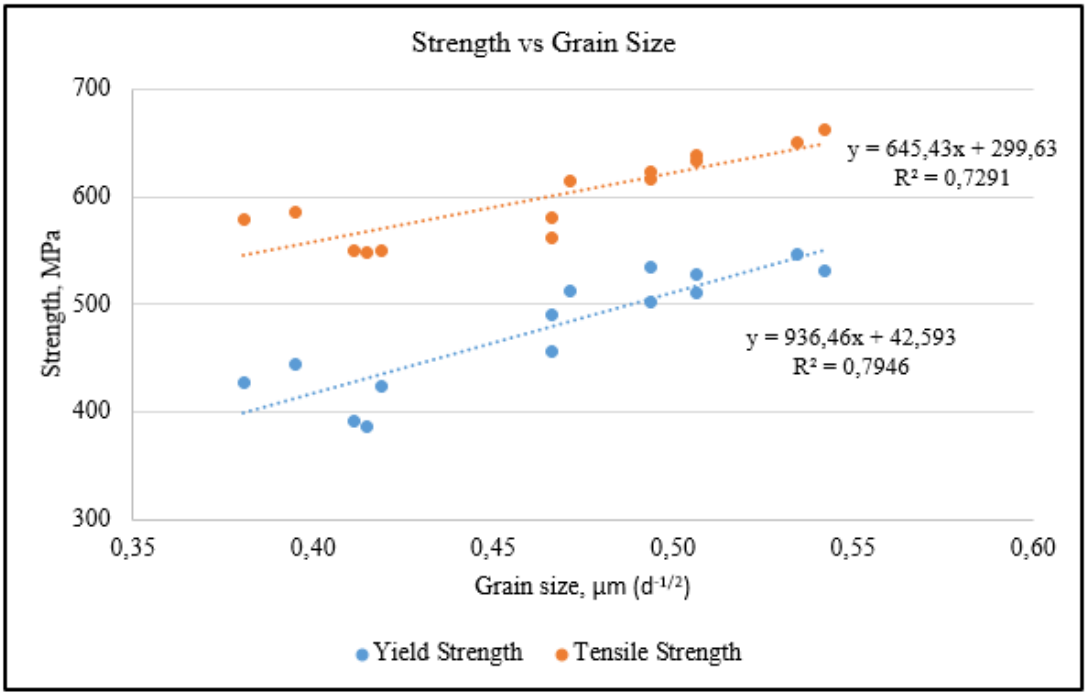

Figure 89 Tensile and yield strengths vs grain size

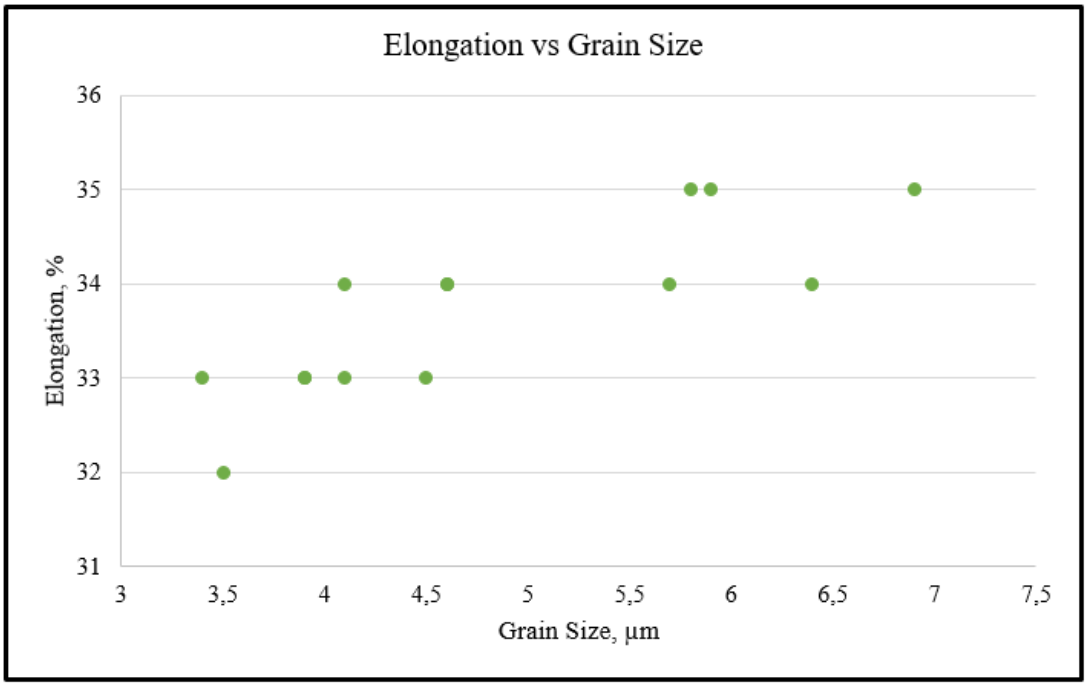

Figure 90 Elongation vs grain size

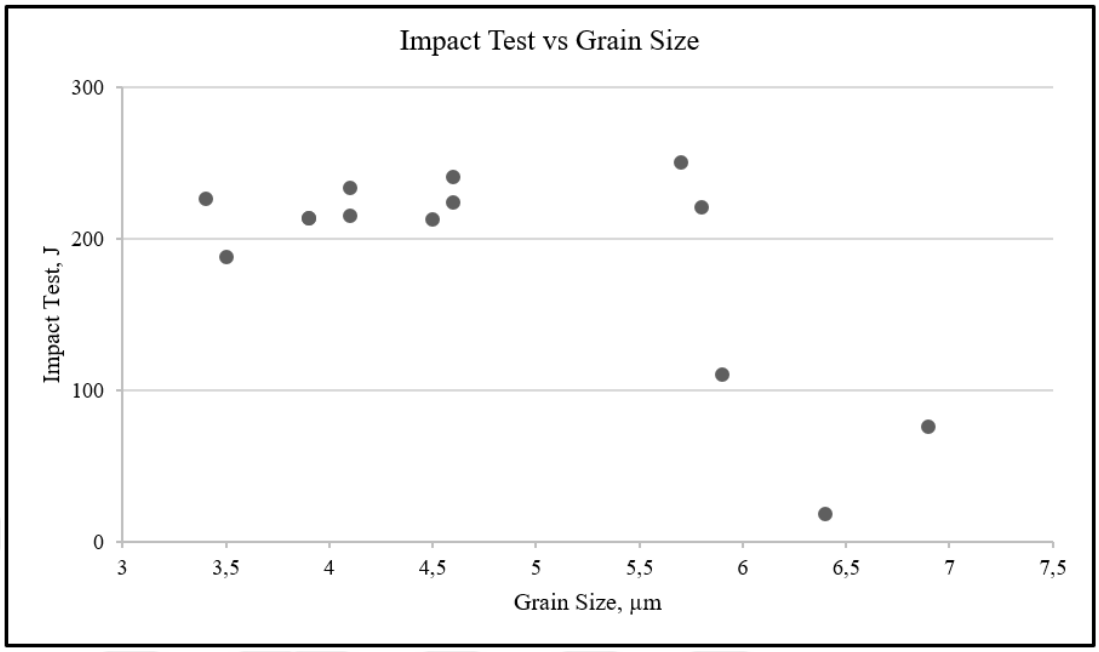

Figure 91 Impact test vs grain size

4.5.4. Effects of Temperature on Strength in TCR and TMCP

B-Slabs were rolled in different controlled temperatures and the graphs are based on controlled temperatures degrees and strength of plates. Conventionally rolled temperatures are taken as 1000°C according to the rolling conditions and the controlled temperature is started with 950°C in TCR and TMCP at 3T.

The strength of plates according to controlled temperature in TCR is given in Figure 92 and the strength of plates according to controlled temperature in TMCP is given in Figure 93.

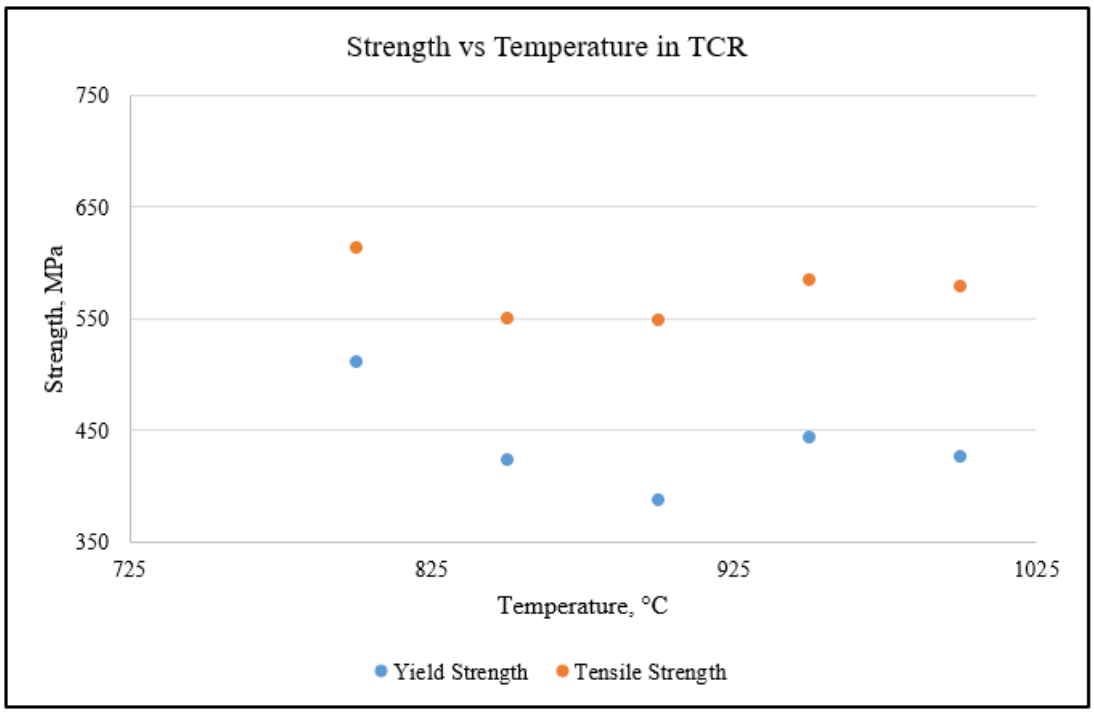

Figure 92 Strength vs controlled temperature in TCR

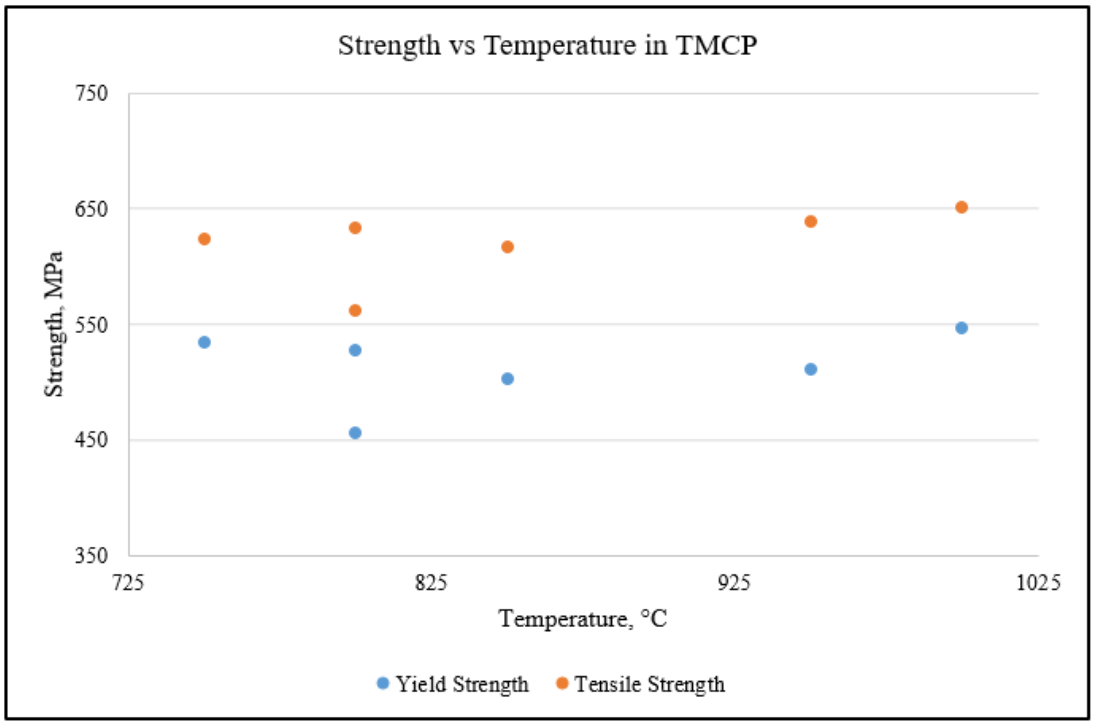

Figure 93 Strength vs controlled temperature in TMCP

4.6. Microstructural Characterization by SEM

Various microstructures are remarkable on the microstructural images taken by SEM. Generally, most of the trial plates' microstructure are composed of ferrite and pearlite composition in ferrite phase domination. Acicular ferrite and bainite microstructure can be defined, uniform and fine acicular ferrite like bainite brings high strength to steel. SEM micrographs of the plates are given in Appendix A.

4.7. Inclusion Classification of B-Slabs

Inclusions are identified by size, shape, concentration and distribution. The types of inclusions are A-Sulfide Type, B-Alumina Type, C-Silicate Type and D-Globular Oxide Type and their thickness are described as Heavy and Thin.

Inclusion rating of B-Slabs are shown in Appendix B and they are classified according to ASTM E45 Standard Test Methods for Determining the Inclusion Content of Steel [41].

4.8. Discussion

4.8.1. The Effect of Finish Rolling Temperature

Austenite non-recrystallization temperature (T_{nr}) and austenite-to-ferrite transformation start temperatures (A_{r3}) are considered to be crucial for grain size then mechanical strength and toughness in hot rolling process.

In this study, conventional process and thermomechanical rolling process were applied to the plates in the trial production. In thermomechanical rolling, the grain sizes are smaller than the conventional process.

In conventional hot rolling, the rolling started above recrystallization temperature and finished just above or below the recrystallization temperature, then recrystallization grains were occurred and getting coarser since the deformation process is finished. That is why the grains of the conventionally rolled product is larger than the thermomechanical rolled products. In addition, except for the rough rolling, the

temperature of last three passes for the deformation plays an important role in thermomechanical rolling.

Although the effect of niobium and vanadium elements restrict recrystallization and grain growth, the effects of different temperatures for last three passes deformation were noticed in this study.

Almost strength and toughness of all the plates comply with the API X60M grade with thermomechanical rolling due to the alloying elements in the chemical composition. According to mechanical properties, controlled temperature rolling in 800°C and 850°C with TCR satisfies the API X70M grade properties. Thus, as the grain size decreases, then mechanical properties, strength, toughness and ductility increases.

4.8.2. The Effect of Partitioning of the Total Reduction between the Rough and Finish Rolling Phases

In order to investigate the reduction ratio effects on rolling process in thermomechanical control rolling, controlled temperature in the last three passes was started at two times final thickness (2T), three times final thickness (3T) and four times final thickness (4T). Although the purpose is to catch the finest grain size, the industrial process was not gone as expected. In the 4T, the number of last three passes increases to five passes due to the thickness, so the thermomechanical control process became out of order.

The results of TCR at 4T meet the API X70 grade, but ductility was not enough for PSL2. The results of TMCP at 4T do not meet the API X60 or API X70 grade due to the mechanical properties. On the other hand, the results of TMCP at 2T meet the requirements of API X70M grades due to the DWTT. The microstructure images of TCR plates at 2T and 4T are given in Figure 94.

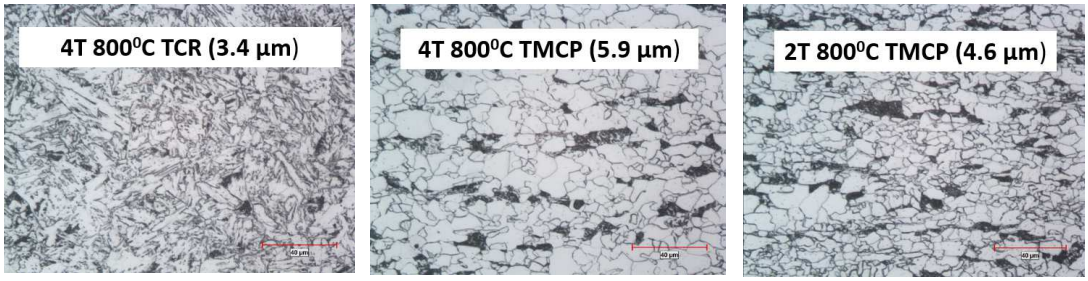

Figure 94 The microstructure images of TCR plates at 2T and 4T (x500)

4.8.3. The Effect of Accelerated Cooling

Thermomechanical control process is an improved process of controlled temperature and cooling operations while rolling of plates. Measuring temperature of plates at multiple locations and implement cooling operation with showering water provides hardening effect and more strength to the plates. Refined and uniform grain size leads to increase in strength, toughness, and ductility.

The production of API X70 grade was accomplished by TCMP. Especially the controlled rolling temperature in 800°C and 850°C with TCMP satisfies the mechanical requirements of API X70M with well ductility. This is the result of fine grain practice in TMCP.

The controlled rolling temperature in 750°C, which was calculated before as a $A_{r3,}$ beginning of the transformation of austenite phase to ferrite phase, forced the rolling mills, thus the last three passes for controlled rolling started at 770°C and with the help of cooling process, the mechanical test results and ductility property also satisfy the API X70M.

Therefore, controlled rolling temperature below T_{nr} temperature and just above A_{r3} temperature result in the best results. In addition, cooling process stops the grain growth that gives the product more strength, toughness and ductility in TMCP.

The microstructure images of conventional rolled plates, TCR plates and TMCP plates are given in Figure 95 and Figure 96.

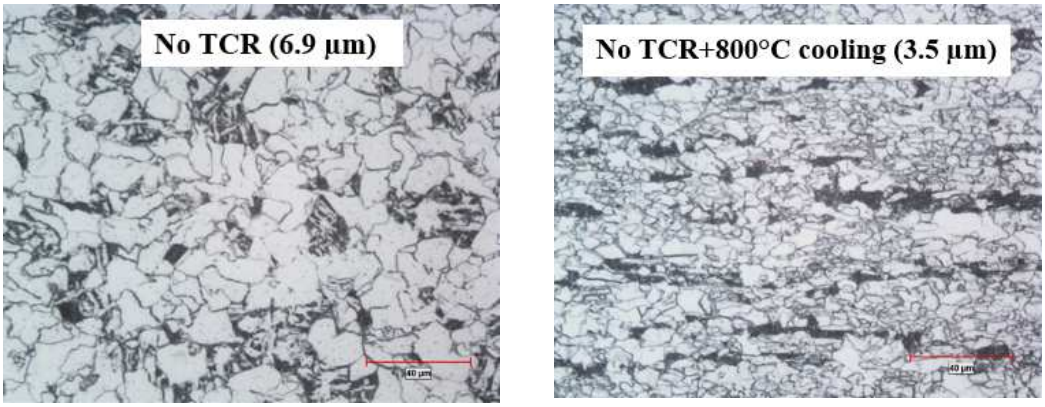

Figure 95 The microstructure images of conventional rolled plates (x500)

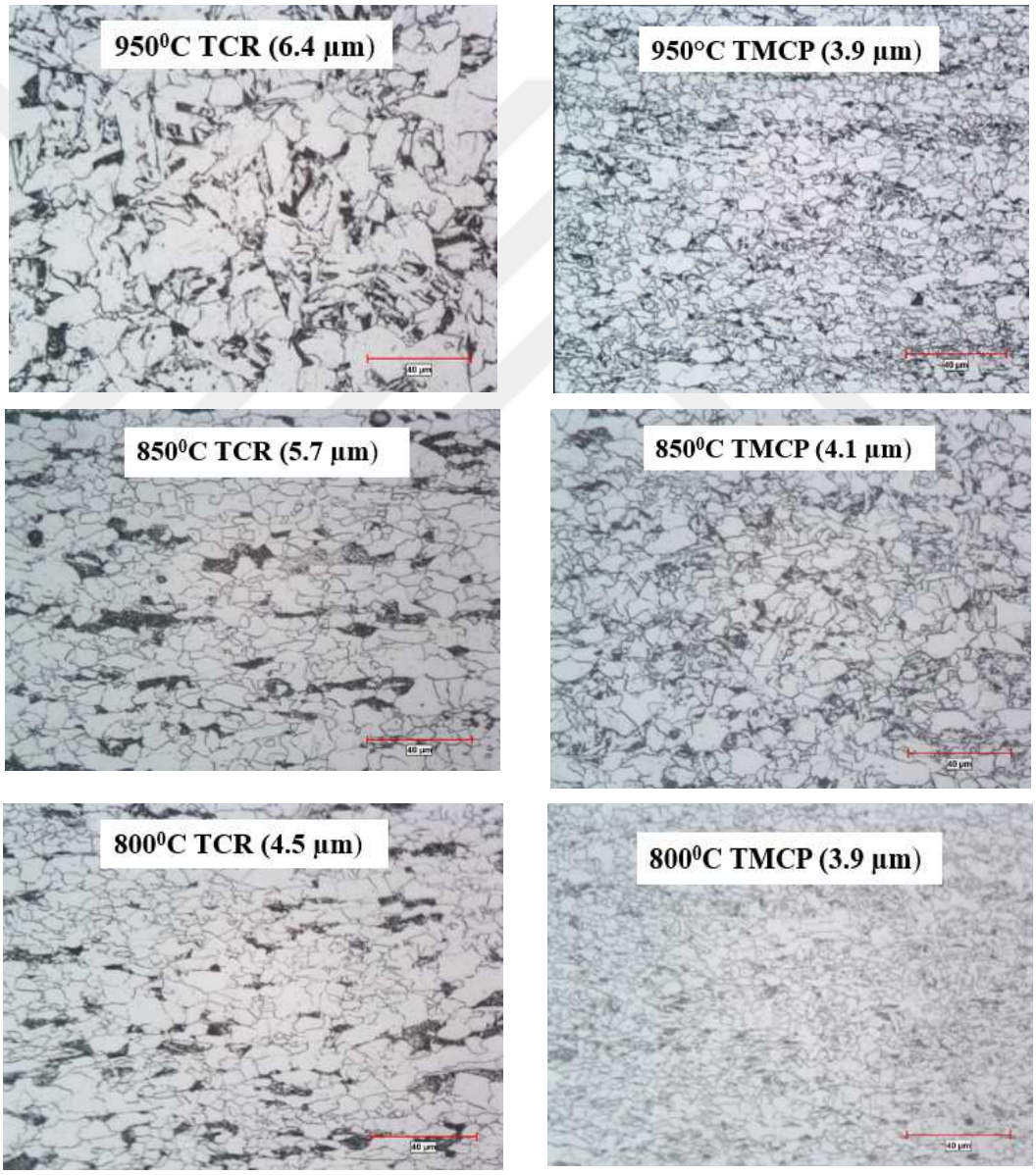

Figure 96 The microstructure images of plates at 3T (x500)

CHAPTER 5

CONCLUSIONS

5.1. Conclusions

The objective of this study was to determine the conditions API X60-X70 grade high strength low alloyed steels as plates for pipeline customers. Although, thermomechanical controlled rolling method which needs just control of temperature while rolling is sufficient for API-X60 grade, thermomechanical controlled process is needed with accelerated cooling process for API-X70 grades.

Temperature control is indispensable for uniform grain refinement in thermomechanical rolling. The temperature of final three pass during rolling should be taken just above the Ar_3 phase transformation temperature. In this study, Ar_3 temperature is approximately 750°C according to chemical analysis and in actual the best mechanical test results were attained in temperatures of 800°C in controlled rolling.

The toughness of steel has been found to increase by the accelerated cooling process. The best results of the DWTT test were obtained from the specimens of accelerated cooling process.

In microstructure, ferrite grain refinement occurs obviously with decrease in thermomechanical control temperature that results in strength and toughness at the same time. Ferrite-pearlite combination and for some regions bainite phase are obtained in addition acicular ferrite microstructure is obtained in temperature 800°C with cooling just after rolling process. Acicular ferrite microstructure with low carbon content offers a perfect combination of high strength and high toughness.

The major findings and accomplishments of this work are:

- Rolling and cooling conditions to produce 20 mm thick steel plates compliant to API-5L PSL2 X60 and X70 grades have been determined.
- Finish rolling at a temperature range of 750-850°C gave the best combination of the mechanical properties.
- It is found that there is an optimum partitioning of the total amount of reduction between the rough and finish rolling phases.

5.2. Suggestions for Future Work

- Production trials should be performed using full size slabs in order to explore repeatability and homogeneity of the results found.
- Further studies should be planned to maximize the strength values of the plates without sacrificing toughness and ductility. For example, a time controlled rough rolling schedule needs to be developed in order to fully benefit from the recrystallization behavior of austenite.
- Slabs with reduced alloying element concentrations (Nb, Ti, V) should be tried.
- In this study, API X60-X70 grades plates were produced with 20 mm in thickness and 1000 mm in width due to the slab dimensions. On the other hand, plates among 1000-3600 mm in width can be manufactured by reversing mill. In the future, the production of plates with width measurements of 2500 mm or more can be tried.

REFERENCES

[1] API, American Petroleum Institute, Oil and Natural Gas Transporting Pipeline, 05/06/2018, www.api.org.

[2] Tekin, E, API Standardı Petrol ve Doğalgaz Boru Çeliklerine Genel Bakış, 2012, Metalurji Mühendisleri Odası Dergisi, no 162, pp. 23-33.

[3] Shin, S.Y., Hwang, B., Lee, S., Kim N.J., Ahn, S.S., Correlation of microstructure and charpy impact properties in API X70 and X80 line-pipe steels, Materials Science and Engineering A 458, 2007, pp. 281–289.

[4] API Specification 5L, Specification for Line Pipe, Forty-Fifth Edition, December, 2012, Errata 1, April 2015, American Petroleum Institute, pp. 13-49.

[5] Xinlinsteel news, Shanghai Xin Lin Co., Ltd., 10/11/2013, http://www.xinlinsteel.com/news/news_show-76.html.

[6] Erdemir, Basic oxygen process, Metallurgy, Encyclopedia Britannica, 05/06/2018, www.erdemir.com.tr/corporate/story-of-steel/.

[7] Türk, U., Entegre Demir Çelik Tesislerinde Çelik Üretimi (Bazik Oksijen Fırını-BOF), 02/06/2018, http://www.muhendisalemi.com/celik-uretimi-bazik-oksijen-firini-bof/

[8] Kundakçı, K., Termomekanik haddeleme yöntemi ile levha üretimi ve karekterizasyonu, Yüksek lisans tezi, Gebze Yüksek Teknoloji Enstitüsü, Mühendislik ve Fen Bilimleri Enstitüsü, 2010, pp. 9-28.

[9] Jonsson, M., TM-Rolling of Heavy Plate and Roll Wear, Luleå University of Technology, Department of Applied Physics and Mechanical Engineering, Division of Material Mechanics, Licentiate Thesis, Sweden, 2006, pp. 1-9.

[10] Siemens VAI, Plate Mill Model – Descriptions, Standard Design Specification, Document No. STD-PM-MODEL-DESC, Version 1.0, March 2005, pp. 1-99.

[11] Barsom, J.M., High Performance Steels and Their Use in Structures, Proceedings of the International Symposium on High Performance Steels for Structural Applications, Pittsburgh, Pennsylvania, USA, CONF-951026- ISBN 0-87170-555-9, U.S. Steel Group, 1995.

[12] Wusatowski, Z., Fundamentals of Rolling, Polytechnical University, Gliwice, Poland, Pergamon Press, 1969, pp. 15-19.

[13] Hillenbrand, H.G, Gras, M and Kalwa, C., Development and production of high strength pipeline steel, International Symposium Niobium 2001, December 02-05, 2001, Orlando, Florida, USA.

[14] Prakasan, N., High strength low alloy steels, slayt 9, published in Technology, 9 Jun 2013, Business, www.slideshare.net/N.Prakasan/hsla-steels.

[15] Benz, J.K., Thomson, S.W., Effect of Vanadium on the Hardening of Low-Carbon Microalloyed Steels during an experimental time temperature study, AISTECH 2018: The Iron & Steel Technology Conference and Exposition, May 7-10, 2018, Philadelphia, PA, USA, pp. 221-224.

[16] Ataçelik, Çeliğe alaşım elementlerinin etkileri, Ataçelik Dökümhanesi, 01/06/2018, http://www.atacelik.com/etkileri.html.

[17] Dökümhane, Çeliklerde alaşım elementlerinin etkileri, Türk Döküm Sektörünün Eğitim Platformu, 25/01/2017, https://dokumhane.net/2017/01/25/celiklerde-alasim-elementlerinin-etkileri/

[18] Malcolm, G.J., Kirkwood, P.R., Evolution of Niobium Microalloyed Line Pipe Steels and Associated Welding Technology, AISTECH 2018: The Iron & Steel Technology Conference and Exposition, May 7-10, 2018, Philadelphia, PA, USA, pp. 189-191.

[19] Avner, S.H., Introduction to Physical Metallurgy, Second Edition, New York, Indian Edition, Mc Graw Hill Book Company, 1974, pp. 355-369.

[20] Zheng, L., Gao, S., Microstructure and Properties of Pipeline Steel with Acicular Ferrite, Baoshan Iron & Steel Co. Ltd., Materials Science Forum Online, ISSN: 1662-9752, Vols. 539-543, Shanghai 201900, China, 15/03/2007, pp. 4750-4755.

[21] Ginzburg, V.B., Flat-Rolled Steel Processes, Advanced Technologies, chapter 4, CRC Press, 2009, pp. 55-60.

[22] Wright, William J., Steel Bridge Design Handbook, Bridge Steels and Their Mechanical Properties, Washington, D.C. 20590 Publication No FHWA-IF-12-052 - Vol. 1, November 2012, pp. 15-20.

[23] Yoshıe, A., Fujioka, M., Watanabe, Y., Nıshıoka, K., Morıkawa, H., Modelling of Microstructural Evolution and Mechanical Properties of steel plates produced by Thermomechanical Control Process, ISIJ International, Vol 32, 1992, pp. 395-404.

[24] Shigeru, E., Naoki, N., Development of Thermo-Mechanical Control Process (TMCP) and High Performance Steel in JFE Steel, JFE Technical Report No 20, 2015, pp. 1-6.

[25] Gorni, A.A., Silveira, J.H., Accelerated Cooling of Steel Plates, The Time Has Come, Journal of ASTM International, Vol. 5, No 8, Paper ID JAI101777, 2008, pp. 1-7.

[26] JMatPro-V10, Sente Software, Ltd., Surrey Research Park, Guildford GU2 7YG, United Kingdom

[27] ASTM E112-13, Standard Test Methods for Determining Average Grain Size, ASTM Standard, 2013, pp. 1-28.

[28] Andres, C.G., Bartolome, M.J., Capdevila, C., San Martın, D., Caballero, F.G., Lopez, V., Metallographic techniques for the determination of the austenite grain size in medium-carbon microalloyed steels, Materials Characterization, Volume 46, Issue 5, May 2001, pp. 389-398

[29] Digges, T.G., Rosenberg, S.J., Heat Treatment and Properties of Iron and Steel, Arizona Library, U.S. Department of Commerce, National Bureau of Standards, 1960, pp. 2-11.

[30] ASM International, Fundamentals of the Heat Treating of Steel, Practical Heat Treating, chapter 2, Second Edition, 2006, pp. 1-18.

[31] Manna, R., Heat Treatment, Assistant Professor Centre of Advanced Study Department of Metallurgical Engineering, Institute of Technology, Banaras Hindu University, India, 12/03/2018, https://www.phase-trans.msm.cam.ac.uk.

[32] Gomez, M., Oscar, H., Sebastian, M., Pascual, T., Determination of Residual Stress and Critical Rolling Temperatures in a Microalloyed Steel with Low Carbon and Niobium Contents, October 2002, Steel Research 73(10) pp. 446-452

[33] Mishra, D.K., Thermo-mechanical Processing of API-X60 Grade Pipe Line Steel, Master in Technology in Mechanical Engineering, Department of Metallurgical and Materials Engineering National Institute of Technology, May 2014, pp. 5-20.

[34] Homsher, C.N., Determination of the non-recrystallization temperature in multiple microalloyed steels, Thesis in Colorado School of Mines, Publication Number AAT 1535618, ISBN 9781303018862, 2013, pp. 15-70.

[35] Takayama, N., Murakami, Y., Murota, Y., Nishimachi, R., Heavy-Thickness, Abrasion-Resistant Steel Plate with Excellent Low-Temperature Toughness, AISTECH 2018: The Iron & Steel Technology Conference and Exposition, May 7-10, 2018, Philadelphia, PA, USA, pp. 411-413.

[36] Quchi, C., Sampei, T., and Kozasu, I., The Effect of Hot Rolling Condition and Chemical Composition, Research Article, Transactions ISIJ, Vol. 22, 1982, pp. 214-221.

[37] ASTM A370-17a, Standard Test Methods and Definitions for Mechanical Testing of Steel Products, ASTM Standard, 2017, pp. 1-50.

[38] API-5L3, Drop-Weight Tear Tests on Line Pipe, Fourth Edition, API Recommended Practice 5L3, Copyright American Petroleum Institute, August 2014, pp. 1-20.

[39] ASTM E436-03 (Reapproved 2014), Standard Test Method for Drop-Weight Tear Tests of Ferritic Steels, ASTM Standard, 2014, pp 1-6.

[40] CLEMEX, Clemex Technologies Inc., Longueuil, Quebec, J4G 1T5, Canada

[41] ASTM E45-18, Standard Test Methods for Determining the Inclusion Content of Steel, ASTM Standard, 2018, pp. 1-19.

APPENDICES

A. SEM INVESTIGATION OF THE SAMPLES

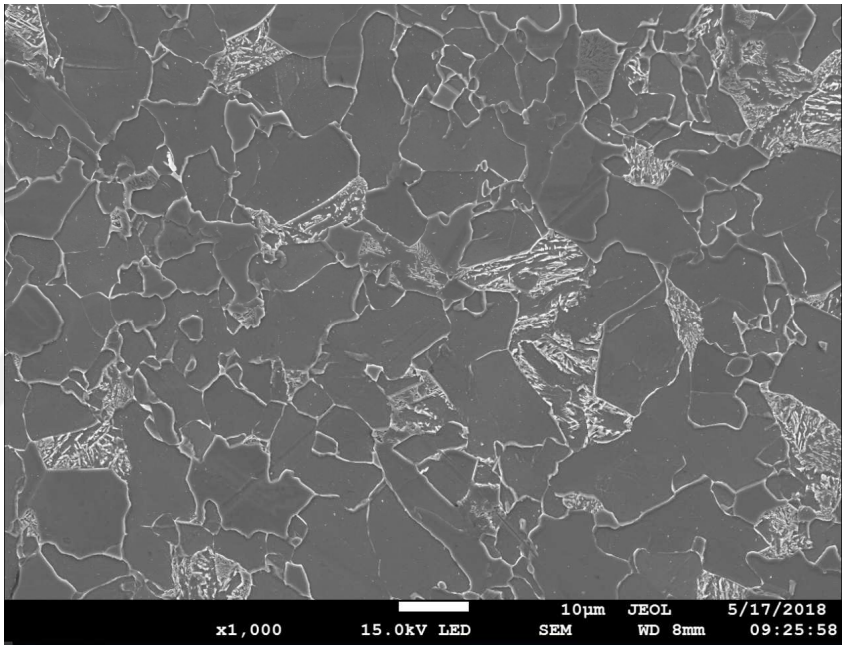

Figure A-1 Image of B-Slab1 by SEM

Ferrite is dominant in ferrite-pearlite microstructure as seen in Figure A-1. Although the ferrite phase is dominant in microstructure, ferrite-pearlite microstructure is obtained.

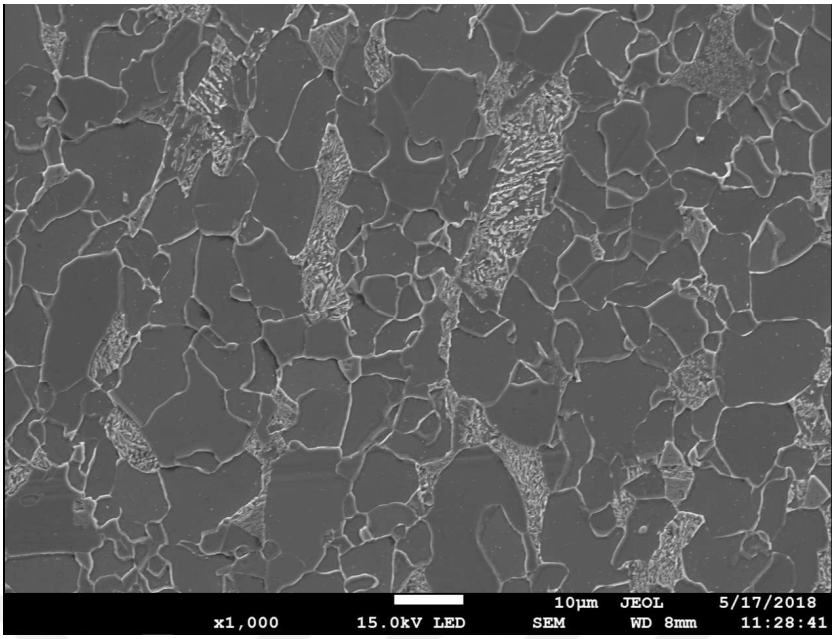

Figure A-2 Image of B-Slab7 by SEM

The grain boundaries are definite. In some regions, bainite is obtained (Figure A-2).

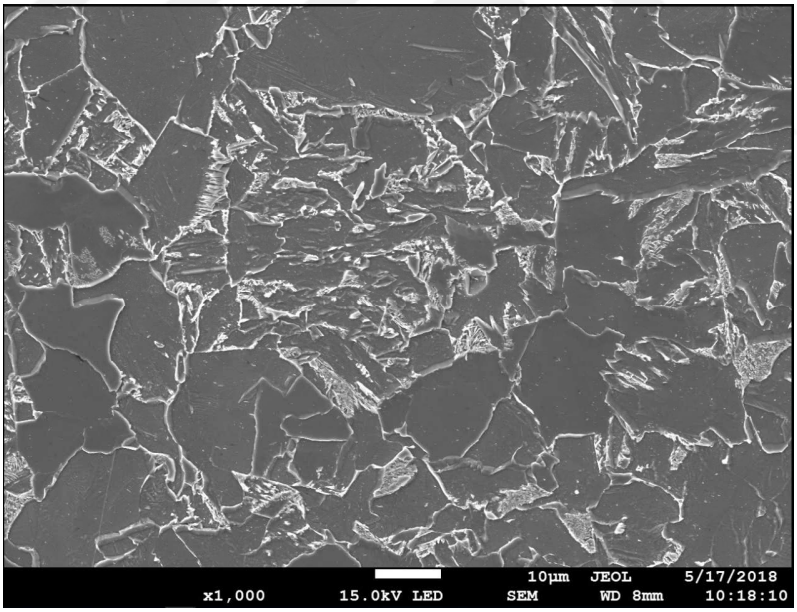

Figure A-3 Image of B-Slab2 by SEM

Although the ferrite phase is dominant in microstructure, ferrite-pearlite microstructure is obtained. In some regions, acicular ferrite is obtained (Figure A-3).

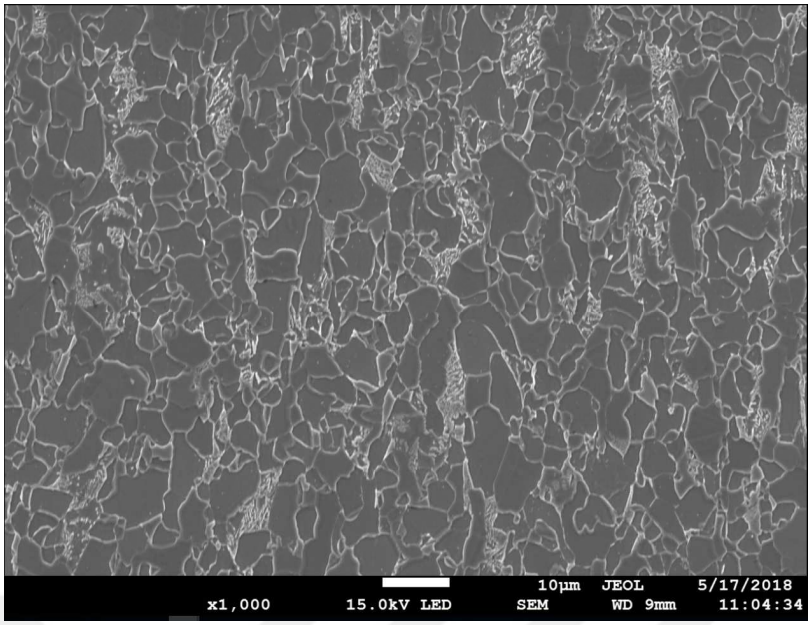

Figure A-4 Image of B-Slab8 by SEM

Ferrite phase is dominant in microstructure. Pearlite is also obtained. The grain boundaries are definite. In some regions, upper bainite phase is obtained (Figure A-4).

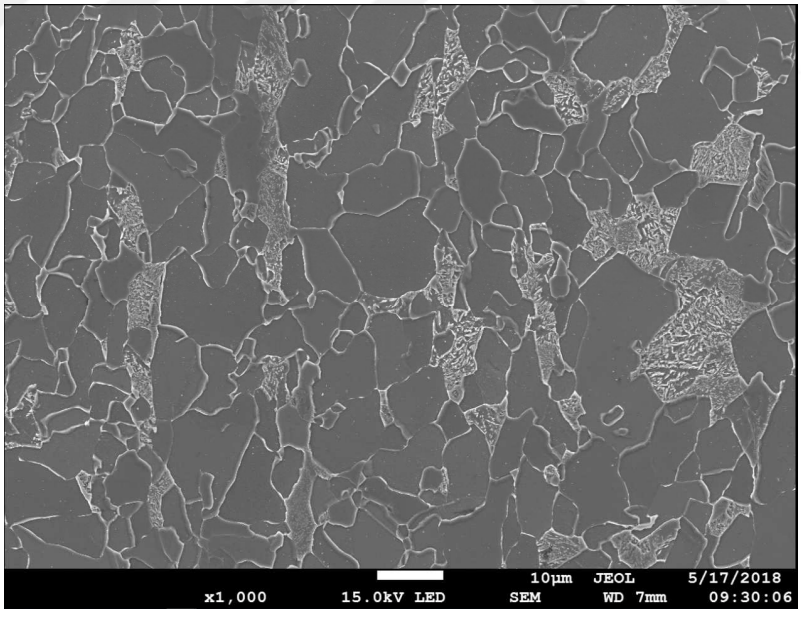

Figure A-5 Image of B-Slab3 by SEM

Although the ferrite phase is dominant in microstructure, fine and coarse pearlite is obtained in microstructure (Figure A-5).

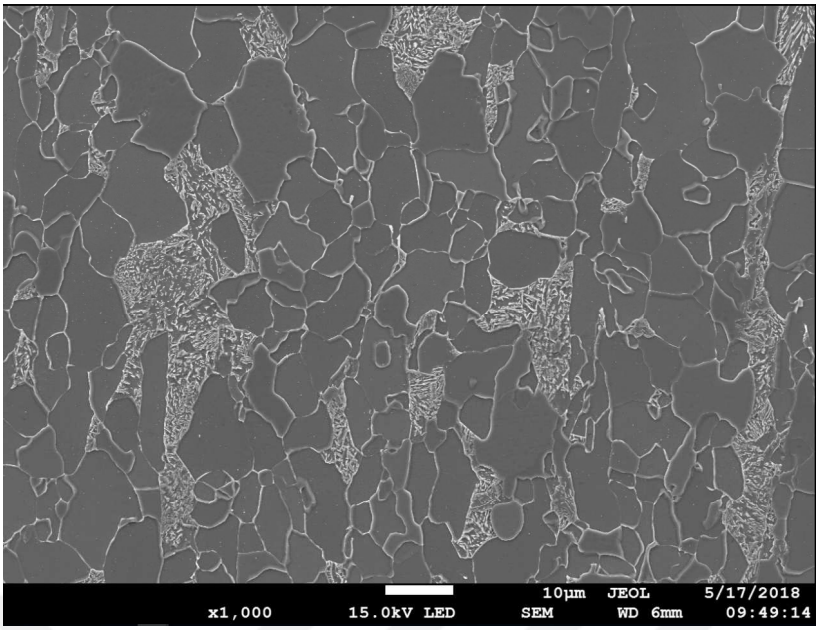

Figure A-6 Image of B-Slab4 by SEM

Ferrite phase is dominant, fine and coarse pearlite is obtained in microstructure (Figure A-6).

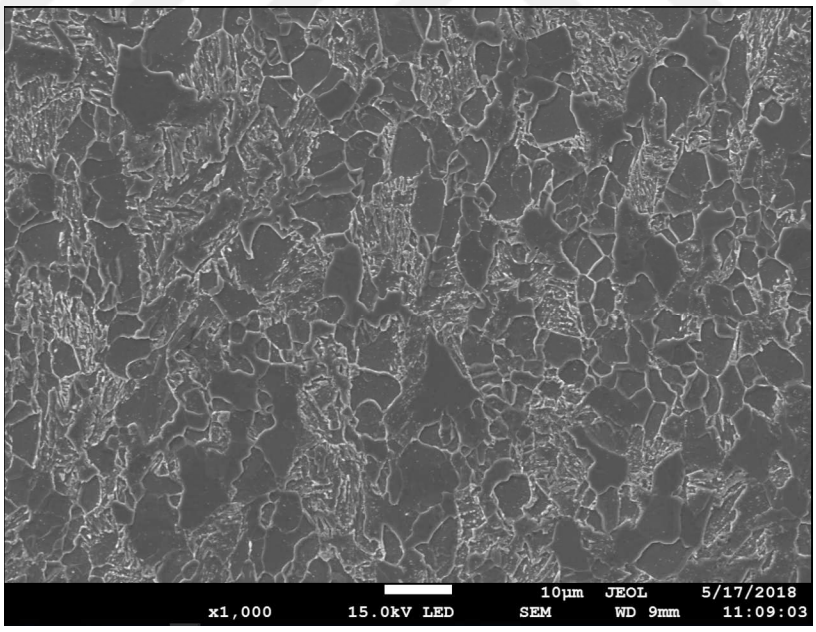

Figure A-7 Image of B-Slab9 by SEM

Ferrite phase is dominant in microstructure. Small amount of pearlite is also obtained. The grain boundaries are definite and upper bainite phase can be distinguished (Figure A-7).

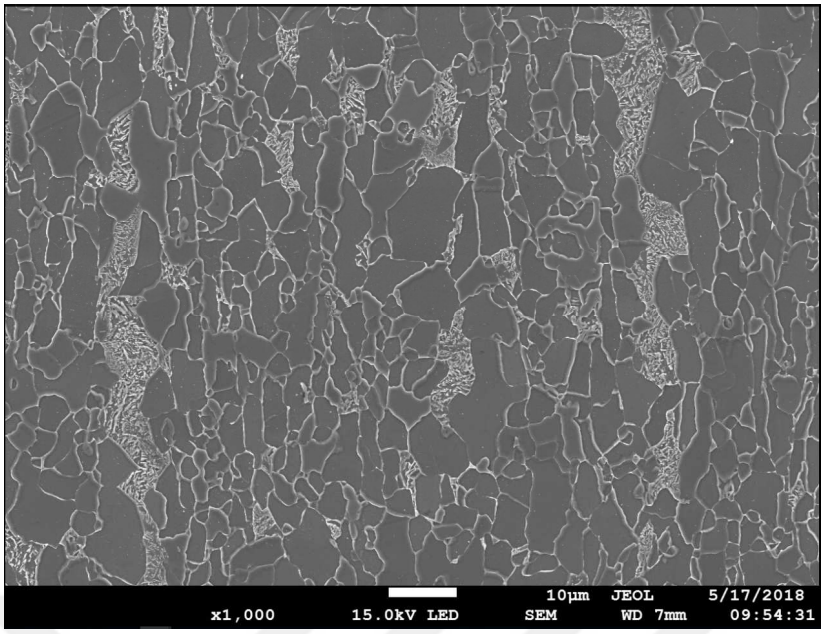

Figure A-8 Image of B-Slab5 by SEM

Ferrite phase is dominant in microstructure and ferrite-pearlite microstructure is obtained. In some regions, bainite is obtained (Figure A-8).

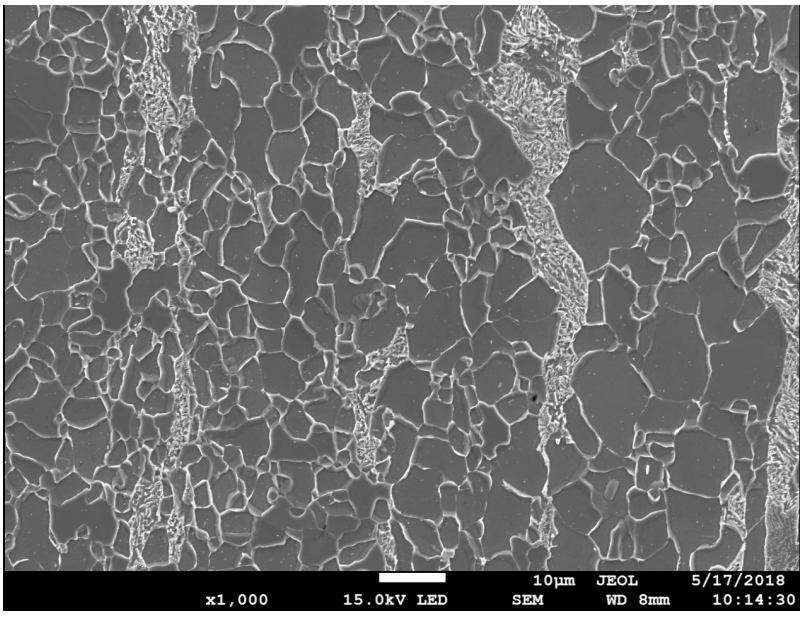

Figure A-9 Image of B-Slab6 by SEM

Ferrite phase is dominant in ferrite-pearlite microstructure. Lower bainite is also obtained (Figure A-9).

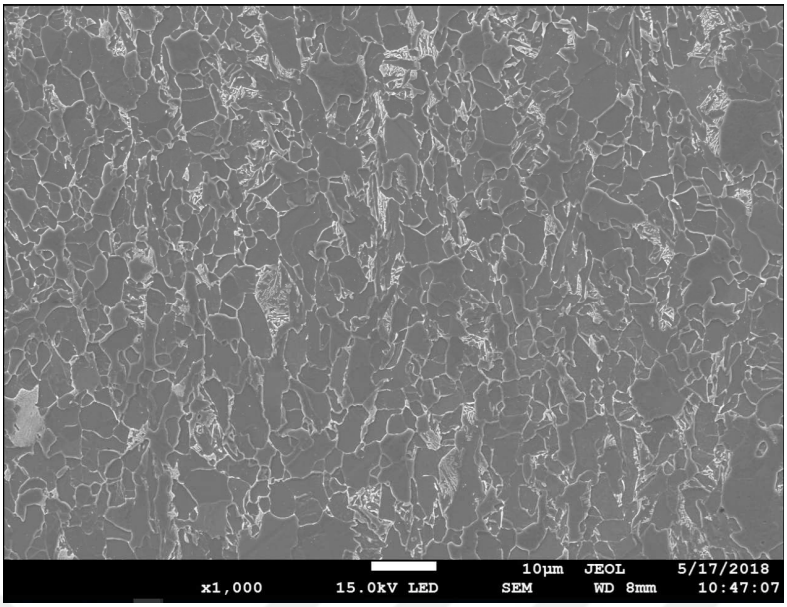

Figure A-10 Image of B-Slab10 by SEM

Ferrite phase is dominant in ferrite-pearlite microstructure. Lower bainite is obtained (Figure A-10).

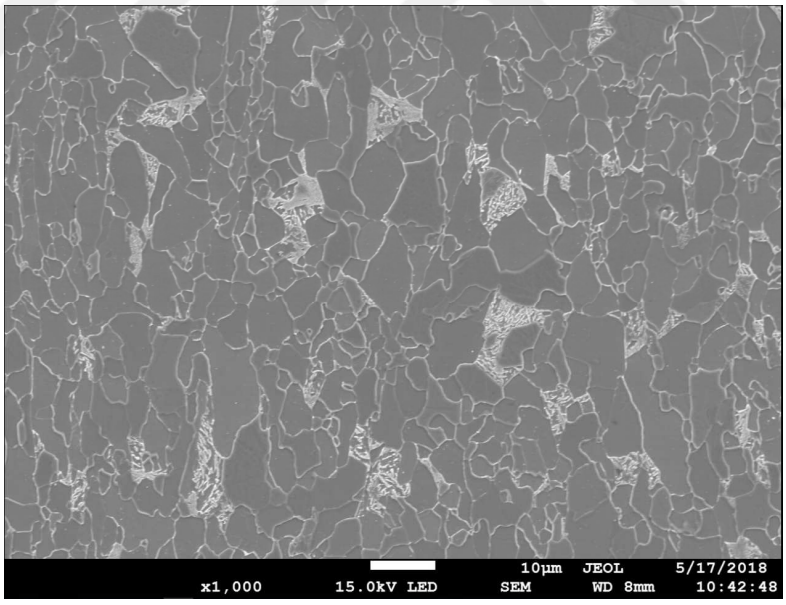

Figure A-11 Image of B-Slab11 by SEM

Ferrite phase is dominant in ferrite-pearlite microstructure. Although not very clear, bainite can be distinguished (Figure A-11).

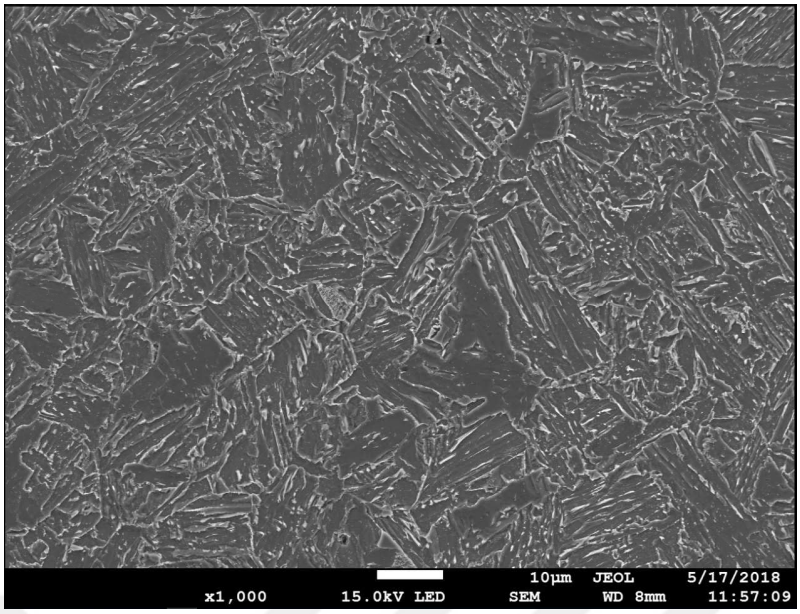

Figure A-12 Image of B-Slab14 by SEM

Ferrite phase is dominant. Acicular ferrite and bainite is obtained and in some regions, small amount of martensitic structure can be seen (Figure A-12).

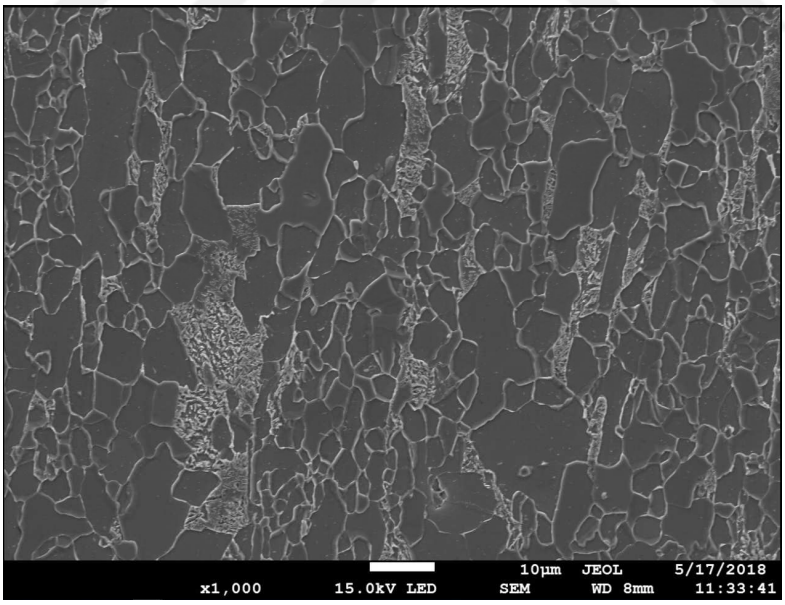

Figure A-13 Image of B-Slab13 by SEM

Ferrite phase is dominant and coarse pearlite is obtained in ferrite-pearlite microstructure (Figure A-13).

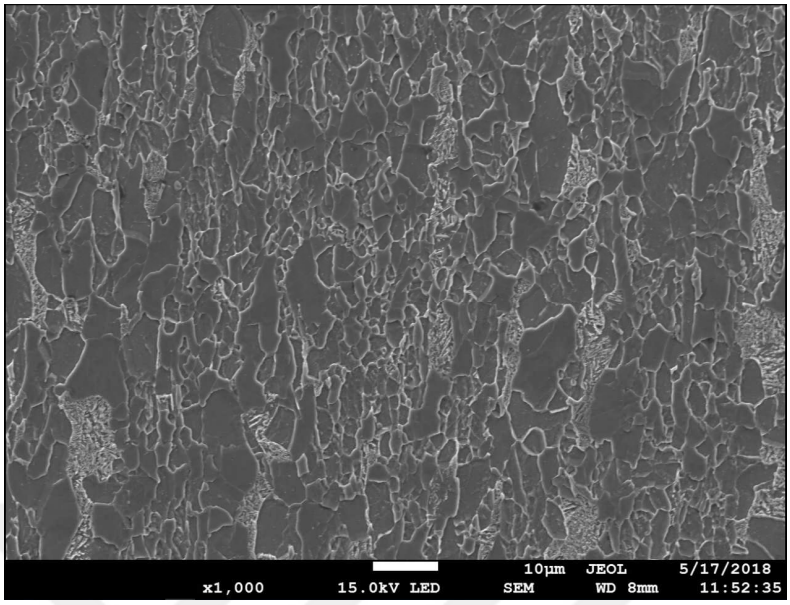

Figure A-14 Image of B-Slab12 by SEM

Ferrite and pearlite is obtained in microstructure (Figure A-14).

B. INCLUSION CLASSIFICATION OF THE SAMPLES

B-Slab1 has D-Globular Oxide Type, Thin, 2 as shown in Figure B-1

Figure B-1 Inclusion rating of B-Slab1

B-Slab7 has D-Globular Oxide Type, Thin, 3 as shown in Figure B-2

Figure B-2 Inclusion rating of B-Slab7

B-Slab2 has D-Globular Oxide Type, Thin, 3 as shown in Figure B-3

Figure B-3 Inclusion rating of B-Slab2

B-Slab8 has D-Globular Oxide Type, Thin, 2 as shown in Figure B-4

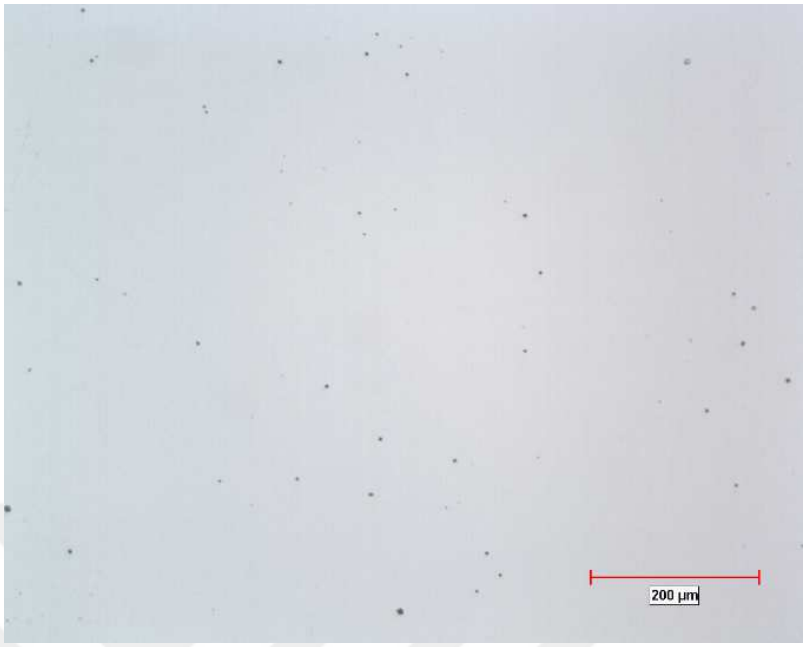

Figure B-4 Inclusion rating of B-Slab8

B-Slab3 has D-Globular Oxide Type, Thin, 3 as shown in Figure B-5

Figure B-5 Inclusion rating of B-Slab3

B-Slab4 has D-Globular Oxide Type, Thin, 3 as shown in Figure B-6

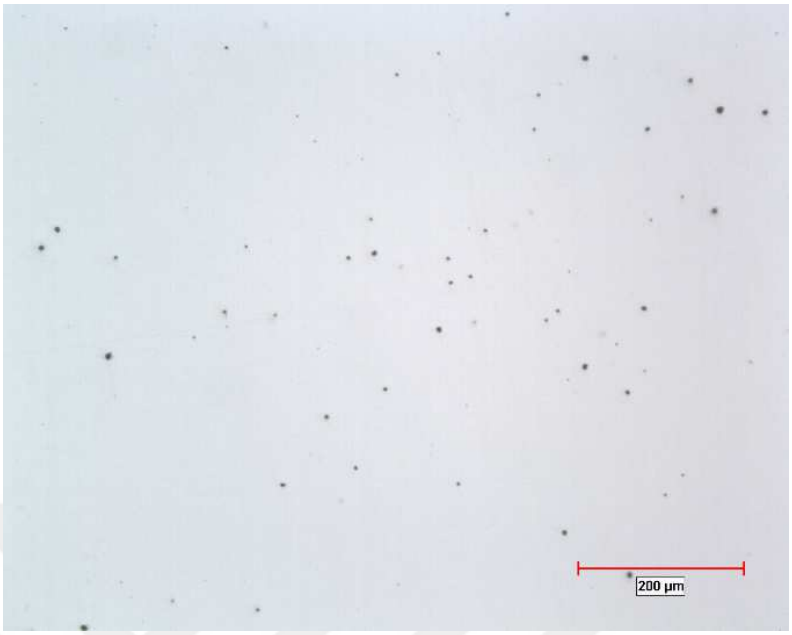

Figure B-6 Inclusion rating of B-Slab4

B-Slab9 has D-Globular Oxide Type, Thin, 2 as shown in Figure B-7

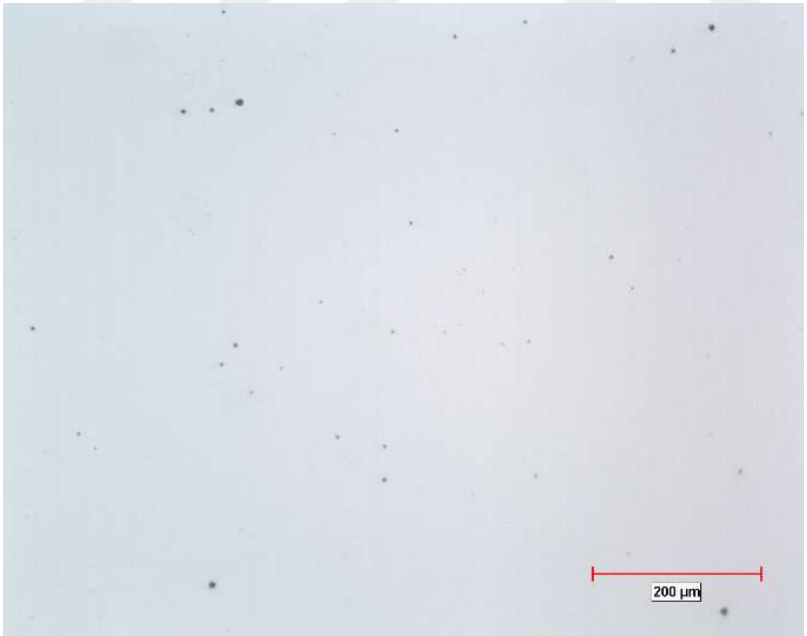

Figure B-7 Inclusion rating of B-Slab9

B-Slab5 has D-Globular Oxide Type, Thin, 3 as shown in Figure B-8

Figure B-8 Inclusion rating of B-Slab5

B-Slab6 has D-Globular Oxide Type, Thin, 2 as shown in Figure B-9

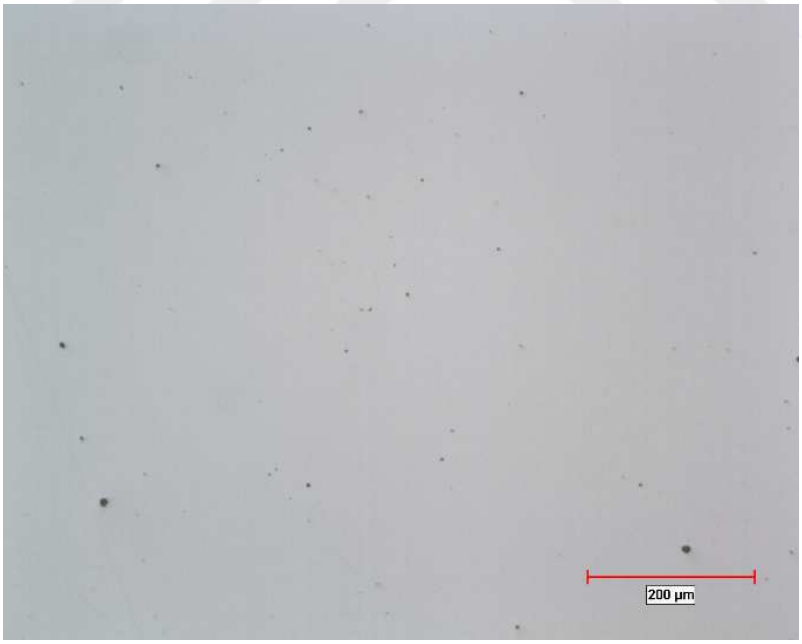

Figure B-9 Inclusion rating of B-Slab6

B-Slab10 has D-Globular Oxide Type, Thin, 2 as shown in Figure B-10

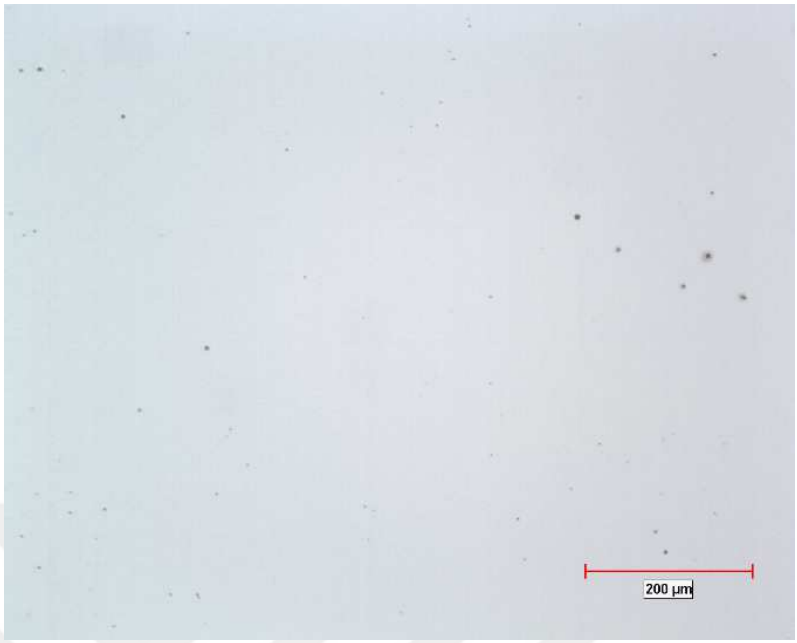

Figure B-10 Inclusion rating of B-Slab10

B-Slab11 has D-Globular Oxide Type, Thin, 2 as shown in Figure B-11

Figure B-11 Inclusion rating of B-Slab11

B-Slab14 has D-Globular Oxide Type, Thin, 2 as shown in Figure B-12

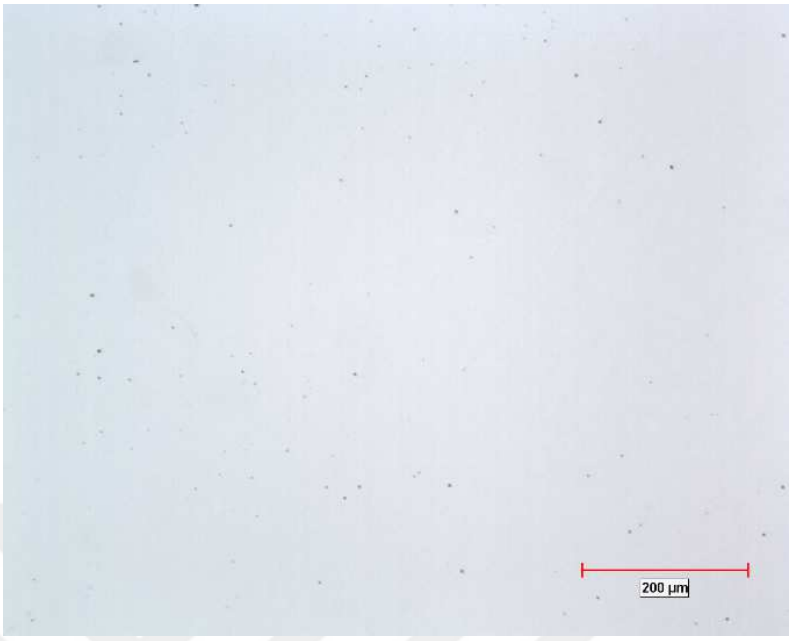

Figure B-12 Inclusion rating of B-Slab14

B-Slab13 has D-Globular Oxide Type, Thin, 3 as shown in Figure B-13

Figure B-13 Inclusion rating of B-Slab13

B-Slab12 has D-Globular Oxide Type, Thin, 2 as shown in Figure B-14

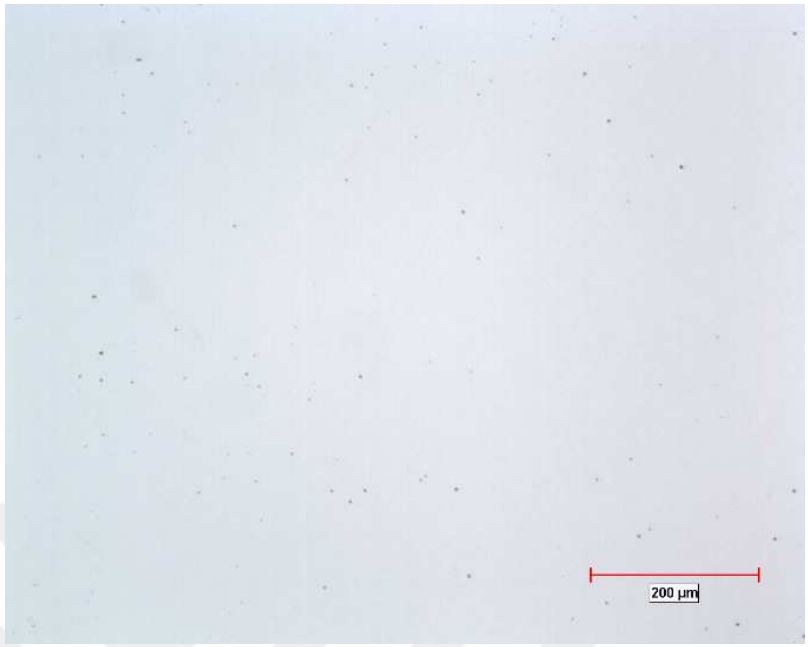

Figure B-14 Inclusion rating of B-Slab12